

An experimental study of liquid-phase separation in the systems $\text{Fe}_2\text{SiO}_4\text{-Fe}_3\text{O}_4\text{-KAlSi}_2\text{O}_6\text{-SiO}_2\text{-H}_2\text{O}$, $\text{Fe}_3\text{O}_4\text{-KAlSi}_2\text{O}_6\text{-SiO}_2\text{-H}_2\text{O}$ and $\text{Fe}_3\text{O}_4\text{-Fe}_2\text{O}_3\text{-KAlSi}_2\text{O}_6\text{-SiO}_2\text{-H}_2\text{O}$ with or without P, S, F, Cl or $\text{Ca}_{0.5}\text{Na}_{0.5}\text{Al}_{1.5}\text{Si}_{2.5}\text{O}_8$: Implications for immiscibility in volatile-rich natural magmas

Gregory W Lester

A thesis submitted to the Department of Geological Science and Geological Engineering

In conformity with the requirements for
the degree of Doctorate of Philosophy

Queen's University

Kingston, Ontario, Canada

April, 2012

Copyright ©Gregory W Lester 2012

D'Villefort "We transcend discourse and enter into dissertation"

Dantes "Surely you do not believe that what you do deserves to be called anything"

~ Dumas

Abstract

Isobaric (200 MPa) experiments have been performed to investigate the effects of H₂O alone or in combination with P, S, F or Cl on the phase relations and elemental and oxygen isotopic partitioning between immiscible silicate melts in the systems Fe₂SiO₄-Fe₃O₄-KAlSi₂O₆-SiO₂, Fe₃O₄-KAlSi₂O₆-SiO₂ and Fe₃O₄-Fe₂O₃-KAlSi₂O₆-SiO₂ +/- plagioclase (An₅₀). Experiments were heated in a newly-designed rapid-quench internally-heated pressure vessel at 1075, 1150 or 1200 °C for 2 hours. Water alone or in combination with P, S, or F significantly increases the temperature and composition range of two-liquid fields at f_{O_2} = NNO and MH buffers. Water-induced suppression of liquidus temperatures, considered with the effects of pressure on two-liquid fields stability in silicate melts, suggests that liquid phase separation may occur in some volatile-rich silicate magmas at pressures up to 2GPa. Two-liquid partition coefficients for Fe, Si, P and S correlate well with the degree of polymerization of the SiO₂-rich conjugate melts and the data can be applied to assess the involvement of liquid-phase separation in the genesis of coexisting volatile-rich magmas.

The partitioning of trace concentrations of selected HFSE, REE and transition elements between immiscible experimental volatile-rich melts at 1200 °C, 200 MPa has been determined at QFM, NNO and MH oxygen buffers. Water generally increases the partitioning of HFSE, REE and transition elements into the Fe-rich melt. Water alone, or combined with P or S, produces nearly parallel partitioning trends for HFSE and REE. Absolute partitioning values of transition elements are strongly dependent on the network-modifier composition of the melt.

^{18}O in experimental immiscible melts with H_2O or H_2O and P or S partitions preferentially into the felsic conjugate melt ($\delta^{18}\text{O}$ felsic melt- $\delta^{18}\text{O}$ mafic melt values range from 0.4 to 0.8 permil) consistent with observations in anhydrous immiscible silicate melts.

The expansion of the P - T - X - $f\text{O}_2$ stability ranges of two- or three-liquid fields observed in the experimental melts demonstrates that liquid-immiscibility may be an important process in the evolution of some volatile-rich natural magmas. The results support an immiscible petrogenetic origin for some iron-oxide dominated, Kiruna-type, ore-deposits.

Acknowledgements

I wish to thank my advisors Alan H. Clark and T. Kurt Kyser and for that rarest of gifts, the opportunity to pursue one's intellectual passions, unfettered, with support and guidance as required.

I wish to thank Dick Naslund, Bruce Watson, Tony Phillpotts, Dan Layton-Matthews, and Peter Roeder whose research, conversation and correspondence have contributed much to this project.

Gordon Moore and John Holloway of the Depths of the Earth Laboratory at Arizona State University, Jim Lee, Paul Alexandre and Alan Grant of Queen's University, Panseok Yang of the University of Manitoba and the laboratory personnel of the Queen's Facility for Isotope Research contributed invaluable time, technical expertise and resources to this endeavour. I would also express my gratitude to Jorge Benavides, Allan Montgomery and the students, staff and faculty of the Queen's University Department of Geological Sciences and Geological Engineering: your professionalism, generosity and friendship have made graduate work a pleasure.

This research was supported by the Natural Sciences and Engineering Research Council of Canada (NSERC) individual discovery grants to A.H. Clark and T.K. Kyser as well as NSERC Major Facilities Access Grants to T.K. Kyser. A Hugh E. McKinstry grant from the Society of Economic Geologists is also acknowledged.

Lastly, my heartfelt thanks are given to David Love, Carol Christiansen, Zabe MacEachren, Julie Hammer, my daughters Evelyn and Becky, and my brothers Garra and Richard, whose contributions have been fundamental to the completion of this dissertation.

Statement of Originality

I hereby certify that all of the work described in this thesis is the original work of the author. Any published (or unpublished) ideas and/or techniques from the work of others are fully acknowledged in accordance with the standard referencing practices.

(Gregory W Lester)

February, 2012

Table of Contents

Abstract	iii
Acknowledgements	v
Statement of Originality	ix
Table of Contents	x
List of Figures.....	x
List of Tables	x
Chapter 1 Introduction.....	1
1.1 Rationale.....	1
1.2 Objectives and Method.....	3
1.3 Thesis organization.....	5
Chapter 2 Experiments on silicate liquid immiscibility with H ₂ O, P, S, F or Cl: implications for natural magmas.....	6
2.1 Abstract	6
2.2 Introduction	7
2.3 Experimental Method	8
2.4 Results	11
2.4.1 General.....	11
2.4.2 Addition of H ₂ O	14
2.4.3 Addition of H ₂ O and Phosphorous.....	16
2.4.4 Addition of H ₂ O and Sulfur.....	18
2.4.5 Addition of H ₂ O and Fluorine.....	19
2.4.6 Addition of H ₂ O and Chlorine.....	19

2.4.7 Addition of H ₂ O plus P, S, F, or Cl to the system Fe ₃ O ₄ Fe ₃ O ₄ - KAlSi ₂ O ₆ -SiO ₂ -CaAl ₂ Si ₂ O ₈ -NaAlSi ₃ O ₈	10
2.4.8 Additional Experiments.....	20
2.5 Discussion.....	29
2.5.1 Partition coefficients and melt structure in volatile rich melts	29
2.5.2 Major element partitioning and melt structure relations in volatile-rich melts.....	29
2.5.2.1 Fe, Si and K partitioning.....	32
2.5.3.2 Partitioning of P, S and F.....	33
2.5.4 Application of partitioning-polymerization relationships in experimental melts to the assessment of coexisting, volatile- rich natural magmas.....	34
2.5.5 Immiscibility in volatile-rich magmas.....	35
2.5.6 Implications for the pressure stability of volatile-rich immiscible magmas.....	37
2.6 Conclusions	40
Chapter 3 The Effect of H ₂ O, P, S, F, or Cl on trace element partitioning between immiscible silicate melts.....	42
3.1 Abstract	42
3.2 Introduction.....	42
3.3 Experimental method.....	44
3.4 Analytical method.....	46

3.5 Results	47
3.5.1 Run products.....	47
3.5.2 Major elements.....	47
3.5.3 Trace elements.....	47
3.6 Discussion and conclusions	51
Chapter 4 Oxygen Isotopic Partitioning between Immiscible Silicate Liquids with H ₂ O, P and S.....	53
4.1 Abstract	53
4.2 Introduction	54
4.3 Experimental procedure	55
4.4 Results	57
4.5 Discussion	57
4.6 Concluding remarks	62
Chapter 5 Discussion.....	64
5.1 Introduction.....	64
5.2 Phase relations volatile-rich immiscible silicate melts.....	63
5.3 Trace element partitioning in volatile-rich immiscible silicate melts..	67
5.4 Stable isotopes.....	68
Chapter 6 Summary and Conclusions.....	70
6.1 Experiments on liquid immiscibility in silicate melt with H ₂ O, P, S, F and Cl: Implications for volatile-rich natural magmas.....	70
6.2 Effect of H ₂ O, P, S, F, or Cl on trace element partitioning between immiscible silicate melts.....	71

6.3 Oxygen isotopic partitioning in immiscible silicate liquids with H ₂ O, P and S.....	72
6.4 Concluding remarks.....	73
References	74
Appendix A Experimental Procedure.....	75
Appendix B Preparation of trace element doping mixtures and major element composition data for trace element partitioning experiments.....	89

List of Figures

Figure 2-1: Back-scattered electron images of experimental results.....	12
Figure 2-2: Phase relations in experimental melts.....	15
Figure 2-3: Phase relations in experimental melts with 10 wt% H ₂ O, and equivalent anhydrous melts.....	17
Figure 2-4: Partition coefficients and nbo/t ^f ratio between conjugate experimental melts.....	31
Figure 2-5: Width of the miscibility gap in experimental melts with; H ₂ O, and H ₂ O with P, S, or F expressed as a function of temperature plotted against nbo/t of conjugate liquid pairs.....	36
Figure 2-6: Inferred <i>T-X</i> H ₂ O range of two-liquid silicate melts in supra-subduction H ₂ O-fluxed melting zone of the mantle wedge.....	39
Figure 3-1: Two-liquid partition coefficients for trace elements in experimental melts...	49
Figure 4-1: Oxygen isotope proportioning in Si- and Fe-rich glasses melt-mineral and mineral-mineral pairs.....	60
Figure 4-2: Oxygen isotope proportioning as a function of tetrahedral oxygen partitioning in conjugate Si- and Fe-rich glasses, melt-mineral, and mineral-mineral pairs.....	61

List of Tables

Table 2-1. Base mixture compositions.....	9
Table 2-2. Experimental starting compositions, run conditions and phase assemblages	13
Table 2-3. Electron microprobe analyses of experimental run products	21
Table 3-1. Starting mixture compositions	45
Table 3-2. Two liquid partition coefficients (Nernst) $D^{Lm/Lf}$ for trace elements	48
Table 4-1. Starting compositions for experimental melts	56
Table 4-2. Major element compositions and $\delta^{18}\text{O}$ values for conjugate immiscible glasses	58

Chapter 1

INTRODUCTION

1.1 Rationale

Liquid-phase separation is accepted as the genetic mechanism for coexisting silicate-sulfide and silicate-carbonatitic magmas (Naldrett, 2010; Hamilton et al. 1979), but the geological importance of conjugate-immiscible silicate and iron-oxide rich melts has remained a matter of contention since it was first proposed as a petrogenetic mechanism in the early 19th century (Scrope, 1825). Immiscible silicate and iron-oxide rich melts have, however, been documented in layered mafic intrusions (McBirney, 1975), massif anorthosite complexes (Darling and Florence, 1995), granitoids (Rajesh, 2003, Johnson et al., 2002), lamprophyres (Philpotts, 1976), and both lunar and terrestrial volcanic rocks (Roedder and Weiblen, 1971), and invoked as a primary genetic mechanism for some iron-oxide dominated mineral deposits, including Kiruna-type magnetite +/- apatite systems (Chen et al. 2010; Clark and Kontak, 2004; Nyström and Henríquez, 1994).

Arguments for silicate liquid immiscibility as a petrogenetic mechanism are generally supported with textural and compositional evidence from rocks (e.g. Clark and Kontak, 2004) or with phase-relationships determined by experimental investigations of chemically simplified systems broadly analogous to natural magmas (e.g. Bogaerts and Schmidt, 2006). Thus, experimental studies have constrained miscibility gaps in silicate melts as a function of parental melt composition, temperature and, to a lesser extent, pressure for the anhydrous system Si - Fe - Al - K - O, alone or in combination with one or more of the following: Na, Ca, Mg, Ti and P (Roedder, 1951, 1978; Watson and Naslund, 1976; Visser and van Groos, 1979b; Naslund, 1983;

Bogaerts and Schmidt, 2006), as well as for more complex lunar and terrestrial basaltic liquids (Hess et al., 1975; Longhi, 1990).

The present study is predicated on the hypothesis that minor quantities of the common volatile constituents, H₂O, P, S, F and Cl are likely to affect the formation and extent of two- or three- liquid fields in magmatic systems, and that composition and phase relation data pertaining to these effects are required to evaluate further the role of silicate liquid-phase separation in petrogenesis. The limited data available indicate that in contrast to the crystal fractionation process, in which small variations in magma composition produce only minor displacements of phase-field boundaries or system mineralogy, liquid phase separation, and concomitant gravitational segregation of the conjugate liquids, may result in significant chemical and spatial segregation of magmatic components, generating fundamentally different lithologies. The stability and extent of miscibility gaps in silicate melts are markedly sensitive to variation in composition. Components such as OH, PO₄, S, F and Cl are commonly present in magmas in the form of anion-metal complexes that have positive enthalpies of formation. Thus, the presence of these common components in magmas act to increase the ΔG_{mix} term in the expression $\Delta G_{\text{mix}} = \Delta H_{\text{mix}} - T\Delta S_{\text{mix}}$, favouring liquid unmixing (Ryerson and Hess, 1978). Further, it has been demonstrated that OH, P, S, F and Cl affect both the position of the liquidus and the degree of melt polymerization in silicate melts, parameters that control the compositions and thermal ranges of two-liquid fields (Botcharnikov 2008; Lester 2002; Moore et al. 1998; Visser and van Groos, 1979c; Haughton et al., 1974; Dolejš and Baker, 2007; Webster, 2002).

1.2 Objectives and method

The objectives of this experimental study are: a) to elaborate the predictive model of immiscibility in silicate magmas by constraining the T - X - fO_2 conditions under which silicate-liquid phase separation occurs; b) to define, in part, the chemical compositions and element partitioning in conjugate immiscible melts that approximate the compositions of natural melts with regard to network-modifying components; and c) to combine the new data with those from previous studies to more fully understand the potential role of silicate immiscibility in magmatic systems and petrogenesis.

This study comprises the presentation and evaluation of data collected from three sets of experiments:

1. *Experiments on liquid immiscibility in silicate melts with H₂O, P, S, F and Cl: implications for natural magmas.*

These experiments were designed to extend previous knowledge of silicate liquid-liquid immiscibility by exploring the effects of the common magmatic constituents H₂O, F, Cl, S and P on phase relations in chemically-simplified magma-analogue melts, and to draw general implications regarding the effects of these components on liquid-phase separation in natural magmas. The implications of the results for the P - T - X - fO_2 stability ranges of two-liquid fields in natural silicate melts, with emphasis on the pressure stability of miscibility gaps in volatile-rich magmas, are discussed. The investigation represents a first step out from the published studies of anhydrous, volatile-free systems. Compositional data from immiscible melt produced in these experiments are used to demonstrate the effects of H₂O, F, Cl, S and P on major-element partitioning between immiscible melts and to test the element partitioning-melt polymerization

assessment method developed by Bogaerts and Schmidt (2006) as a means to evaluate the involvement of liquid-phase separation in coexisting, volatile-rich magmas.

2. Trace element partitioning between immiscible silicate melts with H₂O, P, S, F, or Cl

These experiments investigate the effects of H₂O, P, S, F, or Cl on the partitioning of the trace elements Rb, Cs, Zr, Nb, Hf, Th, U, La, Ce, Nd, Sm, Eu, Dy, Er, Yb, Mn, Co, Mo, Ni, Cu, Zn, Cr, Cr, V, Ti and Ag between immiscible silicate melts with molar equivalent quantities of P, S, F, or Cl in the systems Fe₂SiO₄-Fe₃O₄-KAlSi₂O₆-SiO₂, Fe₃O₄-KAlSi₂O₆-SiO₂ and Fe₃O₄-Fe₂O₃-KAlSi₂O₆-SiO₂, with or without plagioclase (An₅₀) under conditions of variable oxygen fugacity.

3. Oxygen isotope partitioning between immiscible silicate liquids with H₂O, P and S

These experiments quantify oxygen isotope proportioning to evaluate oxygen isotope controls on fractionation between hydrous immiscible silicate melts with P or S. This limited set of experiments assesses the application of stable oxygen isotope analysis as a means to identify silicate liquid phase separation as a petrogenetic mechanism.

The experiments described above involve selected starting mixtures in the systems Fe₂SiO₄-Fe₃O₄-KAlSi₂O₆-SiO₂, Fe₃O₄-KAlSi₂O₆-SiO₂ and Fe₃O₄-Fe₂O₃-KAlSi₂O₆-SiO₂, with or without plagioclase (An₅₀), heated under isothermal/isobaric conditions at fixed oxygen fugacity. Material for chemical and isotopic analyses was obtained by the rapid quench of experimental runs. Details regarding the procedures used in each experimental set are given in Chapters 2 and 4 of this thesis. Comprehensive reviews of previous experimental studies of liquid immiscibility in silicate melts are given in Bogaerts and Schmidt (2006), Veksler et al. (2006) and Lester (2002).

1.3 Thesis organization

This dissertation is constructed in manuscript format, and fulfills the requirements of the Queen's University School of Graduate Studies and Research. Three manuscripts form the body of this thesis. Chapter 2 represents one paper on, "Experiments on liquid immiscibility in silicate melts with H₂O, P, S, F and C: implications for natural magmas" as authored by Lester GW, Clark A.H., Kyser, T.K., and Naslund, H.R. This paper has been accepted for publication in *Contributions to Mineralogy and Petrology* pending revision. Chapter 3 is another paper that describes "The effects of H₂O, P, S, F, or Cl on trace element partitioning between immiscible silicate melts" and is authored by Lester, G.W., Clark, A.H., Kyser, T.K., and Layton-Mathews, D. It has been submitted to the journal *Chemical Geology* and is under review. Chapter 4 is the third paper on "Oxygen isotopic partitioning between immiscible silicate liquids with H₂O, P and S", authored by Lester, GW, Kyser, TK and Clark, AH, to be submitted to a journal as yet undecided. *Contributions to Mineralogy and Petrology* and *Chemical Geology* are major international, peer-reviewed journals.

Chapter 2

EXPERIMENTS ON LIQUID IMMISCIBILITY IN SILICATE MELTS WITH H₂O, P, S, F AND Cl: IMPLICATIONS FOR NATURAL MAGMAS

2.1 Abstract

Isobaric (200 MPa) experiments have been performed to investigate the effects of H₂O alone or in combination with P, S, F or Cl on liquid phase separation in melts in the systems Fe₂SiO₄-Fe₃O₄-KAlSi₂O₆-SiO₂, Fe₃O₄-KAlSi₂O₆-SiO₂ and Fe₃O₄-Fe₂O₃-KAlSi₂O₆-SiO₂, with or without plagioclase (An₅₀). Experiments were carried out in a rapid-quench internally-heated pressure vessel at 1075, 1150 or 1200 °C for 2 hours. Experimental fO_2 was maintained at QFM, NNO or MH oxygen buffers. Water alone, or in combination with P, S, or F, is shown to increase the temperature and composition range of two-liquid fields at NNO and MH buffers. The elements P, S, F and Cl partition preferentially into the Fe-rich immiscible liquid. Two-liquid partition coefficients for Fe, Si, P and S correlate well with the degree of polymerization of the SiO₂-rich liquid (nbo/t) and plot on similar but distinct power law curves compared with equivalent anhydrous or basaltic melts. The addition of 2 wt% S to the system Fe₃O₄-Fe₂O₃-KAlSi₂O₆-SiO₂ stabilizes three immiscible melts with Fe-, FeS- and Si- rich compositions. Water- induced suppression of liquidus temperatures in the experimental systems, in combination with the effects of pressure on the temperature and composition ranges of two-liquid fields in silicate melts, suggests that liquid phase separation may occur in some H₂O-rich silicate magmas at pressures up to 2GPa.

2.2 Introduction

Liquid phase separation is accepted as an important differentiation mechanism in diverse magmas. Immiscibility between felsic silicate and Fe-rich mafic silicate liquids (L^f and L^m) has been documented in layered mafic intrusions (McBirney, 1975) anorthosite complexes (Darling and Florence, 1995), granitoids (Rajesh, 2003, Johnson et al., 2000), lamprophyres (Philpotts, 1976) and lunar and terrestrial volcanic rocks (Roedder and Weiblen, 1971). Immiscibility has also been invoked as a primary genetic mechanism for some iron-oxide dominated base- and precious- metal mineral deposits, including Kiruna-type magnetite +/- apatite systems (Chen et al., 2010, Clark and Kontak, 2004, Nyström and Henríquez, 1994).

Experimental investigations of felsic silicate-mafic silicate liquid immiscibility to date have constrained the configuration of miscibility gaps in silicate melts as a function of parental melt composition, temperature and, to a lesser extent, pressure for the anhydrous system $\text{Fe}_2\text{SiO}_4\text{-KAlSi}_2\text{O}_6\text{-SiO}_2$, with or without one or more of the following: Na, Ca, Mg, Ti and P, (Roedder, 1951; 1978; Watson, 1976a,b; Visser and van Groos, 1979a,b; Naslund, 1983; Bogaerts and Schmidt, 2006), as well as for more chemically complex lunar and terrestrial basaltic liquids (Longhi, 1990; Philpotts, 1982; Hess et al., 1975). To develop further a predictive model of felsic silicate-mafic silicate immiscibility in magmas, I herein document experiments on the effects of the network-modifying component H_2O , alone and in combination with P, S, F or Cl, on selected compositions in the systems $\text{Fe}_2\text{SiO}_4\text{-Fe}_3\text{O}_4\text{-KAlSi}_2\text{O}_6\text{-SiO}_2$, $\text{Fe}_3\text{O}_4\text{-KAlSi}_2\text{O}_6\text{-SiO}_2$ and $\text{Fe}_3\text{O}_4\text{-Fe}_2\text{O}_3\text{-KAlSi}_2\text{O}_6\text{-SiO}_2$ +/- $\text{Ca}_5\text{Na}_5\text{Al}_{1.5}\text{Si}_{2.5}\text{O}_8$, (An_{50}).

The stability and extent of two-liquid solvi in silicate melts are markedly sensitive to minor variations in the enthalpy of mixing term in the expression $\Delta G_{\text{mix}} = \Delta H_{\text{mix}} - T\Delta S_{\text{mix}}$. Common constituents in natural melts, such as OH, P, S, F and Cl, have positive enthalpies of

formation of anion-metal complexes which act to increase the value of the ΔG_{mix} term, thus favoring liquid unmixing (Ryerson and Hess, 1978). Further, it has been demonstrated that OH, P, S, F and Cl influence liquidus-miscibility gap relations and the degree of polymerization in silicate melts, parameters that control the compositions and thermal ranges of two-liquid solvi (Botcharnikov, 2008; Moore et al., 1998; Visser and van Groos, 1979a; Haughton et al. 1974; Dolejš and Baker, 2007; Webster, 2002).

The results reported herein show that H₂O, alone or in combination with P, S, F, or Cl, acts to expand significantly two- liquid miscibility gaps in geologically-relevant temperature-pressure-composition space. The phase relationships documented, considered in conjunction with known chemical-thermal evolution trends in natural melts, provide a more complete framework for discussion of the role of silicate liquid immiscibility in petrogenesis and mass-flux in natural igneous systems.

2.3 Experimental method

Starting materials for the experiments included seven anhydrous base compositions prepared from SiO₂ (cristobalite), Al₂O₃, K₂Si₂O₅, FeO and Fe₂O₃. Each base-mixture plots as a composition point on the 30 wt% FeO isopleth on the ternary join fayalite-leucite-silica (Appendix A, Naslund, 1983). Base-compositions have an Al/K molar ratio of 1 (Table 2-1). To minimize the $f\text{O}_2$ gradient between melts and external solid buffers, $\text{Fe}^{3+} / \Sigma \text{Fe}$ values for the melts synthesized in this study were estimated with the method of Schuessler et al. (2008) at the quartz-fayalite-magnetite (QFM), nickel-nickel oxide (NNO) or magnetite-hematite (MH) oxygen buffers at, $T=1200$ °C and $P=200$ MPa. The 30 wt% FeO_{total} component of each base-mixture comprises FeO and Fe₂O₃, with Fe₂P, FeS, FeCl₂, or FeF₂ in proportions that

approximate the $\text{Fe}^{3+} / \Sigma \text{Fe}$ values calculated for the selected experimental conditions. Oxygen fugacity in the experimental capsules was controlled using the conventional double capsule, metal-metal oxide or metal oxide-silicate + water configuration (Chou and Cygan, 1990).

Table 2-1: Base compositions (wt%).

base composition	SiO ₂	FeO _{total}	Al ₂ O ₃	K ₂ O	An ₅₀ ^a
A - 1	66.05	30	2.06	1.89	-
A - 2	64.46	30	2.88	2.66	-
A - 3	62.86	30	3.71	3.43	-
A - 4	60.13	30	5.13	4.74	-
A - 5	57.48	30	6.51	6.01	-
A - 6	55.88	30	7.34	6.78	-
A - 7	54.32	30	8.15	7.53	-
An ₅₀	65.2	29.62	2.03	1.87	1.3

^a (Ca₅ Na₅) Al_{1.5} Si_{2.5}O₈

Experimental starting compositions containing either 1 wt% P, 2 wt% S, 6 wt% Cl or 6 wt% F (total wt. oxides) were prepared by the addition of Fe₂P, FeS, FeCl₂, or FeF₂ to the anhydrous base- mixtures (Table 2-1). Fe-salts were selected as the source of P, S F and Cl in order to minimize the loss of volatile components during the welding of experimental capsules. Hydrous experiments incorporated 10 wt% H₂O (total wt. solids). Plagioclase-bearing experiments contain 1.3 wt% (total wt. solids) An₅₀, constituting 43 wt% of the normative feldspar component.

Experiments were carried out by loading the desired quantity of starting material, or starting material + H₂O, into a 2mm (outside diameter) platinum capsule. Three- to- five experimental capsules were loaded into a 5 mm (outside diameter) platinum capsule containing H₂O and one of the selected metal-metal oxide or metal oxide-silicate buffers, QFM, NNO or MH. Both inner experimental capsules and outer buffer-bearing capsules were sealed by welding.

Experiments were carried out in Kanthal™ or platinum-wound furnaces placed in an internally-heated pressure vessel under isobaric conditions (200, +/- 10 MPa), isothermally at 1075, 1150 or 1200 °C for two hours using argon as the pressure medium. The pressure vessel, similar in design to that described by Holloway (1971), was modified to allow the vessel to rotate from the horizontal run position to a vertical quench position (Appendix A). Rapid isobaric cooling of the experimental capsules was achieved as the vessel was rotated towards the vertical, causing the capsule to drop from the hot spot to the unheated, water-cooled end of the pressure chamber ($T < 250$ °C). The quench rate is inferred to be 500° C/s, similar to that reported by Holloway et al. (1992) for a rapid-quench furnace with an equivalent thermal profile. The rotating furnace design used in this study provides a significant degree of control on the thermal characteristics of the critical heating zone. The temperature along the length of the experimental capsules was measured using three iconel-sheathed, chrome-alumel thermocouples. Temperature differences between the distal thermocouples ranged from 1 to 16 °C, +/- 2 °C. The argon medium pressure was measured using a Bourdon tube-gauge, accurate to +/- 5 MPa.

Reversal experiments were performed to determine the time required to achieve chemical equilibrium in the experimental charges. Capsules containing experimental base-compositions + 10 wt% H₂O, were heated for two hours at a temperature of 1210 °C and then cooled to 1075, 1150 or 1200 °C for one, two or four hours, and subsequently quenched. The chemical compositions and textural characteristics observed in the experimental products produced in the reverse experiments are identical to those produced in forward experiments run at the same temperature and it is therefore concluded that equilibrium was obtained at heating durations of less than one hour. Solid-oxide buffer reactants were evaluated after cooling using X-ray powder diffraction analysis or microscopic phase identification.

Experimental samples were mounted in epoxy, polished and analyzed with a Cameca SX-100 electron microprobe at the University of Manitoba. Analytical conditions were set to an accelerating voltage of 15 kV, a 15 nA beam current and a counting time of 20s for all elements except P, S, F and Cl (30s). The beam diameters were 5-10 μm for Si-rich and Fe-rich glasses and 2 μm for quenched sulfide melt. Natural and synthetic oxides, silicates or sulfides were used as standards.

2.4 Results

2.4.1 General

Compositions of the starting materials are given in Table 2-1, run conditions and phase relation data are summarized in Table 2-2; and electron microprobe analyses and partition ratios ($D_i = \text{concentration in the felsic liquid } L^f / \text{concentration in the mafic liquid } L^m$) are presented in Table 2-3.

Immiscible liquids in experimental anhydrous silicate melts commonly occur as spheroidal or ellipsoidal droplets that range from sub-micron to over 500 μm in size (Figure 2-1). Exsolving conjugate immiscible liquids nucleate and form droplets which grow and, to a varying degree, coalesce (Figure 2-1a). Each liquid commonly occurs as droplets or pools distributed within a larger volume of the other liquid (Bowen, 1925; Philpotts, 2008). Experimental melts produced in this study in systems with H_2O alone or $\text{H}_2\text{O} + \text{P, S or F}$ exhibit a spherical geometry similar to that observed in anhydrous melts (Figure 2-1b).

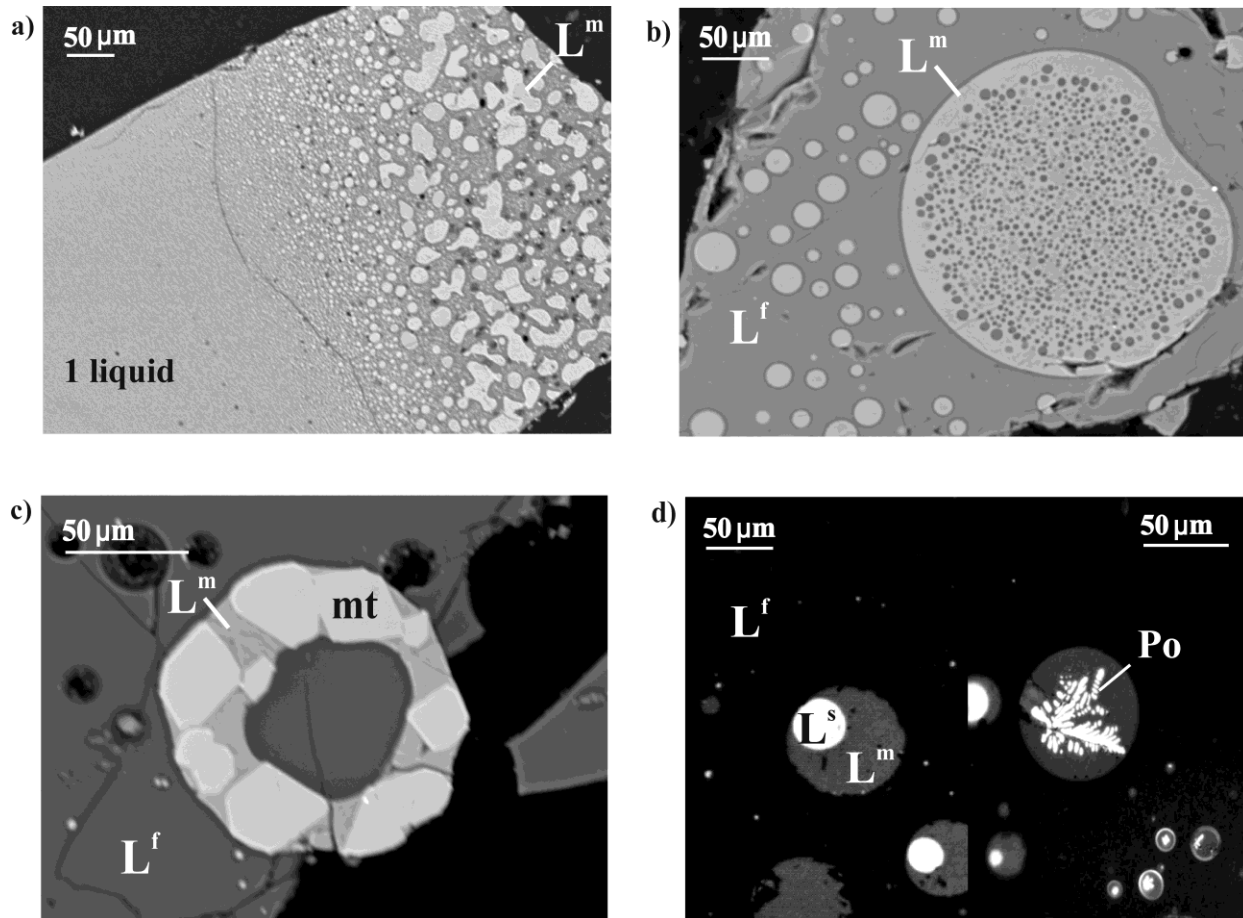


Figure 2-1: Back-scattered electron images of experimental melts: **a)** liquid phase separation and coalescence of liquid droplets (L^m), composition: A-3 + H_2O + F, $fO_2=MH$, $P = 200$ MPa. The phase assemblage is the result of a thermal gradient of ~ 950 - 1230 °C (from left to right); **b)** typical liquid phase separation textures, composition: A-1 + H_2O + P, $fO_2=MH$, $1200^\circ C$, $P= 200$ MPa; **c)** two liquids plus magnetite, composition: A-3 + H_2O + F, $fO_2=MH$, 1075 °C, $P = 200$ MPa; **d)** three-liquid phase assemblage (L^f , L^m and L^s), and three liquids plus pyrrhotite (Po) developed upon cooling, A-3 + H_2O + S, $fO_2=MH$, 1150 °C, $P = 200$ MPa. *NB.* L^f = Si-rich liquid, L^m = Fe-rich liquid, L^s = sulphide-rich liquid, Po = pyrrhotite, mt = magnetite.

All of the experimental immiscible melt phase-assemblages contain a vapor phase. The presumed equilibrium vapor bubbles are generally > 10 μm in diameter and are defined by menisci that appear smooth under high power magnification. These bubbles are easily distinguished from quench-induced vapor exsolution textures which form as small bubbles of < 1 μm or as aggregate masses of bubbles with irregular geometries.

Table 2-2: Experimental run conditions and phase assemblages. $P=200 \pm 1.5$ Mpa
 All experimental melts include a vapor phase. Data for A-2 - A-6 with P, S from Lester (2002).
 liq-liquid, mt-magnetite, sil-silica minerals

base	composition additional components					t (°C)	buffer	phase - assemblage	base	composition additional components					t (°C)	buffer	phase - assemblage
	(wt% base)									(wt% base)							
	H ₂ O	P	S	F	Cl					H ₂ O	P	S	F	Cl			
A - 1	10	-	-	-	-	1200	MH ^b	2 liq.	A - 2	10	1	-	-	-	1075	NNO	2 liq.
A - 2	10	-	-	-	-	1200	MH	2 liq.	A - 3	10	1	-	-	-	1075	NNO	2 liq.
A - 3	10	-	-	-	-	1200	MH	2 liq.	A - 4	10	1	-	-	-	1075	NNO	1 liq.
A - 4	10	-	-	-	-	1200	MH	2 liq.	A - 1	10	1	-	-	-	1200	QFM	2 liq.
A - 5	10	-	-	-	-	1200	MH	2 liq.	A - 1	10	-	2	-	-	1200	MH	3 - liq.
A - 6	10	-	-	-	-	1200	MH	2 liq.	A - 3	10	-	2	-	-	1200	MH	3 - liq.
A - 1	10	-	-	-	-	1150	MH	2 liq.	A - 4	10	-	2	-	-	1200	MH	3 - liq.
A - 3	10	-	-	-	-	1150	MH	2 liq.	A - 5	10	-	2	-	-	1200	MH	3 - liq.
A - 5	10	-	-	-	-	1150	MH	2 liq.	A - 6	10	-	2	-	-	1200	MH	3 - liq.
A - 7	10	-	-	-	-	1150	MH	1 liq. + mt	A - 1	10	-	2	-	-	1150	MH	3 - liq.
A - 1	10	-	-	-	-	1075	MH	1 liq. + mt	A - 3	10	-	2	-	-	1150	MH	3 - liq.
A - 3	10	-	-	-	-	1075	MH	1 liq. + mt	A - 5	10	-	2	-	-	1150	MH	3 - liq.
A - 5	10	-	-	-	-	1075	MH	1 liq. + mt	A - 7	10	-	2	-	-	1150	MH	2 liq. + mt
A - 7	10	-	-	-	-	1075	MH	1 liq. + mt	A - 1	10	-	2	-	-	1075	MH	1 liq. + mt + sil
A - 1	10	-	-	-	-	1200	NNO	2 liq.	A - 3	10	-	2	-	-	1075	MH	1 liq. + mt + sil
A - 2	10	-	-	-	-	1200	NNO	1 liq.	A - 5	10	-	2	-	-	1075	MH	2 liq. + mt
A - 3	10	-	-	-	-	1200	NNO	1 liq.	A - 7	10	-	2	-	-	1075	MH	2 liq. + mt
A - 5	10	-	-	-	-	1200	NNO	1 liq.	A - 1	10	-	2	-	-	1200	NNO	2 liq.
A - 7	10	-	-	-	-	1200	NNO	1 liq.	A - 2	10	-	2	-	-	1200	NNO	2 liq.
A - 1	10	-	-	-	-	1150	NNO	1 liq.	A - 3	10	-	2	-	-	1200	NNO	2 liq.
A - 2	10	-	-	-	-	1150	NNO	1 liq.	A - 4	10	-	2	-	-	1200	NNO	2 liq.
A - 1	10	-	-	-	-	1200	QFM	2 liq.	A - 5	10	-	2	-	-	1200	NNO	1 liq.
A - 1	10	1	-	-	-	1200	MH	2 liq.	A - 6	10	-	2	-	-	1200	NNO	1 liq.
A - 2	10	1	-	-	-	1200	MH	2 liq.	A - 7	10	-	2	-	-	1200	NNO	1 liq.
A - 3	10	1	-	-	-	1200	MH	2 liq.	A - 1	10	-	2	-	-	1150	NNO	2 liq.
A - 4	10	1	-	-	-	1200	MH	2 liq.	A - 2	10	-	2	-	-	1150	NNO	2 liq.
A - 5	10	1	-	-	-	1200	MH	2 liq.	A - 3	10	-	2	-	-	1150	NNO	2 liq.
A - 6	10	1	-	-	-	1200	MH	2 liq.	A - 4	10	-	2	-	-	1150	NNO	1 liq.
A - 7	10	1	-	-	-	1200	MH	1 liq.	A - 1	10	-	2	-	-	1075	NNO	2 liq.
A - 1	10	1	-	-	-	1150	MH	2 liq.	A - 2	10	-	2	-	-	1075	NNO	2 liq.
A - 3	10	1	-	-	-	1150	MH	2 liq.	A - 3	10	-	2	-	-	1075	NNO	1 liq.
A - 5	10	1	-	-	-	1150	MH	2 liq.	A - 3	10	2	-	-	-	1200	QFM	2 liq. + mt
A - 7	10	1	-	-	-	1150	MH	1 liq. + mt	A - 1	10	-	-	6	-	1200	MH	2 liq.
A - 1	10	1	-	-	-	1075	MH	2 liq. + mt	A - 2	10	-	-	6	-	1200	MH	2 liq.
A - 3	10	1	-	-	-	1075	MH	2 liq. + mt	A - 3	10	-	-	6	-	1200	MH	2 liq.
A - 4	10	1	-	-	-	1075	MH	2 liq. + mt	A - 4	10	-	-	6	-	1200	MH	2 liq.
A - 7	10	1	-	-	-	1075	MH	1 liq. + mt	A - 5	10	-	-	6	-	1200	MH	2 liq.
A - 1	10	1	-	-	-	1200	NNO	2 liq.	A - 6	10	-	-	6	-	1200	MH	1 liq.
A - 2	10	1	-	-	-	1200	NNO	2 liq.	A - 1	10	-	-	6	-	1150	MH	1 liq. + sil
A - 3	10	1	-	-	-	1200	NNO	2 liq.	A - 2	10	-	-	6	-	1150	MH	1 liq. + sil
A - 4	10	1	-	-	-	1200	NNO	2 liq.	A - 3	10	-	-	6	-	1150	MH	2 liq.
A - 5	10	1	-	-	-	1200	NNO	2 liq.	A - 4	10	-	-	6	-	1150	MH	2 liq.
A - 6	10	1	-	-	-	1200	NNO	1 liq.	A - 5	10	-	-	6	-	1150	MH	2 liq.
A - 1	10	1	-	-	-	1150	NNO	2 liq.	A - 7	10	-	-	6	-	1150	MH	1 liq. + mt
A - 2	10	1	-	-	-	1150	NNO	2 liq.	A - 1	10	-	-	6	-	1075	MH	1 liq. + sil
A - 3	10	1	-	-	-	1150	NNO	2 liq.	A - 3	10	-	-	6	-	1075	MH	2 liq. + mt
A - 4	10	1	-	-	-	1150	NNO	2 liq.	A - 5	10	-	-	6	-	1075	MH	1 liq. + mt
A - 5	10	1	-	-	-	1150	NNO	1 liq.	A - 7	10	-	-	6	-	1075	MH	1 liq. + mt

Table 2-2: cont.

base	additional components (wt% base)					t (°C)	buffer	phase - assemblage	base	additional components (wt% base)					t (°C)	buffer	phase - assemblage
	H ₂ O	P	S	F	Cl					H ₂ O	P	S	F	Cl			
A - 2	10	-	-	6	-	1200	NNO	1 liq.	A - 5	10	-	-	-	6	1150	MH	1 liq. + mt + sil
A - 3	10	-	-	6	-	1200	NNO	1 liq.	A - 6	10	-	-	-	6	1150	MH	1 liq. + mt + sil
A - 4	10	-	-	6	-	1200	NNO	1 liq.	A - 7	10	-	-	-	6	1150	MH	1 liq. + mt + sil
A - 1	10	-	-	6	-	1150	NNO	2 liq.	An ₅₀	10	-	-	-	-	1200	NNO	2 liq.
A - 2	10	-	-	6	-	1150	NNO	1 liq.	An ₅₀	10	1	-	-	-	1200	NNO	2 liq.
A - 1	10	-	-	6	-	1200	QFM	2 liq.	An ₅₀	10	-	2	-	-	1200	NNO	2 liq.
A - 1	10	-	-	-	6	1200	MH	1 liq. + sil	An ₅₀	10	-	-	6	-	1200	NNO	2 liq.
A - 2	10	-	-	-	6	1200	MH	1 liq. + sil	A - 1	-	-	-	-	-	1200	MH	1 liq. + mt
A - 3	10	-	-	-	6	1200	MH	2 liq.	A - 1	-	-	2	-	-	1200	MH	2 liq + mt
A - 4	10	-	-	-	6	1200	MH	1 liq. + sil	A - 1	-	-	-	-	6	1200	MH	2 liq.
A - 5	10	-	-	-	6	1200	MH	1 liq. + mt + sil	A - 1	-	1	-	-	-	1200	NNO	2 liq.
A - 6	10	-	-	-	6	1200	MH	1 liq. + mt + sil	A - 1	-	-	-	6	-	1200	NNO	2 liq. + mt
A - 7	10	-	-	-	6	1200	MH	1 liq. + mt + sil	A - 1	-	-	-	-	-	1200	QFM	1 liq. + mt
A - 1	10	-	-	-	6	1150	MH	1 liq. + sil	A - 1	-	1	-	-	-	1200	QFM	2 liq.
A - 2	10	-	-	-	6	1150	MH	1 liq. + sil	A - 1	-	-	-	6	-	1200	QFM	2 liq.
A - 3	10	-	-	-	6	1150	MH	1 liq. + sil	A - 1	-	-	-	-	6	1200	QFM	2 liq. + sil

Macroscopic scale liquid-phase aggregation and gravitational segregation have been reported in anhydrous immiscible silicate melts (Kyser et al., 1998). In the present study, the spatial orientation of experimental capsules was recorded prior to the heating of selected charges and the gravitational settling (density segregation) of Fe-rich immiscible liquids was evident in the run products produced in each of the H₂O-bearing experimental systems.

2.4.2 Addition of H₂O

Water-induced liquidus suppression in both natural and synthetic silicate melts is well documented (Medard and Grove, 2008; Gaetani et al., 1994). In the hydrous experimental systems considered here, the H₂O-induced thermal suppression of the liquidus surfaces exposes low-temperature, compositionally-extensive, two- liquid miscibility gaps, some of which lie

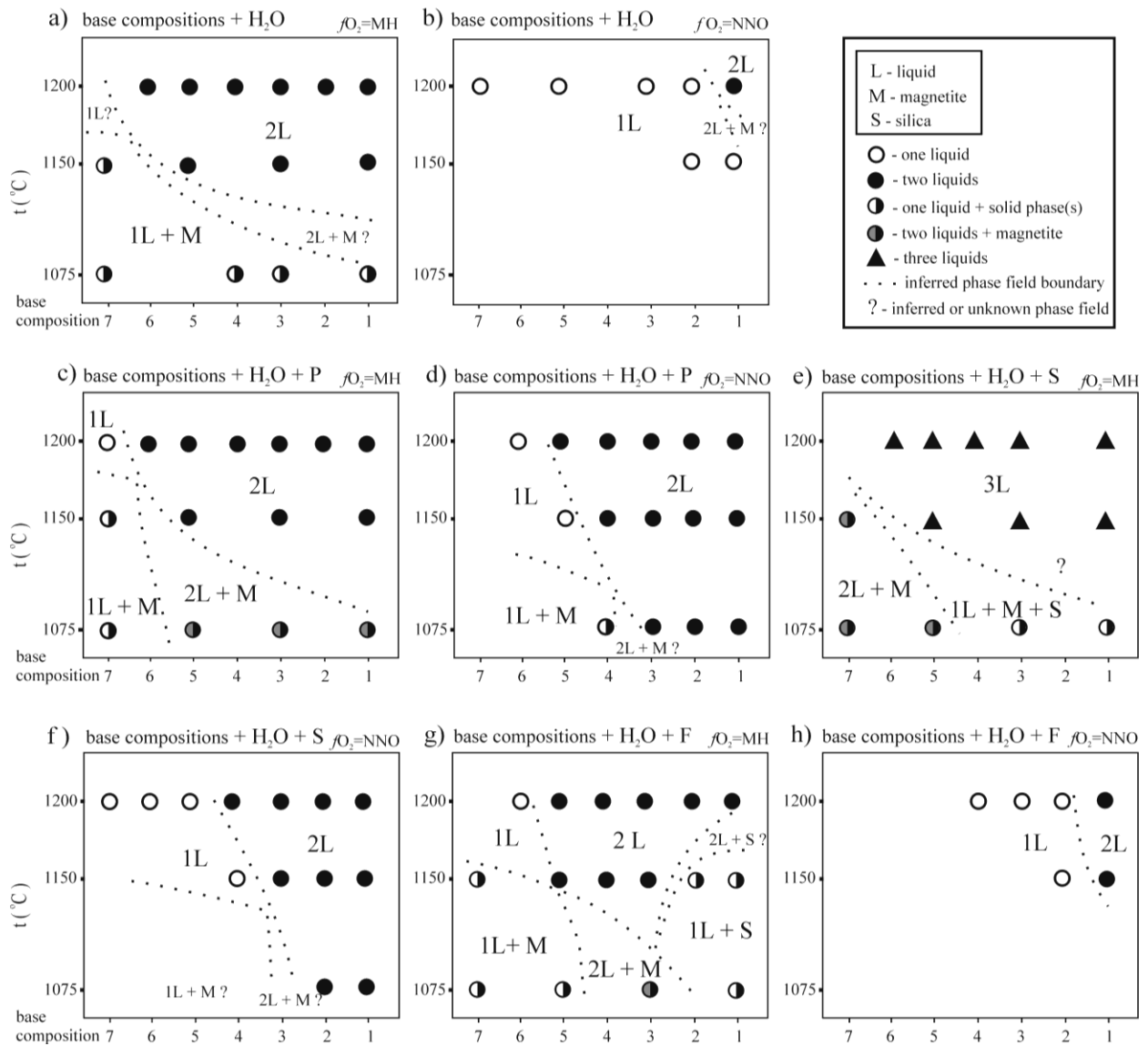


Figure 2-2: Phase relations in experimental melts, a-h. Composition: base mixtures A-1 - A-7, in the systems $\text{Fe}_3\text{O}_4\text{-KAlSi}_2\text{O}_6\text{-SiO}_2$ and $\text{Fe}_3\text{O}_4\text{-Fe}_2\text{O}_3\text{-KAlSi}_2\text{O}_6\text{-SiO}_2$ plus 10 wt% H₂O and either 1 wt% phosphorus, 2 wt% sulfur, or 6 wt% fluorine. Conditions of experiments: $T = 1075, 1150$ or 1200 °C, $P = 200$ MPa, duration- two hours, f_{O_2} - NNO or MH buffers. Dashed lines represent the inferred region of phase-field boundaries.

partially or entirely below the liquidus surfaces in anhydrous systems of similar compositions (Figure 2-2). In the system $\text{Fe}_3\text{O}_4\text{-Fe}_2\text{O}_3\text{-KAlSi}_2\text{O}_6\text{-SiO}_2\text{-H}_2\text{O}$ at $f\text{O}_2=\text{MH}$, the composition range of the miscibility gap is increased relative to that in equivalent anhydrous melts (Figure 2-3). The minimum temperature observed for the two-liquid field in the experimental melts with added H_2O is $1150\text{ }^\circ\text{C}$, whereas in anhydrous melts that are otherwise equivalent in composition it is $1375\text{ }^\circ\text{C}$ (Naslund, 1983). At $f\text{O}_2=\text{NNO}$, the addition of H_2O to the system $\text{Fe}_3\text{O}_4\text{-KAlSi}_2\text{O}_6\text{-SiO}_2$ displaces the range of the miscibility gap to higher SiO_2 compositions, and presumably extends the two-liquid field outside of the experimental composition range. A single experiment performed at $f\text{O}_2=\text{QFM}$, with base composition A-1+ H_2O (10 wt%), $P=200\text{ MPa}$, $T=1200\text{ }^\circ\text{C}$, produced two conjugate liquids. The A-1 base mixture used in the experiment is more SiO_2 -rich (~ 5 wt%) than the most SiO_2 -rich parental melt in equivalent anhydrous melts, suggesting that the miscibility gap either expands or shifts toward more SiO_2 -rich compositions in hydrous melts at $f\text{O}_2=\text{QFM}$.

2.4.3 Addition of H_2O and phosphorus

The miscibility gap in the system $\text{Fe}_3\text{O}_4\text{-Fe}_2\text{O}_3\text{-KAlSi}_2\text{O}_6\text{-SiO}_2\text{-H}_2\text{O-P}$, $f\text{O}_2=\text{MH}$ (Figure 2-2c) shows the same range of composition as that in the melts with H_2O alone, but the extent of the two-liquid-plus-magnetite field is significantly increased in the P-bearing system. In the system $\text{Fe}_3\text{O}_4\text{-KAlSi}_2\text{O}_6\text{-SiO}_2\text{-H}_2\text{O-P}$ at $f\text{O}_2=\text{NNO}$ (Figure 2-2d), the two-liquid field is shifted toward higher SiO_2 compositions, but to a lesser degree than in melts with H_2O only. The temperatures of the magnetite saturation in the system at $f\text{O}_2=\text{NNO}$ are predictably lower than at $f\text{O}_2=\text{MH}$ and consequently the two-liquid field is extended to lower temperatures at more reducing conditions.

2.4.4 Addition of H₂O and sulfur

Immiscibility between silicate and sulfide melts is well documented, e.g., Naldrett (2005), but no experimental investigations of the effect of sulfur on L^m-L^f liquid-phase separation in silicate melts have been documented. Laroque et al. (2000) reported the conversion of Fe-sulfide melts to Fe-oxide melts in basaltic, intermediate and granitic systems, providing chemical and textural evidence that immiscible FeO-rich liquids are widely produced from sulfide liquids as a consequence of sulfur loss during magma devolatilization. The addition of H₂O + 2 wt% S to the system Fe₃O₄-Fe₂O₃-KAlSi₂O₆-SiO₂-H₂O at $fO_2=MH$ stabilizes a three-liquid field (Figure 2-2e), an Fe-rich mafic silicate liquid, an Fe-poor felsic silicate liquid and an Fe-sulfide liquid (FeS_{.63} to FeS_{.74}). The three-liquid field extends from base-compositions A-1 to A-6, delimited in the low-silica portion of the experimental field by a region in which two liquids + magnetite are stable (Figure 2-2e). The three liquids are preserved in experimental glasses as spheroidal droplets, each distributed within the other two, or as crystalline Fe-sulfide that nucleated and grew rapidly in the sulfide liquid upon quench. The sulfide solid phase shows dendritic growth habit, and is best developed on the boundary surface between magnetite crystals in the quenched mafic conjugate-liquids (Figure 2-1c).

Experiments in the system Fe₃O₄-KAlSi₂O₆-SiO₂-H₂O-S at $fO_2=NNO$ did not reach sulfide liquid saturation, but a compositionally-extensive two-liquid field, stable to below 1075 °C, is observed in the intermediate- to- high silica portion of the experimental composition range (Figure 2-2f).

At $fO_2=NNO$, the mafic liquids in the two-liquid portion of the system accommodate over 10 wt% sulfur. At $fO_2 = MH$, sulfur is strongly partitioned into the Fe-S-O melt, which accommodates up to 23 wt% S and 60 to 65 wt% FeO_{total}. The phase relations in the high-silica

portion of the system $\text{Fe}_3\text{O}_4\text{-Fe}_2\text{O}_3\text{-KAlSi}_2\text{O}_6\text{-SiO}_2\text{-H}_2\text{O-S}$ at $f\text{O}_2 = \text{MH}$, i.e., between the three-liquid field and the assemblage one liquid + magnetite + silica (temperature range: 1075-1150 °C) are undetermined. The exsolution of a sulfide liquid in the S-bearing melts is notable, in part, because in typical silicate magmas under oxygen fugacities above NNO, all sulfur should occur as sulfate (Wallace and Carmichael, 1994). The assumption of equilibrium $f\text{O}_2$ conditions is supported by the partitioning trends of S in the two-melt phase assemblages, as well as by composition data from reversal experiments. The simplest explanation for the presence of sulfide is that the speciation of sulfur is controlled by the amount of Fe^{2+} in the melts which, in turn, is probably elevated because of the lack of mono- and di-valent cations required to charge-balance any network-forming Fe^{3+} in the melts.

2.4.5 The addition of H₂O and fluorine

The addition of fluorine to the system $\text{Fe}_3\text{O}_4\text{-Fe}_2\text{O}_3\text{-KAlSi}_2\text{O}_6\text{-SiO}_2\text{-H}_2\text{O}$ at $f\text{O}_2 = \text{MH}$ increases both the composition range and the silica-mineral saturation surface temperatures in the experimental melts (Figure 2-2g). The expansion of the silica-mineral stability region limits the extent of the two-liquid field and shifts the composition range of the miscibility gap to more intermediate silica compositions. The two-liquid field in the system $\text{Fe}_2\text{O}_3\text{-KAlSi}_2\text{O}_6\text{-SiO}_2\text{-H}_2\text{O-F}$ at $f\text{O}_2 = \text{NNO}$ is limited to high-silica compositions (~66 wt% SiO_2).

2.4.6 The addition of H₂O and chlorine

No two-liquid field was observed in this study in the system $\text{Fe}_3\text{O}_4\text{-KAlSi}_2\text{O}_6\text{-SiO}_2\text{-H}_2\text{O-Cl}$, $f\text{O}_2 = \text{NNO}$. The addition of $\text{H}_2\text{O} + \text{Cl}$ to the $\text{Mt-Hm-Lc-Qtz-H}_2\text{O}$, $f\text{O}_2 = \text{MH}$ system increases the temperatures of the silica mineral saturation surface to the extent that two liquids were

observed in only one of the experimental melts, i.e., base-composition A-1 + H₂O + Cl at 1200 °C (table 2-2). Melts produced from starting mixtures of mafic- to- intermediate composition (with respect to silica content) become significantly enriched in iron (40-64 wt% FeO_{total}) and H₂O with decreasing temperature and the progressive crystallization of silica minerals.

2.4.7 The addition of H₂O plus P, S, F, or Cl to the system Fe₃O₄-KAlSi₂O₆-SiO₂-Ca_{0.5}Na_{0.5}Al_{1.5}Si_{2.5}O₈

Experiments were performed in the system Fe₃O₄-KAlSi₂O₆-SiO₂-Ca_{0.5}Na_{0.5}Al_{1.5}Si_{2.5}O₈ (An₅₀) with 10 wt% H₂O, 1 wt % P, 2 wt% S and 6 wt% F or Cl at 1200 °C, *f*O₂=NNO, P=200 MPa. Stable two-liquid assemblages were observed in the melts with H₂O alone, and with H₂O and P, S or F (table 2-2). No liquid phase separation was observed in the melts with H₂O plus Cl.

2.4.8 Additional experiments

Additional experiments were performed using base compositions A-1 or A-3 with or without H₂O, at 1200°C, P=200 MPa and *f*O₂ = QFM, NNO or MH (table 2-2). Two- liquid assemblages were observed in melts with compositions; A-1 + H₂O (QFM), A-1 + H₂O + F (QFM), A-1 + P (QFM), A-1 + F (QFM) and A-1 + Cl (MH). Two-liquid- plus- solid phase assemblage were produced in melts A-3 + H₂O + P (QFM), A-1+ Cl (QFM), A-1 + F (NNO) and A-1 + S (MH). Compositional data for the products of these experiments are listed in Table 2-3.

Table 2-3. Electron microprobe analyses of experimental glasses and element partition coefficients D.
D= (wt% element in Fe-rich liquid)/(wt% element in Si-rich liquid).

starting composition	t (°C)	fO ₂ buffer	conjugate liquid	n	SiO ₂	FeO	Al ₂ O ₃	K ₂ O	P	S	F	Cl	Total
<i>system: SiO₂ - FeO - Al₂O₃ - K₂O +/- H₂O</i>													
A - 1 + H ₂ O	1200	MH	Fe-liq.	5	36.54	55.98	2.91	1.18	-	-	-	-	96.64
			std. dev.		0.21	0.35	0.32	0.10					0.32
			sil-liq.	4	71.19	16.00	5.62	4.67	-	-	-	-	97.49
			std. dev.		0.51	3.50	0.52	0.25					0.39
			D _{Fe-liq/Si-liq}		0.51	3.50	0.52	0.25					
A - 3 + H ₂ O	1200	MH	Fe-liq.	3	38.01	55.20	3.41	1.49	-	-	-	-	98.15
			std. dev.		0.32	0.01	0.03	0.05					0.31
			sil-liq.	5	76.81	9.83	6.17	5.40	-	-	-	-	98.22
			std. dev.		0.68	0.29	0.25	0.25					0.43
			D _{Fe-liq/Si-liq}		0.49	5.62	0.55	0.28					
A - 4 + H ₂ O	1200	MH	Fe-liq.	5	45.91	44.79	4.25	2.77	-	-	-	-	97.80
			std. dev.		0.19	0.42	0.10	0.00					0.44
			sil-liq.	5	65.40	20.79	6.21	5.53	-	-	-	-	97.94
			std. dev.		0.33	0.26	0.04	0.08					0.55
			D _{Fe-liq/Si-liq}		0.70	2.15	0.68	0.50					
A - 5 + H ₂ O	1200	MH	Fe-liq.	4	36.75	55.14	3.51	1.97	-	-	-	-	97.39
			std. dev.		0.46	0.58	0.03	0.23					0.25
			sil-liq.	5	61.70	21.27	8.06	6.81	-	-	-	-	97.89
			std. dev.		1.22	1.40	0.17	0.22					0.14
			D _{Fe-liq/Si-liq}		0.60	2.59	0.44	0.29					
A - 6 + H ₂ O	1200	MH	Fe-liq.	3	39.31	53.51	1.87	0.99	-	-	-	-	96.48
			std. dev.		0.59	1.36	0.20	0.24					0.50
			sil-liq.	4	74.34	14.93	3.95	3.16	-	-	-	-	96.51
			std. dev.		0.74	0.28	0.04	0.98					0.64
			D _{Fe-liq/Si-liq}		0.53	3.58	0.47	0.31					
A-1 + H ₂ O	1150	MH	Fe-liq.	3	43.11	49.09	2.46	1.79	-	-	-	-	96.48
			std. dev.		1.17	1.69	0.12	0.09					0.50
			sil-liq.	4	76.82	8.01	5.96	5.68	-	-	-	-	96.51
			std. dev.		1.01	1.04	0.32	0.41					0.64
			D _{Fe-liq/Si-liq}		0.56	6.13	0.41	0.31					
A - 5 + H ₂ O	1150	MH	Fe-liq.	2	51.72	34.47	6.25	4.35	-	-	-	-	96.80
			std. dev.		1.36	1.20	0.19	0.45					0.86
			sil-liq.	5	69.16	13.57	8.33	6.81	-	-	-	-	97.87
			std. dev.		0.53	0.22	0.09	0.80					0.49
			D _{Fe-liq/Si-liq}		0.75	2.54	0.75	0.64					
A-1	1200	MH	Fe-liq.	1	35.41	58.30	2.27	1.01	-	-	-	-	97.00
			std. dev.										
			sil-liq.	3	72.43	23.22	3.17	1.92	-	-	-	-	100.75
			std. dev.		1.49	2.05	0.09	0.04					0.52
			D _{Fe-liq/Si-liq}		0.49	2.51	0.72	0.53					

Table 2-3. continued

starting composition	t (°C)	fO ₂ buffer	conjugate liquid	n	SiO ₂	FeO	Al ₂ O ₃	K ₂ O	P	S	F	Cl	Total
<i>system: SiO₂ - FeO - Al₂O₃ - K₂O +/- H₂O continued</i>													
A - 1 + H ₂ O	1200	NNO	Fe-liq.	5	40.2	55.7	1.91	0.76	-	-	-	-	98.52
			std. dev.		0.83	1.17	0.18	0.14					0.53
			sil-liq.	5	79.42	11.59	2.71	2.03	-	-	-	-	95.75
			std. dev.		0.43	0.12	0.05	0.12					0.43
			D _{Fe-liq/Si-liq}		0.51	4.8	0.71	0.38					
<i>system: SiO₂ - FeO - Al₂O₃ - K₂O - P +/- H₂O</i>													
A-1 + H ₂ O + P	1200	MH	Fe-liq.	5	29.63	67.95	1.35	0.68	5.75	-	-	-	92.97
			std. dev.		0.10	2.09	0.07	0.04	0.12				0.07
			sil-liq.	5	75.41	7.12	2.55	2.18	0.47	-	-	-	95.40
			std. dev.		1.53	0.10	0.02	0.44	0.10				0.64
			D _{Fe-liq/Si-liq}		0.39	9.55	0.53	0.31	12.12				
A-3 + H ₂ O + P	1200	M-H	Fe-liq.	2	33.11	57.34	2.20	1.18	4.47	-	-	-	98.29
			std. dev.		0.46	1.07	1.51	0.10	0.05				0.17
			sil-liq.	3	80.62	2.55	3.89	2.22	0.26	-	-	-	99.54
			std. dev.		1.58	0.27	0.91	0.78	0.08				0.94
			D _{Fe-liq/Si-liq}		0.37	22.49	0.57	0.53	17.08				
A- 6 + H ₂ O + P	1200	MH	Fe-liq.	5	20.43	59.46	2.28	0.68	2.56	-	-	-	97.80
			std. dev.		0.15	0.49	0.04	0.05	2.09				0.71
			sil-liq.	5	82.94	10.37	6.94	5.68	0.62	-	-	-	98.88
			std. dev.		0.37	1.01	0.29	0.72	0.03				0.43
			D _{Fe-liq/Si-liq}		0.25	5.73	0.33	0.12	4.12				
A- 2 + H ₂ O + P	1150	MH	Fe-liq.	5	29.96	58.68	2.43	0.50	6.17	-	-	-	97.73
			std. dev.		0.25	0.55	0.14	0.05	0.17				0.17
			sil-liq.	5	80.46	5.99	7.15	5.00	0.53	-	-	-	99.13
			std. dev.		1.74	0.11	0.64	1.00	0.09				1.00
			D _{Fe-liq/Si-liq}		0.37	9.79	0.34	0.10	11.68				
A - 5 + P + H ₂ O	1150	MH	Fe-liq.	3	36.85	49.47	2.79	2.20	7.18	-	-	-	98.49
			std. dev.		2.84	3.01	0.49	0.52	0.53				0.50
			sil-liq.	3	76.23	6.64	7.88	7.07	0.43	-	-	-	98.25
			std. dev.		0.84	0.71	0.44	1.15	0.04				0.58
			D _{Fe-liq/Si-liq}		0.48	7.45	0.35	0.31	16.69				
A-1 + H ₂ O + P	1200	MH	Fe-liq.	4	32.78	59.61	1.49	0.35	3.97	-	-	-	98.20
			std. dev.		1.55	2.39	0.37	0.08	0.37				0.84
			sil-liq.	4	83.94	8.19	2.95	2.47	0.29	-	-	-	97.70
			std. dev.		0.86	0.61	0.14	0.63	0.21				1.01
			D _{Fe-liq/Si-liq}		0.39	7.28	0.50	0.14	13.7				
A-1 + H ₂ O + P	1200	QFM	Fe-liq.	3	33.00	59.00	1.44	0.95	3.89	-	-	-	98.29
			std. dev.		0.57	0.93	0.17	0.15	0.14				0.25
			sil-liq.	5	77.54	11.32	4.40	4.49	0.31	-	-	-	98.06
			std. dev.		0.41	0.61	0.17	0.45	0.05				0.86
			D _{Fe-liq/Si-liq}		0.43	5.21	0.33	0.21	12.59				

Table 2-3 continued

starting composition	t (°C)	fO ₂ buffer	conjugate liquid	n	SiO ₂	FeO	Al ₂ O ₃	K ₂ O	P	S	F	Cl	Total
<i>system: SiO₂ - FeO - Al₂O₃ - K₂O - P +/- H₂O continued</i>													
A-1 + P	1200	QFM	Fe-liq.	4	31.62	60.52	1.32	0.70	4.27	-	-	-	98.43
			std. dev.		0.40	0.76	0.10	0.04	0.09				0.79
			sil-liq.	5	77.41	11.26	4.84	4.71	0.33	-	-	-	98.55
			std. dev.		2.16	1.25	0.48	0.86	0.02				0.47
			D _{Fe-liq/Si-liq}		0.41	5.38	0.27	0.15	####				
A-1 + H ₂ O + P	1200	NNO	Fe-liq.	4	35	56.9	1.9	0.44	4.91	-	-	-	99.05
			std. dev.		1.09	0.42	0.08	0.1	2				0.76
			sil-liq.	5	76.17	12.48	2.41	1.58	0.54	-	-	-	93.17
			std. dev.		0.45	0.34	0.04	0.05	0.08				0.39
			D _{Fe-liq/Si-liq}		0.46	4.56	0.79	0.28	8.96				
A-2 + H ₂ O + P	1200	NNO	Fe-liq.	5	30.9	58.9	3.27	0.26	5.71	-	-	-	99.03
			std. dev.		0.36	0.46	0.07	0.04	0.36				0.24
			sil-liq.	5	76.80	9.81	6.62	4.90	0.34	-	-	-	98.46
			std. dev.		0.64	0.42	0.14	0.07	0.05				1.16
			D _{Fe-liq/Si-liq}		0.4	6.01	0.49	0.05	16.9				
A-3 + H ₂ O + P	1200	NNO	Fe-liq.	4	26.5	60.9	1.57	0.54	7.97	-	-	-	97.51
			std. dev.		0.69	0.67	0.13	0.13	0.48				0.96
			sil-liq.	4	74.94	11.49	4.26	3.44	0.51	-	-	-	94.64
			std. dev.		0.27	0.18	0.12	0.05	0.03				0.32
			D _{Fe-liq/Si-liq}		0.35	5.3	0.37	0.16	15.6				
A-4 + H ₂ O + P	1200	NNO	Fe-liq.	5	28.2	59.5	2.72	1.35	7.47	-	-	-	99.21
			std. dev.		0.59	1.09	0.21	0.29	1.3				0.42
			sil-liq.	5	74.79	9.95	6.34	5.37	0.62	-	-	-	97.08
			std. dev.		1.36	0.95	0.58	0.23	0.15				0.37
			D _{Fe-liq/Si-liq}		0.38	5.98	0.43	0.25	12.1				
A-5 + H ₂ O + P	1200	NNO	Fe-liq.	3	32.9	55.5	4.03	2.71	1	-	-	-	96.13
			std. dev.		1.97	2	0.25	0.21	0.38				0.09
			sil-liq.	3	65.02	18.78	7.61	5.42	2.17	-	-	-	98.99
			std. dev.		0.55	0.53	0.06	0.07	0.06				0.04
			D _{Fe-liq/Si-liq}		0.51	2.96	0.53	0.5	0.46				
A-1 + H ₂ O + P	1150	NNO	Fe-liq.	2	29.8	54.3	3.66	2.04	11.8	-	-	-	101.6
			std. dev.		1.54	3.91	0.29	0.23	4.96				2.07
			sil-liq.	5	66.05	17.86	7.61	5.57	2.04	-	-	-	99.12
			std. dev.		0.58	0.27	0.07	0.05	0.08				0.78
			D _{Fe-liq/Si-liq}		0.45	3.04	0.48	0.37	5.79				
A-2 + H ₂ O + P	1150	NNO	Fe-liq.	3	31.48	58.9	4.48	0.19	5.94	-	-	-	97.31
			std. dev.		0.75	0.28	0.05	0.05	0.36				0.47
			sil-liq.	3	79.40	10.16	6.16	3.89	0.4	-	-	-	100
			std. dev.		0.34	0.39	0.03	0.80	0.02				0.37
			D _{Fe-liq/Si-liq}		0.40	5.44	0.73	0.05	14.8				

Table 2-3 continued

starting composition	t (°C)	fO ₂ buffer	conjugate liquid	n	SiO ₂	FeO	Al ₂ O ₃	K ₂ O	P	S	F	Cl	Total
<i>system: SiO₂ - FeO - Al₂O₃ - K₂O - P +/- H₂O continued</i>													
A-3 + H ₂ O + P	1150	NNO	Fe-liq.	2	44.4	40.8	2.78	1.83	7.73	-	-	-	97.45
			std. dev.		1.37	0.91	0.07	0.08	2.67				2.06
			sil-liq.	2	66.47	20.15	4.21	2.72	2.06	-	-	-	95.61
			std. dev.		0.75	1.15	0.01	0.11	0.03				0.32
			D _{Fe-liq/Si-liq}		0.67	2.02	0.66	0.67	3.76				
A-4 + H ₂ O + P	1150	NNO	Fe-liq.	2	11.7	66.2	2.19	1	0.19	-	-	-	81.29
			std. dev.		2.01	6.67	0	0.15	0.06				8.46
			sil-liq.	3	63.07	19.75	5.46	3.05	2.41	-	-	-	93.74
			std. dev.		0.02	0.18	0.01	0.03	0.10				0.08
			D _{Fe-liq/Si-liq}		0.19	3.35	0.4	0.33	0.08				
A-1 + H ₂ O + P	1075	NNO	Fe-liq.	2	32	56.1	5.13	0.43	5.3	-	-	-	98.92
			std. dev.		0.32	0.64	0.08	0.1	0.05				0.25
			sil-liq.	5	73.60	9.73	8.02	5.29	0.33	-	-	-	96.97
			std. dev.		0.63	0.61	0.10	0.08	0.11				0.94
			D _{Fe-liq/Si-liq}		0.43	5.76	0.64	0.08	15.8				
A-2 + H ₂ O + P	1075	NNO	Fe-liq.	4	31.7	58.4	2.23	0.97	5.47	-	-	-	98.72
			std. dev.		0.86	2.05	0.38	0.18	0.44				1.1
			sil-liq.	5	76.17	8.31	5.67	4.21	0.17	-	-	-	94.53
			std. dev.		0.87	0.11	0.07	0.09	0.03				0.80
			D _{Fe-liq/Si-liq}		0.42	7.02	0.39	0.23	33.1				
A-3 + H ₂ O + P	1075	NNO	Fe-liq.	4	26.4	60.2	1.48	0.72	10.8	-	-	-	99.56
			std. dev.		2.01	1.39	0.21	0.22	2.74				0.96
			sil-liq.	5	77.91	9.35	6.40	5.56	0.30	-	-	-	99.52
			std. dev.		0.62	0.62	0.07	0.06	0.09				0.35
			D _{Fe-liq/Si-liq}		0.34	6.44	0.23	0.13	35.9				
A-1 + P	1200	NNO	Fe-liq.		30.6	57.9	3.01	1.04	6.25	-	-	-	98.85
			std. dev.		1.08	3.7	1.29	0.28	1.04				1.44
			sil-liq.		77.77	9.62	5.86	5.23	0.26	-	-	-	98.74
			std. dev.		0.39	6.02	0.51	0.20	0.21				1.00
			D _{Fe-liq/Si-liq}		0.39	6.02	0.51	0.2	23.9				
<i>system: SiO₂ - FeO - Al₂O₃ - K₂O - S +/- H₂O</i>													
A-1 + H ₂ O + S	1200	MH	Fe-liq.	5	35.98	58.07	2.61	0.57	-	1.96	-	-	99.20
			std. dev.		1.58	1.21	1.22	0.05		1.28			0.55
			sil-liq.	5	86.69	7.14	2.71	2.04	-	0.06	-	-	98.64
			std. dev.		5.75	2.56	1.57	0.95		0.05			1.27
			D _{Fe-liq/Si-liq}		0.42	8.14	0.96	0.28	-	33.09			1.01
			sulfide	3	0.62	61.49	0.04	0.01	-	25.89			88.05
			std. dev.		0.03	0.50	0.02	0.01		0.50			0.93
A-3 + H ₂ O + S	1200	MH	Fe-liq.	5	30.66	62.74	2.34	0.12	-	6.29	-	-	99.16
			std. dev.		1.02	0.42	0.29	0.01		0.81			0.42
			sil-liq.	2	87.92	3.45	4.19	3.40	-	0.05	-	-	99.00
			std. dev.		3.86	1.65	1.55	1.14		0.03			0.50
			D _{Fe-liq/Si-liq}		0.35	18.20	0.56	0.04		135.8			1.03

Table 2-3 continued

starting composition	t (°C)	fO ₂ buffer	conjugate liquid	n	SiO ₂	FeO	Al ₂ O ₃	K ₂ O	P	S	F	Cl	Total
<i>system: SiO₂ - FeO - Al₂O₃ - K₂O - S +/- H₂O continued</i>													
A-5 + H ₂ O + S	1200	MH	Fe-liq.	5	24.24	66.73	2.05	0.16	-	10.29	-	-	99.47
			std. dev.		0.41	0.99	0.04	0.02		0.10			1.41
			sil-liq.	5	75.18	8.23	8.89	6.28	-	0.11	-	-	98.69
			std. dev.		0.20	0.22	0.04	0.35		0.01			0.24
			D _{Fe-liq/Si-liq}		0.32	8.10	0.23	0.02		94.72			1.05
A-6 + H ₂ O + S	1200	MH	sulfide	4	1.77	60.76	0.06	0.07	-	22.68	-	-	85.34
			std. dev.		0.10	0.15	0.01	0.01		1.00			0.85
			Fe-liq.	5	24.45	66.97	1.59	0.12	-	10.75	-	-	103.88
			std. dev.		0.30	0.58	0.05	0.02		0.13			0.60
			sil-liq.	4	73.16	8.22	9.73	7.32	-	0.35	-	-	98.79
A-1 + H ₂ O + S	1150	MH	std. dev.		1.07	0.81	0.20	0.15		0.35			0.42
			D _{Fe-liq/Si-liq}		0.33	8.14	0.16	0.02		30.95			1.05
			sulfide	5	1.59	62.68	0.23	0.03	-	19.60	-	-	84.13
			std. dev.		0.03	1.51	0.37	0.01		0.67			1.79
			Fe-liq.	5	40.78	51.63	3.84	1.30	-	1.69	-	-	99.24
A-3 + H ₂ O + S	1150	MH	std. dev.		0.89	2.87	0.05	0.09		0.13			1.80
			sil-liq.	2	79.75	3.69	6.90	5.75	-	0.04	-	-	94.87
			std. dev.		1.97	0.40	1.13	0.46		0.03			1.92
			D _{Fe-liq/Si-liq}		0.51	14.00	0.56	0.23		45.31			
			Fe-liq.	3	28.76	63.37	3.09	0.19	-	8.33	-	-	103.74
A-5 + H ₂ O + S	1150	MH	std. dev.		0.47	0.43	0.10	0.02		0.28			0.28
			sil-liq.	5	73.77	9.04	8.98	6.84	-	0.13	-	-	98.76
			std. dev.		0.42	0.24	0.11	0.11		0.01			0.27
			D _{Fe-liq/Si-liq}		0.39	7.01	0.34	0.03		65.57			1.05
			Fe-liq.	5	32.77	60.33	2.76	1.57	-	2.46	-	-	99.89
A-1 + H ₂ O + S	1200	NNO	std. dev.		1.08	0.65	0.43	0.18		0.99			0.85
			sil-liq.	4	67.56	12.12	10.67	8.88	-	0.12	-	-	99.35
			std. dev.		1.61	1.34	0.25	0.52		0.01			0.72
			D _{Fe-liq/Si-liq}		0.49	4.98	0.26	0.18		20.82			1.01
			Fe-liq.	5	43.99	44	2.19	1	-	1.16	-	-	92.69
A-2 + H ₂ O + S	1200	NNO	std. dev.		1.21	3.34	0.17	0.09		0.29			3.09
			sil-liq.	5	77.3	15.4	2.41	1.52	-	0.21	-	-	96.84
			std. dev.		0.63	0.56	0.03	0.07		0.05			0.30
			D _{Fe-liq/Si-liq}		0.57	2.85	0.91	0.66		5.64			
			Fe-liq.	3	26.5	61.7	1.31	0.8	-	8.77	-	-	99.11
A-3 + H ₂ O + S	1200	NNO	std. dev.		0.29	0.52	0.12	0.01		0.17			0.46
			sil-liq.	5	73.42	13.09	5.68	5.49	-	0.68	-	-	98.37
			std. dev.		1.54	1.07	0.17	0.17		0.11			0.20
			D _{Fe-liq/Si-liq}		0.36	4.71	0.15	0.15		13			
			Fe-liq.	4	23.7	69.3	1.52	0.59	-	8.16	-	-	103.2
A-3 + H ₂ O + S	1200	NNO	std. dev.		1.1	1.86	0.11	0.2		1.32			1.65
			sil-liq.	4	68.76	18.46	6.21	3.52	-	0.62	-	-	97.58
			std. dev.		2.00	2.63	0.17	0.17		0.07			0.99
			D _{Fe-liq/Si-liq}		0.34	3.75	0.24	0.17		13.1			

Table 2-3 continued

starting composition	t (°C)	fO ₂ buffer	conjugate liquid	n	SiO ₂	FeO	Al ₂ O ₃	K ₂ O	P	S	F	Cl	Total
<i>system: SiO₂ - FeO - Al₂O₃ - K₂O - S +/- H₂O continued</i>													
A-4 + H ₂ O + S	1200	NNO	Fe-liq.	5	22.9	69	0.8	0.5	-	6.98	-	-	100.1
			std. dev.		1.09	2.1	0.03	0.11		1.43			1.14
			sil-liq.	5	69.44	18.40	4.32	3.12	-	0.56	-	-	95.85
			std. dev.		1.26	2.25	0.08	0.17		0.06			1.55
			D _{Fe-liq/Si-liq}		0.33	3.75	0.18	0.16		12.4			
A-1 + H ₂ O + S	1150	NNO	Fe-liq.	3	25.6	68.3	1.06	0.21	-	8.29	-	-	103.4
			std. dev.		1.2	2.43	0.12	0.09		1.25			0.44
			sil-liq.	4	83.38	7.94	2.43	1.72		0.15	-	-	95.61
			std. dev.		0.36	0.20	0.08	0.02	-	0.01			0.19
			D _{Fe-liq/Si-liq}		0.31	8.6	0.44	0.12		56.6			
A-2 + H ₂ O + S	1150	NNO	Fe-liq.	3	35.9	57.7	2.41	0.95	-	2.57	-	-	99.54
			std. dev.		1.17	1.41	0.2	0.12		0.33			1.1
			sil-liq.	5	73.34	16.94	3.83	2.01	-	0.32	-	-	96.44
			std. dev.		0.80	1.37	0.07	0.05		0.07			0.78
			D _{Fe-liq/Si-liq}		0.49	3.41	0.63	0.47		8.13			
A-3 + H ₂ O + S	1150	NNO	Fe-liq.	3	25.8	69.2	1.26	0.25	-	6.95	-	-	103.5
			std. dev.		0.93	0.16	0.09	0.08		0.63			1.13
			sil-liq.	5	76.05	11.73	4.67	3.55	-	11.73	-	-	96.37
			std. dev.		0.80	0.95	0.04	0.10		0.95			0.44
			D _{Fe-liq/Si-liq}		0.34	5.9	0.27	0.07		5.9			
A-4 + H ₂ O + S	1150	NNO	Fe-liq.		29.4	64.5	1.81	0.73	-	4.87	-	-	101.2
			std. dev.		0.28	0.35	0.03	0.05		0.3			0.25
			sil-liq.		70.19	15.48	6.39	4.60	-	0.29	-	-	96.69
			std. dev.		0.44	0.71	0.07	0.11		0.01			0.18
			D _{Fe-liq/Si-liq}		0.42	4.16	0.28	0.16		16.7			
A-1 + H ₂ O + S	1075	NNO	Fe-liq.	5	7.14	72.8	0.7	0.12	-	16.6	-	-	97.3
			std. dev.		3.32	2.85	0.59	0.08		16.3			9.48
			sil-liq.	3	82.17	7.24	3.05	1.66	-	0.28	-	-	94.40
			std. dev.		0.14	0.60	0.04	0.06		0.13			0.70
			D _{Fe-liq/Si-liq}		0.09	10.1	0.23	0.07		59.2			
A-2 + H ₂ O + S	1075	NNO	Fe-liq.		34	59.6	1.97	0.57	-	6.68	-	-	102.8
			std. dev.		2.12	2.63	0.15	0.02		0.91			0.92
			sil-liq.		79.71	9.29	4.00	1.86	-	0.27	-	-	95.14
			std. dev.		0.51	1.18	0.11	0.06		0.21			1.36
			D _{Fe-liq/Si-liq}		0.43	6.41	0.49	0.31		24.6			
<i>system: SiO₂ - FeO - Al₂O₃ - K₂O - F +/- H₂O</i>													
A-1 + H ₂ O + F	1200	MH	Fe-liq.	3	34.73	60.91	2.09	0.31	-	-	5.15	-	99.70
			std. dev.		1.44	0.21	0.25	0.04		0.26			1.50
			sil-liq.	5	62.22	12.33	5.67	4.36	-	-	4.99	-	88.95
			std. dev.		0.69	0.87	0.24	0.52		0.31			0.42
			D _{Fe-liq/Si-liq}		0.56	4.94	0.37	0.07		1.03			

Table 2-3 continued

starting composition	t (°C)	fO ₂ buffer	conjugate liquid	n	SiO ₂	FeO	Al ₂ O ₃	K ₂ O	P	S	F	Cl	Total
<i>system: SiO₂ - FeO - Al₂O₃ - K₂O - F +/- H₂O continued</i>													
A-2 + H ₂ O + F	1200	MH	Fe-liq.	4	34.10	60.83	2.19	0.32	-	-	1.61	-	99.04
			std. dev.		0.35	0.10	0.13	0.03			0.22		0.26
			sil-liq.	5	73.98	13.16	5.37	5.29	-	-	1.27	-	99.06
			std. dev.		0.76	0.52	0.04	0.21			0.08		0.44
			D _{Fe-liq/Si-liq}		0.46	4.62	0.41	0.06			1.27		
A-3 + H ₂ O + F	1200	MH	Fe-liq.	3	44.63	48.47	3.49	1.74	-	-	0.13	-	98.47
			std. dev.		0.36	0.60	0.02	0.05			0.05		0.30
			sil-liq.	3	74.41	8.48	6.53	*	-	-	0.16	-	89.59
			std. dev.		0.22	0.34	0.02	*			0.07		0.43
			D _{Fe-liq/Si-liq}		0.60	5.72	0.53	*			0.82		
A-4 + H ₂ O + F	1200	MH	Fe-liq.	5	34.86	60.18	1.61	0.83	-	-	1.50	-	98.97
			std. dev.		0.08	0.40	0.13	0.09			0.11		0.18
			sil-liq.	5	77.19	7.67	6.24	6.11	-	-	2.98	-	100.20
			std. dev.		0.49	0.34	0.04	0.03			0.07		0.41
			D _{Fe-liq/Si-liq}		0.45	7.84	0.26	0.14			0.50		
A-5 + H ₂ O + F	1200	MH	Fe-liq.	5	61.47	20.00	7.38	5.71	-	-	1.66	-	99.71
			std. dev.		1.08	1.67	0.15	0.22			0.22		0.44
			sil-liq.	5	77.66	0.44	9.69	6.77	-	-	4.37	-	99.55
			std. dev.		0.31	0.03	0.06	0.24			0.91		0.32
			D _{Fe-liq/Si-liq}		0.79	45.72	0.76	0.84			0.38		
A-3 + H ₂ O + F	1150	MH	Fe-liq.	5	32.63	59.29	2.12	0.93	-	-	5.61	-	100.59
			std. dev.		1.25	0.80	0.17	0.13			1.24		0.66
			sil-liq.	3	78.34	6.28	5.92	4.50	-	-	5.45	-	100.48
			std. dev.		0.73	0.06	0.08	0.66			0.11		0.43
			D _{Fe-liq/Si-liq}		0.42	9.44	0.36	0.21			1.03		
A-4 + H ₂ O + F	1150	MH	Fe-liq.	4	34.24	57.83	1.14	0.48	-	-	5.16	-	98.86
			std. dev.		0.25	0.10	0.01	0.13			0.34		0.07
			sil-liq.	4	82.07	6.98	3.56	1.89	-	-	4.58	-	94.55
			std. dev.		0.57	0.13	0.58	0.50			0.07		1.27
			D _{Fe-liq/Si-liq}		0.42	8.28	0.32	0.25			1.13		
A-5 + H ₂ O + F	1150	MH	Fe-liq.	4	40.21	50.76	3.64	2.22	-	-	3.05	-	99.89
			std. dev.		0.40	1.73	0.36	0.34			0.24		0.96
			sil-liq.	5	66.22	13.51	8.39	7.36	-	-	4.83	-	100.32
			std. dev.		0.30	0.19	0.09	0.04			0.09		0.44
			D _{Fe-liq/Si-liq}		0.61	3.76	0.43	0.30			0.63		
A-1 + H ₂ O + F	1200	QFM	Fe-liq.	2	37.68	46.47	1.08	0.84	-	-	1.70	-	87.78
			std. dev.		4.14	12.38	0.12	0.04			0.11		7.97
			sil-liq.	2	84.21	10.73	2.63	1.63	-	-	5.60	-	96.40
			std. dev.		0.94	0.04	0.02	0.57			0.04		0.39
			D _{Fe-liq/Si-liq}		0.45	4.33	0.41	0.52			0.30		

Table 2-3 continued.

starting composition	t (°C)	fO ₂ buffer	conjugate liquid	n	SiO ₂	FeO	Al ₂ O ₃	K ₂ O	P	S	F	Cl	Total
<i>system: SiO₂ - FeO - Al₂O₃ - K₂O - Cl +/- H₂O</i>													
A-3 + H ₂ O + Cl	1200	MH	Fe-liq.	2	68.91	19.36	4.33	3.57	-	-	2.02	0.02	98.19
			std. dev.		0.60	0.43	0.06	0.65			0.09	0.03	0.33
			sil-liq.	5	84.18	0.30	8.33	6.39	-	-	0.26	0.08	99.46
			std. dev.		0.60	0.01	1.08	0.35			0.08	0.05	0.76
			D _{Fe-liq/Si-liq}		0.82	63.94	0.52	0.56			7.66	0.30	
<i>system: SiO₂ - FeO - Al₂O₃ - K₂O - Na - Ca + H₂O +/- (P, S, or F)</i>													
An ₅₀ + H ₂ O	1200	M-H	Fe-liq.	3	41.31	49.43	2.13	1.34	0.19	0.63	-	-	95.07
			std. dev.		0.52	0.36	0.07	0.04	0.03	0.02			0.39
			sil-liq.	5	74.55	14.02	3.94	3.89	0.41	0.20	-	-	97.03
			std. dev.		0.62	0.49	0.14	0.19	0.04	0.01			0.74
			D _{Fe-liq/Si-liq}		0.55	3.53	0.54	0.35	0.45	3.15			
An ₅₀ + H ₂ O + P	1200	MH	Fe-liq.	2	20.71	72.25	1.32	0.50	0.13	0.14	1.84	-	96.94
			std. dev.		1.46	1.70	0.05	0.06	0.03	0.00	0.11		0.27
			sil-liq.	5	85.26	6.25	2.44	2.25	0.23	0.06	0.31	-	96.83
			std. dev.		0.16	0.07	0.04	0.08	0.04	0.01	0.02		0.14
			D _{Fe-liq/Si-liq}		0.24	11.57	0.54	0.22	0.59	2.26	5.90		
An ₅₀ + H ₂ O + S	1200	MH	Fe-liq.	5	81.96	7.40	3.08	1.77	0.20	0.36	-	0.10	87.13
			std. dev.		0.84	0.33	0.60	0.02	0.03	0.01		0.10	0.06
			sil-liq.	5	35.52	44.24	2.46	0.38	0.09	1.72	-	0.27	86.52
			std. dev.		3.12	2.63	0.53	0.06	0.03	0.13		0.01	0.10
			D _{Fe-liq/Si-liq}		0.43	5.98	0.80	0.21	0.46	4.75	2.72		
An ₅₀ + H ₂ O + F	1200	MH	Fe-liq.	5	37.86	49.75	2.06	0.70	0.17	1.52	-	2.51	94.58
			std. dev.		2.53	1.34	0.40	0.21	0.07	0.91		1.48	1.53
			sil-liq.	5	83.68	7.43	2.99	2.51	0.34	0.18		1.29	98.43
			std. dev.		0.24	0.12	0.08	0.01	0.03	0.01		0.11	0.14
			D _{Fe-liq/Si-liq}		0.45	6.69	0.69	0.28	0.51	8.71	1.94		

2.5 Discussion

2.5.1 Effects of H₂O, P, S, F and Cl on the *T-X* range of two-liquid fields

The temperature and compositional ranges of two-liquid fields in silicate melt systems are dependent on the position and configuration of the miscibility gap relative to the saturation surfaces of liquidus minerals. The phase relations illustrated in Figure 2-2 reflect the combined and, in some instances, competing effects of H₂O and P, S or F on the liquidus surface configuration in each of the experimental systems. Water clearly has the most pronounced effects on the phase relations in the experimental melts. Thus, the addition of H₂O dramatically suppresses liquidus surface temperatures, expands the stability field of magnetite and decreases that of silica minerals, thereby increasing the *T-X* range of the miscibility gap (Figure 2-3). In anhydrous melts in the systems Fe₂SiO₄-KAlSi₂O₆-SiO₂, and Fe₂SiO₄-KAlSi₃O₈-SiO₂, +/- CaO, TiO₂ and MgO, the addition of phosphorus expands the two-melt field, decreasing the extent of the fayalite field and increasing that of silica-minerals (Bogaerts and Schmidt, 2006). It is likely that P and S (at concentrations below sulfide saturation) have a similar effect in the H₂O-rich melts, but H₂O-induced suppression of the silicate-mineral liquidus surface limits the stability of silica-minerals to high-SiO₂ compositions at low temperatures in the S-bearing melts and eliminates it in the P-bearing melts. In contrast, F increases the silica-mineral stability field to the extent that the two-liquid field is truncated by the silica-mineral saturation surface.

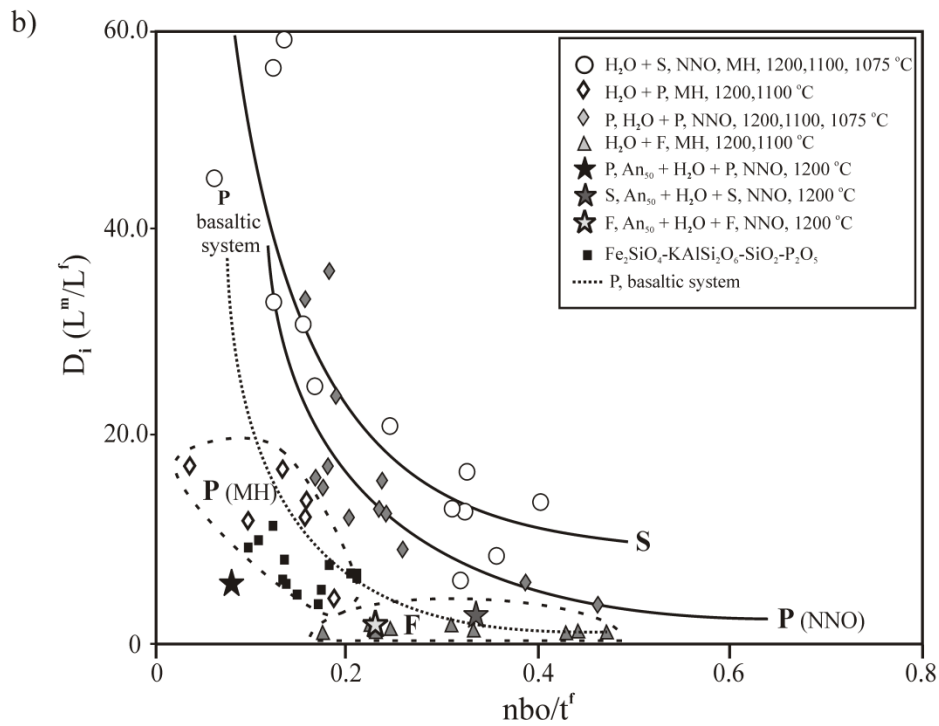
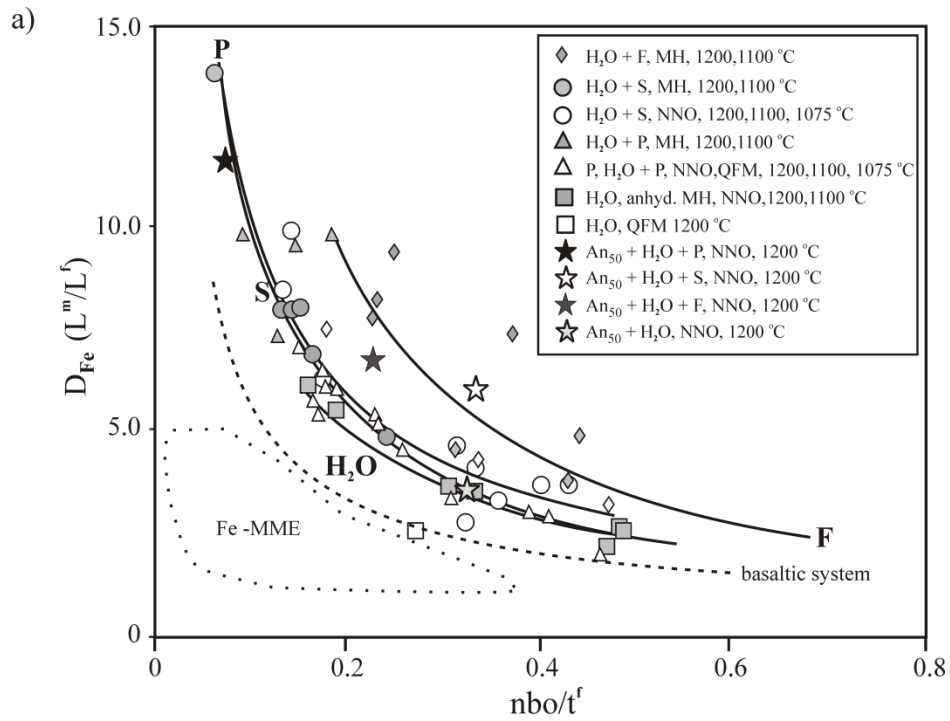
2.5.2 Major element partitioning and melt structure relations in volatile-rich melts

Major element partitioning trends in the volatile-rich experimental melts are similar to those reported in equivalent anhydrous melts (Watson, 1976; Naslund, 1983; Bogaerts and Schmidt, 2006), wherein Fe, Ca and P preferentially partition into the mafic melt and Si, Al, K

and Na into the felsic melt. No data has been presented in the literature regarding the partitioning of S and F between anhydrous immiscible silicate melts, but in the H₂O-bearing melts produced in this study, S partitions strongly into the mafic melt (Figure 2-4b). In contrast, F partitions nearly equally into the mafic and silicate liquids ($D_F = 1 \pm 0.6$). The absolute values of major element partition coefficients between coexisting experimental melts are generally higher than in equivalent anhydrous melts.

The relationship between major element partition ratios and melt structure in immiscible silicate melts has been used to assess the role of liquid phase separation in the evolution of coexisting silicate magmas of differing composition. Specifically, major element partition ratios (D_i) plotted as a function of the melt polymerization parameter nbo/t^f (nbo: number of non-bridging oxygens, t: tetrahedrally-coordinated network-forming cations; f = the felsic member of conjugate immiscible liquids pairs), define power-law relationships that are distinct from those for coexisting melt pairs that have not undergone liquid phase separation. Bogaerts and Schmidt (2006) demonstrated that power-law curves (for D_i as a function of nbo/t) for the elements Fe, Ti, P, Si and K for immiscible melts of basaltic composition can be applied as a means to assess rocks formed from coexisting magmas over a wide range of compositions and petrogenetic conditions.

To test whether the power-law relationships for major element partition data and nbo/t^f in anhydrous silicate melts can be applied to the assessment of melts with H₂O, P, S or F, the D_i for the elements Fe, Si, K, P, S and F are plotted as a function of the nbo/t^f values of the volatile-rich melts produced in this study (Figure 2-4). For purposes of comparison, nbo/t^f values are calculated using the method of Bogaerts and Schmidt (2006), in which $t = Si + Al + P$, and all Fe is treated as non-network forming, an assumption,



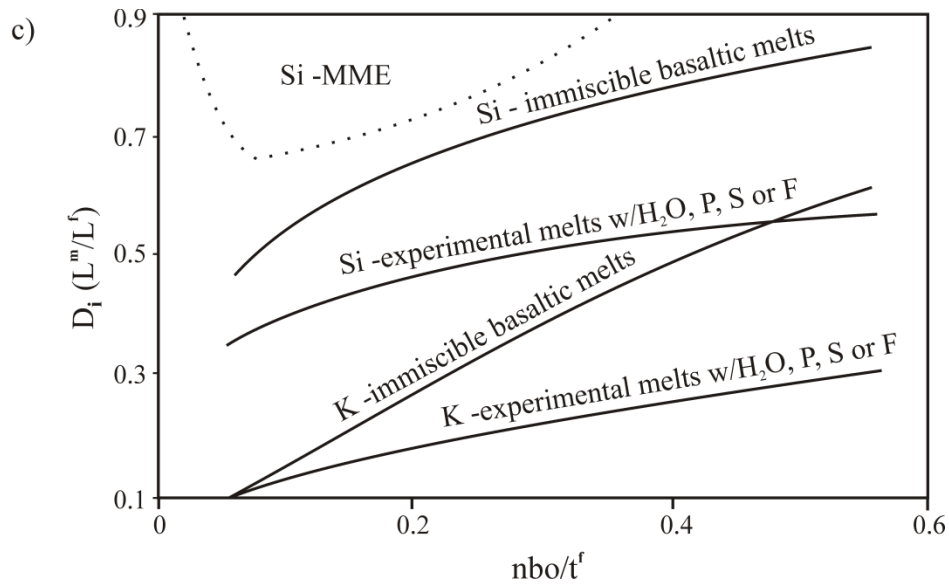


Figure 2-4: Partition coefficients and nbo/t^f between conjugate experimental melts (L^m ; FeO-rich melt, L^f ; SiO_2 -rich melt). **a** variation of the partition coefficients between melts for Fe as a function of nbo/t^f , **b** variation of the partition coefficients between melts for P, S, and F as a function of nbo/t^f . Data for P in the system Fe_2SiO_4 - $KAlSi_2O_6$ - SiO_2 are from Visser and Koster Van Groos (1979a) and Freestone and Powell (1983), and those for the basaltic system (tholeiitic and lunar basalts) are from Rutherford et al (1974), Ryerson and Hess (1980), Dixon and Rutherford (1979), Ryerson and Hess (1980), Philpotts and Doyle (1983) and Longhi (1990), modified from Bogaerts and Schmidt (2006). MME partition data are from non-equilibrium, coexisting microgranular enclaves in granitic melts (Bogaerts and Schmidt, 2006). **c** variation of the partition coefficients between melts for Si and K as a function of nbo/t^f in experimental melts with H_2O and H_2O plus P, S or F (this study), and in immiscible basaltic melts (Bogaerts and Schmidt, 2006).

justified, in part, because the $Al/K = 1$ molar ratio in the experimental melts severely limits the number of cations available to charge-balance any network-forming Fe^{3+} . Water is not included in the nbo/t calculation scheme because its concentration in both natural and synthetic melts is difficult to quantify and the method would be impractical if the power-law relationship between partitioning and the nbo/t^f parameter were strongly dependent on the H_2O content of the melt.

2.5.2.1 Fe, Si and K partitioning

D_{Fe} and nbo/t^f data in melts with H_2O only, or with P or S overlap (Figure 2-4a), yielding indistinguishable power-law curves. Power-law equations fitting the data are: for melts with H_2O

only, $D_{\text{Fe}} = 1.29 (\text{nbo}/t^{\text{f}})^{-0.84}$ ($r^2 = 0.82$); for melts with $\text{H}_2\text{O} + \text{P}$, $D_{\text{Fe}} = 1.22 (\text{nbo}/t^{\text{f}})^{-0.95}$ ($r^2 = 0.82$); and for melts with S , $D_{\text{Fe}} = 1.62 (\text{nbo}/t^{\text{f}})^{-0.82}$ ($r^2 = 0.93$). The curve for D_{Fe} as a function of nbo/t^{f} in F-bearing melts (Figure 2-4b) differs from the curves calculated for melts with H_2O , S or P reflecting both higher D_{Fe} values and a shift in the miscibility gap toward more polymerized compositions (Figure 2-5). The power-law equation fitting the data for F-bearing melts is $D_{\text{Fe}} = 1.75 (\text{nbo}/t^{\text{f}})^{-0.99}$ ($r^2 = 0.74$).

The addition of plagioclase (An_{50}) to melts with H_2O , or H_2O plus P or F , does not induce significant changes in Fe partitioning, but D_{Fe} values in melts with plagioclase and S are significantly greater than those for the plagioclase-bearing melts with H_2O , or H_2O plus P or F . Temperature and oxygen fugacity have a minimal effect on the relationship between Fe partitioning and nbo/t in both the volatile-rich experimental melts and similar anhydrous immiscible melts (Bogaerts and Schmidt, 2006).

Partitioning data for Si and K in melts with H_2O , P , S or F show significant overlap and are more dispersed than those for Fe , but data for D_{Si} as a function of nbo/t^{f} in the experimental melts, considered *in toto*, yield a power-law curve that is clearly distinct from that defined by Si in coexisting melts that have not undergone liquid phase separation (Figure 2-4c).

2.5.3.2 Partitioning of P, S and F

Power-law curves for D_{S} ($f\text{O}_2 = \text{NNO}$ or MH) and D_{P} ($f\text{O}_2 = \text{NNO}$) in the experimental melts are similar to those for D_{Fe} and plot above the curve for D_{P} in immiscible basaltic liquids (Figure 2-4b). Partitioning coefficient values (D_{P}) at $f\text{O}_2 = \text{MH}$ are greater than D_{P} at $f\text{O}_2 = \text{NNO}$ but increased polymerization of the felsic melt shifts the $D_{\text{P}}\text{-nbo}/t^{\text{f}}$ field toward more polymerized compositions that plot closer to the power-law curve for P in immiscible basaltic melts than the data from melts at $f\text{O}_2 = \text{NNO}$. Power-law equations fitting the data for the hydrous

melts are: $D_P(\text{NNO}) = 1.07 (\text{nbo}/t^f)^{-1.79}$ ($r^2 = 0.79$) and, $D_S(\text{NNO}, \text{MH}) = 4.15(\text{nbo}/t^f)^{-1.08}$ ($r^2 = 0.72$). Partitioning coefficients for melts with F ($D_F = 1 \pm 0.6$), however, do not yield a power-law curve. The addition of plagioclase (An_{50}) to melts in the system $\text{Fe}_3\text{O}_4\text{-KAlSi}_2\text{O}_6\text{-SiO}_2$ increases the quantities of P, S and F that can be accommodated in the felsic melt, but does not result in significant change in the partitioning of Fe.

2.5.4 Application of partitioning-polymerization relationships in experimental melts to the assessment of coexisting, volatile-rich natural magmas

Bogaerts and Schmidt (2006) demonstrated that power-law curves for D_i as a function of nbo/t^f for the elements Fe, Si, and Ti in immiscible melts in the basaltic system can be used to discriminate between coexisting melts generated by liquid phase separation and those resulting from other processes. Major element partitioning data determined for rocks formed from coexisting immiscible magmas plot either proximal to, or as extensions of, the power-law curves derived for immiscible melts in the basaltic system. Major element partitioning data from rocks formed from coexisting magmas that were generated by other processes are distinct from those of the immiscible basaltic system. The method has been applied to rocks generated by both intrusive and extrusive coexisting magmas over a wide range of P - T - X - $f\text{O}_2$ conditions. A comparison of power-law relationships established for D_i - nbo/t^f relationships for the elements Fe, Si, and P in the melts produced in this study with those calculated for the same elements in the basaltic system shows that the power-law equations calculated for the basaltic system can be applied to volatile-rich magmas (Figure 2-4) over a wide $f\text{O}_2$ interval e.g. QFM-MH. Further, the method is applicable even if the H_2O and Fe^{3+} contents of the magmas are not considered in calculating the polymerization parameter nbo/t . The finding is non-trivial because quantification of the volatile constituents and Fe^{3+} in igneous rocks and magmas is often problematic.

2.5.5 Immiscibility in volatile-rich magmas

Water, P, S, F and Cl are common constituents in most magmatic systems and understanding their effects on silicate liquid phase separation constitutes a critical step in the assessment of the role of silicate immiscibility in petrogenesis. Although the melt compositions employed herein are simplified, the documented effects of H₂O, P, S, F and Cl in the experimental systems provide a basis for understanding the potential influence of these constituents in natural magmatic systems.

The effect of H₂O alone or in combination with P or S is to increase the *T-X* range of miscibility gaps in silicate melts (Figure 2-5) through suppression of the saturation temperatures of liquidus minerals. Fluorine and Cl increase the activity of Si in the melt, thereby expanding the *T-X* stability fields of SiO₂ minerals. The addition of H₂O and F or Cl to the experimental melts increases the SiO₂ mineral saturation surface, reducing the compositional extent of the miscibility gap in the F-bearing system and eliminating it in the melts with Cl.

Predictably, the stability fields of SiO₂ minerals and magnetite expand with increasing oxygen fugacity. The phase relations demonstrated here have general implications for the long controversial genesis of magnetite deposits of the Kiruna and El Laco type. Sillitoe (2003) and Hitzman et al. (1992) among others propose that these deposits are products of hydrothermal activity whereas Chen et al. (2010), Naslund et al. (2003) and others invoke liquid phase separation of immiscible volatile-rich Fe- and Si- rich magmas as a petrogenetic mechanism. Rocks associated with these deposits are typically enriched in phosphorus and sulfur and have mineralogical and textural characteristics typical of H₂O enrichment (Nyström and Henríquez, 1994; Naslund et al., 2003).

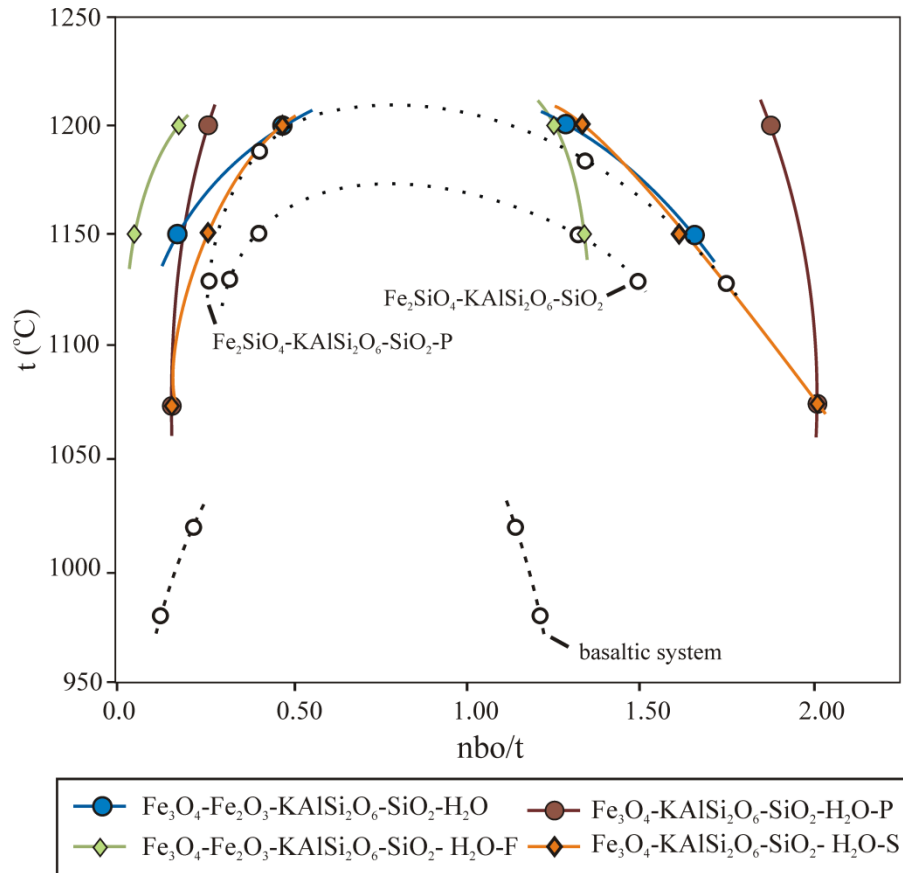


Figure 2-5: Width of the miscibility gap expressed as a function of temperature plotted against nbo/t of conjugate liquid pairs in experimental melts with H₂O, and H₂O with P, S, or F. Data for the basaltic system are from Ryerson and Hess (1980), for the systems; Fe₂SiO₄-KAlSi₂O₆-SiO₂-P, Visser and Koster Van Groos (1979c), modified from Bogaerts and Schmidt (2006), Fe₂SiO₄-KAlSi₂O₆-SiO₂, Bogaerts and Schmidt (2006).

The expanded $T-X$ range of the silicate-liquid miscibility gap and the extreme Fe enrichment of the mafic conjugate melts (up to 72 wt% FeO_{total}) produced by the addition of H₂O, P and S to melts in this study, although by no means conclusive, supports an immiscible petrogenetic hypothesis for some Fe-oxide deposits. In addition, the reduction of viscosity in the silicate melt produced by the presence of H₂O favors the mechanical separation of conjugate liquids by density, an important component of the immiscible petrogenetic model for the ore deposit type.

2.5.6 Implications for the pressure stability of volatile-rich immiscible magmas.

The effects of H₂O on the T - X configuration of the liquidus surface relative to the miscibility gap in the experimental melt systems have important implications for the pressure stability of two-melt fields in H₂O-rich natural magmas. To clarify the effects of pressure on liquid-phase separation in H₂O-rich silicate melts it is useful to consider: a) the effects of pressure on the mixing parameters in the melts and specifically, on the T - X range of the two-liquid field, independent of the liquidus surface configuration; b) the differences in the effects of pressure on the T - X configuration of the liquidus mineral saturation surface between anhydrous and H₂O-rich melts; and c) the net effects of (a) and (b) on the T - X configuration of two-melt fields relative to the liquidus surface and the upper temperature limit of the miscibility gap. In anhydrous silicate melts, increasing pressure has either little effect on, or expands the T - X extent of two-melt fields (Hudon and Baker, 2002; Visser and Van Groos, 1979c; Watson and Naslund, 1978). However, pressure, commonly elevates liquidus surface temperatures above the miscibility gap, with the net effect that two-liquid fields are rarely intersected during the liquid line of descent of most H₂O-poor magmas, particularly at pressures exceeding those typical of shallow to mid-crustal depths.

The effect of pressure on two-melt fields in H₂O-rich melts is likely to differ significantly from that in anhydrous systems because the suppression of liquidus temperatures produced by H₂O is nearly independent of pressure up to 2GPa (Medard and Grove, 2008; Almeev et al., 2007; Gaetani et al., 1994). Assuming the requisite composition, the extent of stable immiscibility in H₂O-rich melts at pressures commensurate with mid- to deep- crustal and upper mantle environments is therefore dependent on two competing effects, viz. the increase in anhydrous melt liquidus temperatures as a function of increasing pressure and the magnitude of

H₂O- induced liquidus suppression in H₂O-rich melts. For example, in basaltic melts at 2 GPa (f_{O_2} =NNO), 5 wt% H₂O lowers the olivine liquidus temperature by ~137 °C, whereas the dry olivine liquidus temperature is increased as a function of pressure over a 2 GPa range by 130 °C. The net result is that at 2 GPa, the olivine liquidus temperature in H₂O- rich basaltic melts is slightly lower than that in the corresponding anhydrous melt at 0.101 MPa, 1241 °C and 1248 °C (Medard and Grove, 2008).

The H₂O-rich experimental melts produced in this study differ from the basaltic system in that they have fewer network- modifying species, and magnetite rather than forsterite is the primary liquidus mineral. Nonetheless, the magnitude of the H₂O-induced liquidus suppression in the experimental melts, although f_{O_2} dependent, is similar to that in the basaltic system, e.g. ΔT liquidus of the experimental melts, ~120 °C at f_{O_2} = NNO, ~200 °C at f_{O_2} = MH and ~137 °C in basaltic melt at f_{O_2} = NNO. Considering that liquid miscibility gaps (sensu stricto) in silicate liquids are either independent of, or enhanced by, increasing pressure, and that H₂O-induced suppression of liquidus temperatures is nearly independent of pressure over a wide range of compositions at pressures up to 2 GPa, we infer that the T - X configuration of two-liquid fields in H₂O-rich silicate melts at 2 GPa will be similar to that of compositionally-equivalent anhydrous melts at low pressures. In addition, although the upper critical temperatures of the miscibility gaps in the experimental systems considered here have not been established, they must be above 1210 °C (the upper limit of the experimental thermal range) which is in excess of the upper critical temperature of similar anhydrous melts (Figure 2-5). The increased upper critical temperature in the hydrous melts is likely to extend further the area of the two-liquid field above the liquidus in H₂O-rich silicate melts.

Water-rich primary melts are typically generated in subduction zones by volatile flux melting, or in highly evolved late-stage melts that become enriched in volatile components during the crystal fractionation process. Magmas in supra-subduction zone environments that contain sufficient H₂O (≥ 5 wt%) to lower liquidus temperatures enough to stabilize two-liquid fields at depth have been described in experimental and theoretical models of mantle wedge melting (e.g. Grove et al., 2006; Ulmer, 2001). The studies delineate an extensive polythermal region within the mantle wedge, where primary, H₂O-rich melts (5-28 wt% H₂O) are generated (Figure 2-6).

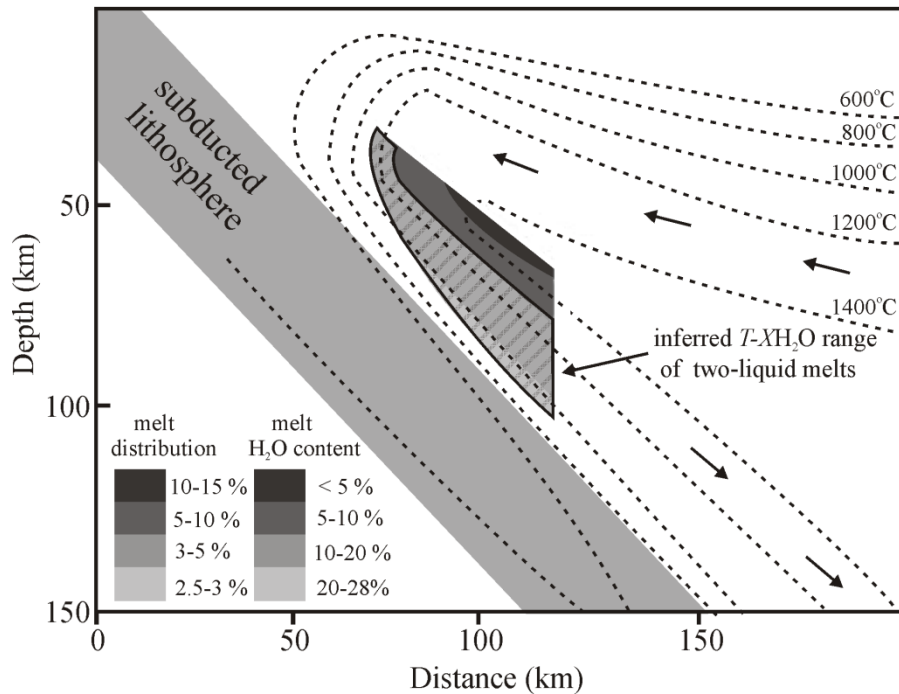


Figure 2-6: Inferred $T-X$ H₂O range of two-liquid silicate melts in supra-subduction H₂O-fluxed melting zone of the mantle wedge. Temperature and H₂O distribution and flux- melting processes in the mantle wedge are modified from Grove et al., 2006.

The $T- XH_2O$ field that we infer to be permissive of silicate-liquid immiscibility lies within the $T-X$ region where volatile-enriched primary melts are generated (Figure 2-6),

suggesting that conjugate immiscible magmas can be generated in deep sub-arc environments. The process, though conjectural, describes a mass-flux mechanism which, in conjunction with the contemporaneous mechanical segregation of conjugate melts, could transport and concentrate small but cumulatively significant quantities of Fe and volatile elements in supra-subduction zone environments.

2.6 Conclusions

The addition of H₂O alone or in combination with small amounts of P, S or F (1, 2, and 6 wt% oxide totals respectively) to melts in the systems Fe₂SiO₄-Fe₃O₄-KAlSi₂O₆-SiO₂, Fe₃O₄-KAlSi₂O₆-SiO₂ and Fe₃O₄-Fe₂O₃-KAlSi₂O₆-SiO₂ expands the *T-X* range of the two-liquid miscibility gap. Phosphorus and S partition strongly into the mafic melt, whereas F is nearly equally partitioned between the conjugate melts. Liquid-phase separation in melts with H₂O + Cl is restricted to a narrow composition range as the result of the Cl-induced increase in the stability of silica minerals. The addition of 2 wt% S to the system Fe₃O₄-Fe₂O₃-KAlSi₂O₆-SiO₂ stabilizes three immiscible melts, with Fe-rich mafic silicate, Fe-poor felsic silicate, and FeS compositions.

Power-law curves calculated for D_i - nbo/t^f relationships for the elements Fe, Si, and P in the melts produced in this study are similar to, but distinct from, those calculated for the same elements in immiscible basaltic melts. The results show that the power-law equations calculated for the basaltic system by Bogaerts and Schmidt (2006) can be applied to assess coexisting volatile rich magmas over a wide range of *P-T-X-fO₂* conditions. Further, the method is applicable even if the H₂O and Fe³⁺ contents of the magmas are not considered in calculating the polymerization parameter nbo/t^f . Water-induced suppression of liquidus temperatures in the experimental systems, combined with the effects of pressure on the temperature and composition

ranges of two-liquid fields in silicate melts suggests that liquid phase separation may occur in some H₂O-rich silicate magmas at pressures up to 2GPa.

Chapter 3

TRACE ELEMENT PARTITIONING BETWEEN IMMISCIBLE SILICATE MELTS WITH H₂O, P, S, F, or Cl

3.1 Abstract

The partitioning of the trace elements Rb, Cs, Zr, Nb, Hf, Th, U, La, Ce, Nd, Sm, Eu, Dy, Er, Yb, Mn, Co, Mo, Ni, Cu, Zn, Cr, V, Ti and Ag between immiscible silicate melts in the systems Fe₂SiO₄-Fe₃O₄-KAlSi₂O₆-SiO₂, Fe₃O₄-KAlSi₂O₆-SiO₂ and Fe₃O₄-Fe₂O₃-KAlSi₂O₆-SiO₂, with or without H₂O P, S, Cl, F or plagioclase (An₅₀) at 1200 °C, 200 MPa has been determined at $fO_2 =$ QFM, NNO and MH oxygen buffers. Water is shown to increase the partitioning of HFSE, REE and transition elements into the Fe-rich melt. Water alone or with 6.66×10^{-4} mols/g of P or S produces nearly parallel partitioning trends for HFSE and REE, at experimental $fO_2 =$ QFM, NNO and MH. Water + F causes Rb and Cs to partition into the Fe-rich melt and significantly increases U partitioning into the Fe-rich melt. Absolute partitioning values of transition elements are strongly dependent on the network-modifier composition of the melt.

3.2 Introduction

Experimental studies of major and trace element partitioning between immiscible Si- and Fe- rich melts have examined the effects of melt composition on element partitioning to clarify the understanding of partitioning systematics between melts and crystalline phases (Hudon and Baker, 2002; Ryerson and Hess, 1978; Watson, 1976), and to predict the compositions of rocks resulting from liquid immiscibility in magmas (Veksler et al., 2007; Vincenzi et al., 1994).

These experiments indicate that melt composition and structure, and particularly the degree of silica polymerization, affect the equilibrium distribution of both major and trace elements between immiscible felsic-silicate and mafic-silicate- melts. Systematic trends have been identified in element partitioning as a function of constituent charge and ionic radii (Watson, 1976), the degree of polymerization in the felsic silicate melt (Bogaerts and Schmidt, 2006), and fO_2 (Naslund, 1983 and Vincenzi et al., 1994).

Studies to date have examined major or trace element partitioning between liquids in the anhydrous systems Si - Fe - Al - K - O alone, or in combination with one or more of the following: Na, Ca, Mg, Ti, B and P (Watson, 1976a,b; Naslund,1983; Bogaerts and Schmidt, 2006; Veksler et al., 2007), as well as for more complex lunar and terrestrial basaltic liquids (Longhi, 1990; Hess et al., 1975; Rutherford et al.; 1974). However, the effects of H₂O, alone or in combination with P, S, F and Cl, on trace element partitioning in these systems have not been investigated.

Water, P, S, F and Cl have been shown to affect both the structure and the concomitant degree of Si - Al - O polymerization in silicate melts (Botcharnikov et al., 2008; Moore et al., 1998; Mysen, 1981; Watson, 1976; Haughton et al., 1974; Dolejš and Baker, 2007; Webster, 2002) as well as the thermal range of miscibility gaps in felsic-silicate and mafic-silicate melts (Lester, 2002; Watson, 1976). Thus, it would be predicted that H₂O, P, S, F, and Cl should influence trace element partitioning between immiscible silicate melts and that partitioning behavior in the experimental melts produced in this study may approximate those in natural systems of similar composition. To explore these relationships we have conducted isobaric (200 MPa) melt-melt partitioning experiments using trace-element doped charges in the systems Fe₂SiO₄-Fe₃O₄-KAlSi₂O₆-SiO₂, Fe₃O₄-KAlSi₂O₆-SiO₂ and Fe₃O₄-Fe₂O₃-KAlSi₂O₆-SiO₂, with or

without H₂O P, S, Cl, F or plagioclase (An₅₀), at 1200 °C and under conditions of variable oxygen fugacity (QFM, NNO or MH buffers). Nernst partition coefficients D (D = concentration in the felsic liquid L^f/concentration in the mafic liquid L^m) calculated for a broad array of trace elements show that the involvement of H₂O, alone or in combination with, P, S, F, or Cl generally acts to increase trace element partitioning into the Fe-rich liquid and for some elements, partitioning trends are reversed relative to anhydrous melts of similar composition.

3.3 Experimental method

Starting materials for the experiments included three anhydrous base-mixtures (Table 3-1) prepared from admixtures of SiO₂ (cristobalite), Al₂O₃, K₂Si₂O₅, FeO and Fe₂O₃. These plot as composition points on the 30 wt% FeO isopleth on the ternary join fayalite-leucite-silica (Al/K ratio of 1), or contain 1.3 wt. % Al in excess of the feldspar normative composition (Appendix A). To minimize the fO_2 gradient between melts and external solid buffers, $Fe^{3+}/\Sigma Fe$ values for the melts synthesized in this study were estimated by the method of Schuessler et al. (2008) at $T = 1200$ °C, $fO_2 =$ quartz-fayalite-magnetite (QFM), nickel-nickel oxide (NNO) or magnetite-hematite (MH) buffers at 200 MPa pressure. The FeO_x component of each base-mixture comprises FeO and Fe₂O₃ in proportions that approximate the $Fe^{3+}/\Sigma Fe$ values calculated for the selected experimental conditions. Oxygen fugacity in the experimental capsules was regulated using the conventional double-capsule, metal-metal oxide + water configuration (Chou and Cygan, 1990). The oxygen fugacities of the experimental melts were quantified using the pressure correction expression of Frost (1991).

Experimental starting compositions containing 2.06 wt% P, 2.14 wt% S, 1.26 wt% F or 2.36 wt% Cl total solids (i.e. 6.66×10^{-4} mols /gr) were prepared by the addition of Fe₂P, FeS,

FeCl₂, or FeF₂ to the anhydrous base-mixtures (Table 3-1). Hydrus experiments incorporated 10 wt% H₂O (total wt. solids). Plagioclase-bearing experiments contain 1.3 wt% (total wt. solids) An₅₀, constituting 43 wt% of the normative feldspar component. Trace elements were added as mixtures of 7, 8 or 10 oxides in the amount of 1.25 wt% total weight solids (Table 3-1).

Table 3-1: Starting mixtures: base compositions A-1, A-1_p (peraluminous), A-3, and An₅₀ plus 10 wt% H₂O (total wt. solids) and 6.66 X 10⁻⁴ mols/gr of P, S, F or Cl.

base compositions (wt% oxide)	SiO ₂	FeO _{total}	Al ₂ O ₃	K ₂ O	An ₅₀
A-1	66.05	30.0	2.06	1.89	-
A-1 _p	66.05	30.0	2.06	1.89	-
A-3	62.86	30.0	3.71	3.43	-
An ₅₀ ^a	65.20	29.62	2.03	1.87	1.3

^a (Ca₅ Na₅) Al_{1.5} Si_{2.5}O₈

Peraluminous compositions contain 1.3 wt % Al₂O₃ total weight % solids in addition to the alumina content of the base composition. Experimental capsules were prepared by loading the desired quantity of starting material, or starting material + H₂O, into a 2mm. (outside diameter) platinum capsule. Three-to-five experimental capsules were loaded into a 5 mm. (outside diameter) platinum capsule containing H₂O and one of the selected solid-oxide oxygen buffers, QFM, NNO or MH. Both inner experimental capsules and outer buffer-bearing capsules were sealed by welding.

Experimental capsules were annealed in KanthalTM or platinum-wound furnaces placed in a rapid-quench, internally heated pressure vessel under isobaric conditions (200 +/- 10 MPa). Capsules were annealed isothermally at 1200 °C for two hours using argon as the pressure medium. A description of the annealing apparatus, quench method and the method used to

determine chemical equilibrium in the experiments is given in sections 2-2 and Appendix A of this thesis.

3.4 Analytical method

Experimental samples were mounted in epoxy and polished. Major element compositions of conjugate immiscible phases were analyzed with a Cameca SX-100 electron microprobe at the University of Manitoba. Analytical conditions were set to an accelerating voltage of 15 kV, a 15 nA beam current and a counting time of 20 s for all elements except P, S, F and Cl (30 s). The beam diameters were 5-10 μm for Si-rich and Fe-rich glasses and 2 μm for quenched sulfide. The concentrations of Rb, Zr, Nb, Cs, Hf, Th, U, La, Nd, Ce, Sm, Eu, Dy, Er, Yb, Ti, V, Cr, Mn, Co, Ni, Cu, Zn, Mo and Ag in quenched conjugate, immiscible liquid pairs were determined using a Thermo Scientific X Series 2 Quadrupole ICP-MS instrument, coupled with a New Wave 213 nm laser ablation system at the Queen's Facility for Isotope Research, Queen's University, Kingston, Ontario. The laser beam was fired at 5 Hz repetition rate with the laser energy in the range of 0.36–0.51 mJ per pulse. A spot size of 30 μm was used, which represented the optimum for a good spatial resolution at the desired level of analytical precision and detection limit. The detection limit was calculated (3x RSD) based on replicate analyses of KL2-G and was found to be 0.03-0.08 ppm for the elements Rb, Cs, Zr, Nb, Hf, Th, U, La, Ce, Nd, Sm, Eu, Dy, Er, Yb, however the transition metal elements Mn, Co, Mo, Ni, Cu, Zn, Cr, Cr, V, Ti and Ag, have slightly higher detection limits of 0.05- 0.1 ppm. All data were collected in a transient time-resolved mode and data acquisition consisted of 20 s of measurement of the gas background, followed by a 120 s of line scan ablation. Data reduction and calculation of elemental contents were performed with the X-Series 2 PlasmaLab software package. Calibration for a quantitative determination of elements was done using NIST 612 as an external reference

material. Iron as ^{57}Fe was used as an internal standard element in both the reference material and the unknown samples.

3.5 Results

3.5.1 Run products

Experimental run products consist of quenched, conjugate immiscible liquids occurring as spheroidal-sub-spheroidal volumes of Si- and Fe- rich glass ~1 - 600 μm in diameter. The addition of refractory trace oxides to some of the starting mixtures acted to raise melt liquidus surface temperatures, producing the assemblage, two immiscible liquids + magnetite. Quench-overgrowth textures were observed on magnetite crystals in some of the experimental glasses and the analytical data obtained from these experiments are discounted here because equilibrium cannot be assumed.

3.5.2 Major elements

The major element compositions and conjugate-liquid partition coefficients for melts with starting compositions A-1, A-3, and An_{50} with H_2O and P, S, F, or Cl are reported in Appendix B. Major element partition coefficient values for conjugate peraluminous and peralkaline melts (compositions A-1, A-3 and An_{50}) do not deviate significantly from melts of similar composition with a 1:1 Al_2O_3 : K_2O molar ratio.

3.5.3 Trace elements

Nernst partition coefficients calculated for trace elements in synthesized immiscible conjugate liquids (Table 3-2) show that nearly all of the trace elements partition preferentially into the siderophile melt regardless of the network modifier present, (e.g. H_2O and P, S, F or Cl), $f\text{O}_2$, or the base composition. Previous studies of trace element partitioning between anhydrous melts of similar composition show that Rb and Cs preferentially partition into the Si- rich melt,

as does K, presumably acting to charge-balance Al in the Si-Al-O structure (Veksler et al., 2007; Vincenzi et al., 1994; Watson, 1976).

In contrast, Rb and Cs preferentially partition into the Fe-rich melt in hydrous melts with base compositions of $An_{50} + P$, $fO_2 = NNO$, and $A-1 + F$, $fO_2 = NNO$, $A-1$ $fO_2 = QFM$, in association with the high-field-strength elements (Figure 3-1a,b), in melts with P, F or H_2O alone. The high-field-strength elements Zr, Nb, Hf, Th, and U have parallel-to-subparallel partitioning trends (Figure 3-1a,b). The data for U and Th in anhydrous melts (Vincenzi et al., 1994) and in melts with similar major elements compositions and $H_2O + P$ or H_2O alone show that both elements partition into the Fe-rich melt in nearly equivalent proportions, whereas, in melts with $H_2O + F$, U and Th partitioning trends are decoupled, with D_U being four-times greater than D_{Th} . Uranium is weakly partitioned into the silicate liquid in melt with composition An_{50} with $H_2O + S$ (Figure 3-1b).

Rare-earth elements show the same partitioning at any fixed experimental condition with the exception of europium in composition $A-1 + H_2O$, $fO_2 = QFM$, where it shows a minor positive anomaly. Partitioning coefficient values for REE's (D_{REE}) decrease in the following order as a function of melt compositions ($fO_2 = NNO$): peraluminous compositions with $P >$ metaluminous compositions with $P >$ anorthite-bearing composition with $P >$ peraluminous composition with $F >$ $Al:K = 1$, with $Cl >$ $Al:K = 1$ with S .

The transition elements studied herein preferentially partition into the mafic melt, but the degree of partitioning varies significantly for each element (Figure 3-1), depending on Al/CNK , fO_2 , $Na + Ca$ contents, and the network-modifying constituent. Thus D values for Cu, V, and Ag in plagioclase-bearing and metaluminous melts with S are higher than in those with P .

A survey experiment with base-composition A-1 + 6.66×10^{-4} mols /gr of both P and S at $fO_2 =$ NNO was conducted to evaluate potential additive effects of two network modifiers on transition element partitioning (Figure 3-1e). Partition coefficients for the elements Mo, Cu, and Ag were found to be higher in the melt with P + S than in melts of equivalent major element composition with either component.

3.6 Discussion and conclusions

Trace element partition coefficients calculated for experimental melts (Table 3.2) confirm the prediction that H₂O alone, or in combination with geologically reasonable quantities of P, S, F or Cl, influences trace element partitioning behavior between conjugate immiscible-liquid pairs. The addition of H₂O to experimental melts significantly increases the partitioning of HFSE and REEs into the Fe-rich melt relative to anhydrous melts of similar composition, regardless of fO_2 . Partitioning trends for Rb and Cs in anhydrous immiscible melts are strongly reduced or even reversed in the H₂O-bearing melts produced here, particularly those with F. Partitioning trends of REE in the experimental melts are generally flat, and rocks formed from volatile-rich, immiscible conjugate magma pairs will probably exhibit similar patterns for the elements La, Ce, Nd, Sm, Dy, Er and Yb, with the concentrations of these elements being significantly enriched in the mafic conjugate melt. The REE trends documented here are similar in configuration to those reported by Shearer et al. (2001) for lunar high-Fe basalt-rhyolite immiscible pairs, but the absolute values of partition coefficients are higher in hydrous melts with P, S or Cl.

Table 3-2: Partition coefficients (D) for trace elements in volatile-rich immiscible experimental melts. Starting compositions are listed in Table 3.1.

	A-1 Fluorine $f_{O_2} = \text{NiNiO}$			A-1 Phosphorus $f_{O_2} = \text{NiNiO}$ peraluminous			A-1 Phosphorus $f_{O_2} = \text{MH}$			A-1 $f_{O_2} = \text{QFM}$			An50 Sulfur $f_{O_2} = \text{NiNiO}$			An50 Phosphorus $f_{O_2} = \text{NiNiO}$			A-1 Phosphorus $f_{O_2} = \text{NiNiO}$					
	D	stdv	n	D	stdv	n	D	stdv	n	D	stdv	n	D	stdv	n	D	stdv	n	D	stdv	n	D	stdv	n
Rb	38.5	1.1	9	0.4	0.1	8	0.3	0.1	9	1.2	0.5	6	0.9	0.1	7	1.2	0.5	7	0.1	0.0	7			
Zr	12.0	0.1	5	9.9	1.1	9	7.6	0.7	8	7.0	1.0	5	3.3	0.9	4	2.6	0.5	7	3.4	1.4	8			
Nb	6.9	0.2	4	16.4	3.0	8	12.6	2.9	8	3.7	0.3	6	3.6	0.3	8	4.2	0.8	7	5.9	0.6	7			
Cs	20.6	0.2	5	0.2	0.0	7	0.2	0.0	9	1.1	0.6	7	0.1	0.1	8	1.2	0.7	7	0.9	0.4	6			
Hf	20.0	0.0	5	20.5	2.5	8	15.8	1.0	8	2.3	0.9	6	1.2	0.3	4	3.8	0.7	7	4.9	0.4	5			
Th	12.1	0.1	5	28.6	2.3	8	22.0	2.1	7	3.7	1.7	6	1.5	0.8	9	4.9	0.7	8	17.2	1.1	6			
U	48.2	0.2	4	24.4	3.8	8	18.8	1.9	7	2.8	1.3	6	0.8	0.5	6	7.5	0.1	7	13.6	1.5	7			
	A-1 Chlorine $f_{O_2} = \text{NiNiO}$			A-1 Fluorine $f_{O_2} = \text{NiNiO}$ peraluminous			A-3 Sulfur $f_{O_2} = \text{NiNiO}$			A-1 Phosphorus $f_{O_2} = \text{QFM}$ peraluminous			An50 Phosphorus $f_{O_2} = \text{NiNiO}$			A-1 Phosphorus $f_{O_2} = \text{NiNiO}$			A-1 $f_{O_2} = \text{QFM}$					
	D	stdv	n	D	stdv	n	D	stdv	n	D	stdv	n	D	stdv	n	D	stdv	n	D	stdv	n	D	stdv	n
La	4.4	0.7	6	9.3	0.7	5	2.8	0.5	6	33.6	5.8	7	30.9	0.5	5	3.9	0.7	6	3.0	0.7	5			
Ce	4.0	0.2	6	9.1	0.4	6	2.4	0.8	6	29.5	6.1	7	25.8	0.2	6	4.9	0.4	6	3.8	0.8	5			
Nd	4.5	0.9	6	8.7	0.5	7	2.8	0.5	6	29.6	5.9	7	15.4	0.8	7	4.2	1.0	6	2.9	0.6	5			
Sm	4.6	0.9	6	9.1	0.9	6	3.0	0.7	6	30.8	6.0	7	14.4	0.1	6	3.5	0.4	6	2.8	0.6	5			
Eu	3.9	0.3	6	8.8	0.8	6	-	-	-	-	-	-	-	-	-	-	-	-	-	-	-			
Dy	4.4	0.6	6	9.2	0.6	5	3.1	0.8	6	30.4	5.9	7	13.8	0.6	6	4.6	0.2	6	3.6	1.1	5			
Er	4.2	0.3	6	9.2	0.6	5	3.1	0.8	6	32.1	6.1	7	13.6	0.3	7	4.9	0.7	6	2.5	0.7	5			
Yb	4.1	1.0	6	9.1	0.9	5	3.5	0.2	6	26.7	6.4	7	12.2	0.9	5	5.3	0.8	6	1.3	0.7	5			
	A-1 Phosphorus $f_{O_2} = \text{QFM}$			A-1 Phosphorus $f_{O_2} = \text{MH}$ peraluminous			A-1 $f_{O_2} = \text{NiNiO}$			A-1 Fluorine $f_{O_2} = \text{NiNiO}$ peraluminous			An50 Phosphorus $f_{O_2} = \text{NiNiO}$			A-1 Phosphorus Sulfur $f_{O_2} = \text{NiNiO}$			A-1 Phosphorus $f_{O_2} = \text{NiNiO}$					
	D	stdv	n	D	stdv	n	D	stdv	n	D	stdv	n	D	stdv	n	D	stdv	n	D	stdv	n	D	stdv	n
La	5.5	0.8	5	43.4	3.6	6	Mn	4.6	0.4	6	7.7	0.8	5	15.1	0.5	6	5.3	0.5	8	12.3	1.4	8		
Ce	6.2	0.1	5	42.5	1.8	6	Co	0.8	0.1	8	6.3	0.6	5	12.6	1.5	6	13.3	1.7	8	21.8	3.0	8		
Nd	5.4	0.6	5	44.8	2.4	6	Mo	5.6	1.1	8	9.4	4.0	5	11.7	2.2	5	8.8	1.2	4	5.7	1.2	8		
Sm	4.7	1.1	5	44.6	4.0	6	Ni	7.1	0.7	8	6.3	0.9	5	9.8	2.0	6	18.1	1.6	8	33.5	1.9	8		
Eu	8.0	0.8	5	-	-	-	Cu	6.1	1.7	8	5.1	1.4	5	8.0	2.6	6	7.0	1.5	8	4.1	1.1	8		
Dy	5.4	0.8	5	40.9	4.6	6	Zn	3.0	0.5	8	13.9	2.5	5	14.8	0.9	6	12.5	0.1	8	12.5	0.7	8		
Er	5.6	0.3	5	37.4	4.0	6	Cr	9.0	1.1	5	6.9	1.1	5	3.6	0.2	6	3.2	0.5	8	37.1	4.8	8		
Yb	4.9	0.6	5	30.9	3.2	6	V	6.9	0.9	3	6.8	2.0	5	1.7	0.9	6	6.3	1.6	8	9.2	1.2	8		
							Ti	8.3	1.5	7	7.2	2.3	5	5.3	0.4	6	3.1	0.9	5	2.3	0.6	8		
							Ag	3.6	0.9	8	14.5	2.9	5	4.3	0.4	6	4.1	0.5	8	1.7	0.8	8		
	A-1 Phosphorus $f_{O_2} = \text{MH}$			A-1 Sulfur $f_{O_2} = \text{NiNiO}$ peraluminous			A-1 Phosphorus $f_{O_2} = \text{QFM}$			An50 Sulfur $f_{O_2} = \text{NiNiO}$			A-3 Sulfur $f_{O_2} = \text{NiNiO}$			A-1 Sulfur $f_{O_2} = \text{NiNiO}$			A-1 $f_{O_2} = \text{NiNiO}$ peraluminous					
	D	stdv	n	D	stdv	n	D	stdv	n	D	stdv	n	D	stdv	n	D	stdv	n	D	stdv	n	D	stdv	n
Mn	11.8	1.7	8	7.6	1.0	7	7.8	1.5	9	7.2	1.1	5	4.9	0.5	8	7.51	3.1	5	16.1	2.2	7			
Co	16.8	2.7	8	5.9	0.5	7	14.5	1.01	9	8.4	0.9	5	4.2	1.5	8	9.84	2.0	5	15.3	2.8	7			
Mo	8.6	0.8	7	9.8	1.7	7	42.1	3.2	9	5.7	1.6	5	22.8	2.7	5	7.85	1.1	6	14.6	1.3	7			
Ni	16.3	2.7	9	10.5	0.8	7	36.2	2.4	9	8.7	4.1	5	3.1	0.3	5	3.50	0.6	7	16.9	1.7	7			
Cu	3.6	1.0	9	8.9	0.4	7	3.5	0.7	9	22.3	3.0	5	6.9	0.6	8	2.94	0.4	6	23.4	3.7	7			
Zn	24.7	3.0	9	4.1	1.5	7	3.6	1.0	4	8.5	1.6	5	5.2	0.4	5	17.32	3.9	6	14.6	3.4	7			
Cr	14.6	3.3	9	26.1	3.8	7	21.8	5.5	9	5.5	1.2	5	41.1	5.1	8	2.12	0.3	8	18.0	4.2	7			
V	6.1	0.9	9	16.7	1.5	7	6.2	0.5	9	4.4	0.6	5	3.0	0.5	8	5.47	1.2	5	12.4	1.3	7			
Ti	1.9	0.6	9	18.7	2.8	7	7.1	1.4	9	6.5	1.7	5	4.3	0.7	8	4.38	0.7	6	16.5	2.3	7			
Ag	1.0	0.8	9	6.3	1.4	7	5.8	0.6	9	12.3	1.5	5	6.8	5.5	8	2.08	0.6	7	11.1	1.4	7			

^a standard deviation

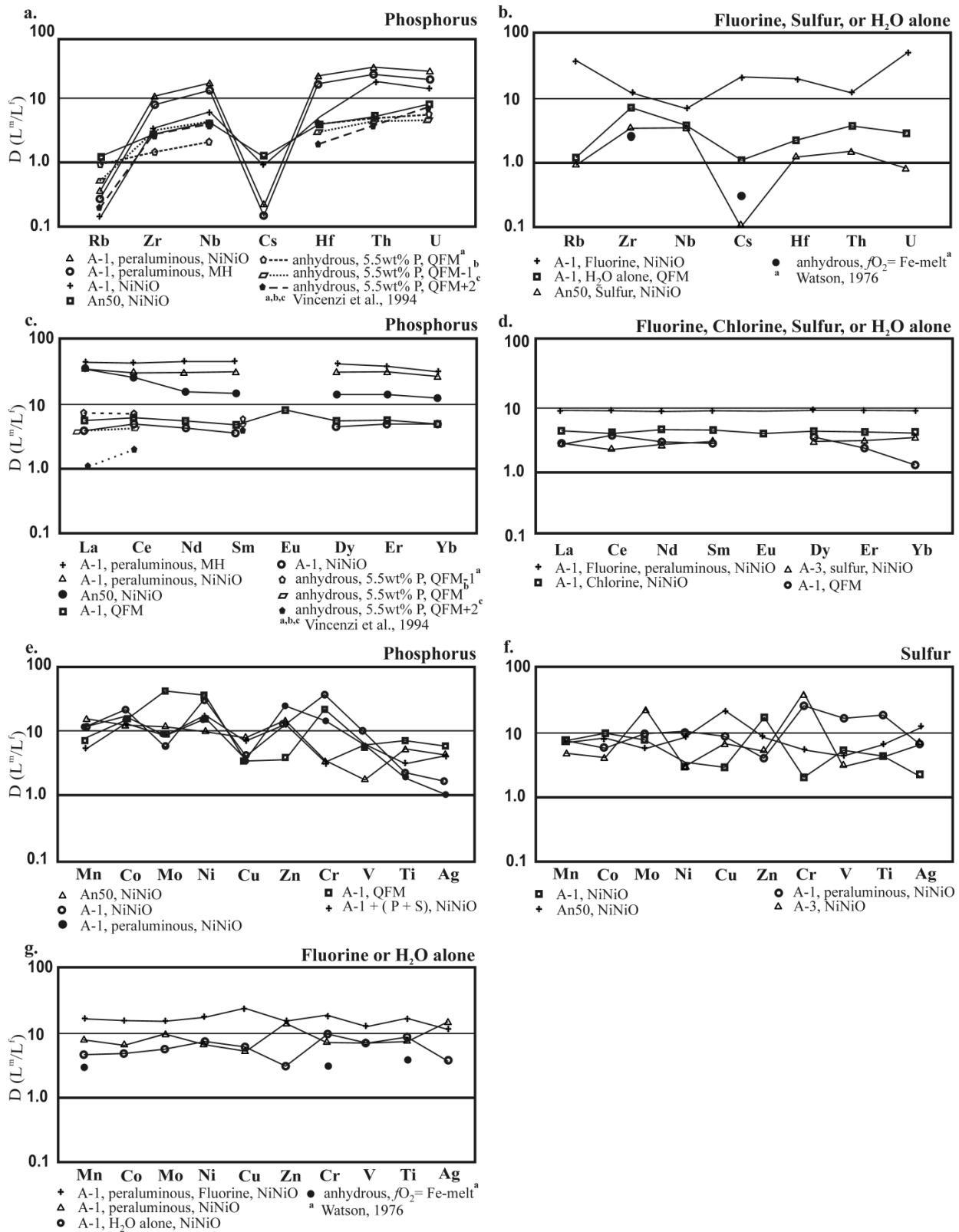


Figure 3-1: Trace element partitioning trends between immiscible silicate melts with H₂O and H₂O with P, S, F or Cl.

Partitioning trends of REE and HFSE are generally subparallel, regardless of initial melt composition, but partitioning trends for transition elements vary significantly as a function of the species of the network modifier in the melt and, to a lesser degree, the major element composition.

Natural magmas generally contain multiple network-modifying constituents such as H₂O, P, S, F and Cl, and trace element partitioning trends in natural two-liquid systems will reflect the combined effects of these components. This and previous studies (Veksler et al., 2006; Vincenzi et al., 1994; Watson, 1976) clearly demonstrate that liquid phase separation in silicate melts is an effective mechanism for concentrating a broad array of trace elements in Fe-rich, Si-poor melts. The transition element partitioning patterns that result from the inclusion of H₂O, P, S, F or Cl in the immiscible melts produced in this study (Figure 3-1) are remarkably similar to element enrichment trends observed in some ore deposit types e.g., iron oxide-copper-gold (Naslund et al., 2003) and Cu-Mo-Au porphyry (Aude'tat and Pettke, 2006) systems, suggesting the need for further study of the potential role played by silicate melt immiscibility in the genesis and evolution of magmatic-hydrothermal ore systems.

Trace element partitioning trends in Fe- and Si- rich lithologies that result from the un-mixing of volatile-rich magmas should conform to the general patterns described above. However, conjugate-immiscible magmas with H₂O, P, S, F, or Cl are subject to continued chemical evolution, including the exsolution of a vapor phase, magmatic recharge and the assimilation of country rock that may further alter trace-element partitioning trends.

Chapter 4

OXYGEN ISOTOPE PARTITIONING BETWEEN IMMISCIBLE SILICATE MELTS WITH H₂O, P AND S

4.1 Abstract

Differences between the $\delta^{18}\text{O}$ values of immiscible Si-rich and Fe-rich melts in the systems Fe_2SiO_4 - Fe_3O_4 - KAlSi_2O_6 - SiO_2 , Fe_3O_4 - KAlSi_2O_6 - SiO_2 , and Fe_3O_4 - Fe_2O_3 - KAlSi_2O_6 - SiO_2 , with H_2O and $\text{H}_2\text{O} + \text{P}$ or S have been determined in isothermal, isobaric experiments at 1100 °C and 1200 °C and 200 MPa. The $\Delta^{18}\text{O}$ values for conjugate Fe_2SiO_4 - Fe_3O_4 - KAlSi_2O_6 - $\text{SiO}_2 + \text{H}_2\text{O}$ and, Fe_3O_4 - KAlSi_2O_6 - SiO_2 KAlSi_2O_6 - $\text{SiO}_2 + \text{H}_2\text{O}$ melts are only 0.4- 0.6 permil and do not differ significantly from those for anhydrous melts of similar composition. The $\Delta^{18}\text{O}$ values for melts with added $\text{H}_2\text{O} + \text{P}$ or S are more variable, ranging from nil to 0.8 permil. Preferential partitioning of ^{18}O into the Si-rich melt is consistent with observations in melt-mineral and mineral-mineral pairs wherein ^{18}O is enriched in the more polymerized phase but the nearly equal proportioning of ^{18}O in the network modifier-bearing immiscible melts is not controlled by the relative degree of polymerization or $f\text{O}_2$. The upper limit of the range of $\Delta^{18}\text{O}$ values (<1 permil), and the variation in the $\delta^{18}\text{O}$ values of conjugate melts that occurs with the inclusion of network modifying constituents, suggest that variations in oxygen isotope ratios cannot be used as a means to identify liquid-phase separation in silicate melts.

4.2 Introduction

Revived interest in the petrogenetic role of silicate immiscibility has called attention to the need to constrain further the chemical and physical characteristics of two-liquid systems, particularly the effects of P - T - X parameters on partitioning between conjugate liquids (Philpotts, 2008; Veksler et al., 2006). The fractionation of oxygen isotopes between phases in natural silicate liquids is normally small, generally less than 1 permil (Taylor and Sheppard, 1986; Kyser 1990). However, processes involving phases with distinct chemical or physical properties, such as CO_2 degassing (Pineau et al., 1976) or fractional crystallization (Taylor and Epstein, 1962), can affect the isotopic composition of silicate liquids. Kyser et al. (1998) determined experimentally that differences in the crystallochemical properties of Si- and Fe- rich immiscible liquids in the system Fe_2SiO_4 - KAlSi_2O_6 - SiO_2 at 1180 °C and 0.1 MPa were sufficient to induce oxygen isotope fractionation between conjugate immiscible melts, the Si-rich liquids having $\delta^{18}\text{O}$ values 0.5 - 0.6 ‰ higher than those of the Fe-rich liquids.

Major and trace element partitioning between immiscible silicate liquids is similarly controlled by differences in the crystallochemical properties of the conjugate melts, in particular the ratio of network-modifying to network-forming components in the melts (Bogaerts and Schmidt, 2006; Vincenzi et al., 1994; Watson, 1976). The effects of H_2O +/- P or S and $f\text{O}_2$ on silicate immiscibility (Lester, 2002) indicate that the addition of these components or variations in $f\text{O}_2$ in the system Fe_2SiO_4 - Fe_3O_4 - KAlSi_2O_6 - SiO_2 (Fa-Mt-Lc-Qtz), Fe_3O_4 - KAlSi_2O_6 - SiO_2 (Mt-Lc-Qtz) and Fe_3O_4 - Fe_2O_3 - KAlSi_2O_6 - SiO_2 (Mt-Hm-Lc-Qtz) influence the crystallochemical properties of conjugate immiscible liquids, broadening the miscibility gap, and increasing the partitioning ratios of most major and trace elements. In theory, the demonstrated changes to the

crystallochemical properties of the immiscible liquids could similarly produce changes to the oxygen isotope proportioning between the conjugate liquids.

This study assesses the magnitude of oxygen isotope fractionation between Fe- and Si- rich conjugate melts incorporating H₂O +/- P or S, and with variation in fO_2 , in the systems Fa-Lc-Sil and Mt-Lc-Sil. Oxygen isotope fractionation in the systems Fa-Lc-Sil and Mt-Lc-Sil + H₂O is consistent with that observed in the anhydrous system regardless of fO_2 . In the systems Fa-Lc-Sil-H₂O and Mt-Lc-Sil-H₂O with P or S, there are small, but significant differences in $\Delta^{18}O$ ($\delta^{18}O_{\text{sil-liquid}} - \delta^{18}O_{\text{Fe-liquid}}$) values relative to those observed in the anhydrous, or H₂O- only systems, suggesting that the inclusion of P or S in silicate melts can cause sufficient change in the crystallochemical properties of the melts to influence the proportioning of oxygen isotopes.

4.3 Experimental procedure

The effect of immiscibility on oxygen isotope ratios in silicate melts with H₂O, P or S was examined using a base-composition plotting on the 30 wt% FeO isopleth in the system Fe₂SiO₄-KAlSi₂O₆-SiO₂ (Fa-Lc-Q) incorporating 10 wt% H₂O (total wt. solids) and either 2.06 wt% P or 2.14 wt% S (i.e..6.66 x 10⁻⁴ mols /gr.) at 1100 and 1200 °C and 200 MPa.

Experimental charges were prepared from admixtures of SiO₂ (cristobalite), Al₂O₃, K₂Si₂O₅, FeO, Fe₂O₃, and Fe₂P or FeS (Table 4-1).

To minimize the fO_2 gradient between melts and external solid buffers, $Fe^{3+} / \Sigma Fe$ values for the melts synthesized in this study were estimated by the method of Schuessler et al. (2008) at $T = 1200$ °C, fO_2 of quartz-fayalite-magnetite (QFM), nickel-nickel oxide (NNO) or magnetite-hematite (MH) buffers at 200 MPa pressure. The FeO_(total) component of each base-mixture comprises FeO and Fe₂O₃, or FeO, Fe₂O₃ and Fe₂P or FeS in proportions that

approximate the $\text{Fe}^{3+} / \Sigma \text{Fe}$ values calculated for the selected experimental conditions. Oxygen fugacity in the experimental capsules was regulated using the conventional double-capsule, metal-metal oxide + water configuration (Chou and Cygan, 1990).

Table 4-1: Starting compositions for experimental melts (wt%). H_2O , P and S values are wt% total wt. oxides; P and S comprise 6.66×10^{-4} mols/gram of total weight oxides.

Sample	SiO_2	$\text{FeO}_{\text{total}}$	Al_2O_3	K_2O	H_2O	P	S
A-1	60.05	27.27	1.87	1.72	9.09	-	-
AP-1	59.50	27.03	1.86	1.70	9.01	2.06	-
AS-1	58.97	26.79	1.89	1.69	8.93	-	2.14

Experimental capsules were prepared by loading the desired quantity of starting material, or starting material + H_2O , into a 2 mm. (outside diameter) platinum capsule. Experimental capsules were loaded into a 5 mm. (outside diameter) platinum capsule containing H_2O and one of the selected solid-oxide oxygen buffers, QFM, NNO or MH. Both inner experimental capsules and outer buffer-bearing capsules were sealed by welding.

Experimental capsules were heated in KanthalTM or platinum-wound furnaces placed in a rapid-quench, internally heated pressure vessel under isobaric conditions (200 +/- 10 MPa). Capsules were heated isothermally at 1100 °C or 1200 °C for two hours using argon as the pressure medium. A description of the furnace, quench method and the method used to determine chemical equilibrium in the experiments is given in section 2-3 of this thesis.

A part of the experimental product was mounted in epoxy and polished. Major element compositions of conjugate immiscible phases were analyzed with a Cameca SX-100 electron microprobe at the University of Manitoba. Analytical conditions were set to an accelerating voltage of 15kV, 15 nÅ beam current, with a beam diameter of 5-10 microns for silicate and Fe-rich glasses. Material for stable oxygen isotope analysis was prepared by magnetic separation of

finely-ground quench products under suspension in ethanol. The process was repeated until samples containing over 95% of the desired conjugate glass were produced. Oxygen isotope analyses were carried out using the BrF_5 procedure of Clayton and Mayeda (1963). The estimated uncertainty in the isotope analyses is ± 0.2 permil. All values are reported in the δ notation ($\delta^{18}\text{O} = \{[(^{18}\text{O}/^{16}\text{O})_{\text{sample}} / (^{18}\text{O}/^{16}\text{O})_{\text{standard}}] - 1\} * 1000$) in units of permil relative to VSMOW.

4.4 Results

Six of the experiments produced immiscible Si-rich felsic silicate and Fe-rich mafic silicate (L^f and L^m) conjugate liquids (Table 4-2) from which the phases could be separated. Differences in the $\delta^{18}\text{O}$ values of the conjugate liquids in the two-liquid field range from 0.4 - 0.8 permil at 1100 °C, and from 0 to 0.4 permil at 1200 °C. The Si-rich liquid is more ^{18}O -rich, as is expected given the correlation between ^{18}O enrichment and the concentration of network-forming components that has been documented for silicate minerals (Taylor and Epstein, 1962).

Composition AS-1, run at $f\text{O}_2 = \text{MH}$, $T = 1200$ °C, produced 3 liquids, an Si-rich liquid, an Fe-rich liquid and an Fe-S-O liquid. The differences in the $\delta^{18}\text{O}$ values of the conjugate Si- and Fe-rich liquids in equilibrium with the Fe-S-O liquid is 0.2 permil, but in contrast to all other experiments, the Fe-rich liquid is more ^{18}O rich.

4.5 Discussion

The addition of H_2O alone and with P or S, to the systems Fe_2SiO_4 - Fe_3O_4 - KAlSi_2O_6 - SiO_2 , Fe_2SiO_4 - Fe_3O_4 - Fe_2O_3 - KAlSi_2O_6 - SiO_2 , and Fe_3O_4 - Fe_2O_3 - KAlSi_2O_6 - SiO_2 widens the two-liquid immiscibility field at temperatures between 1075 °C and 1200 °C, producing conjugate

liquids with strongly divergent compositions (Watson, 1976; Visser and van Groos, 1979; Lester, 2002).

Table 4-2: Major element compositions and $\delta^{18}\text{O}$ values for conjugate immiscible glasses in the systems $\text{Fe}_2\text{SiO}_4\text{-Fe}_3\text{O}_4\text{-KAlSi}_2\text{O}_6\text{-SiO}_2$, $\text{Fe}_3\text{O}_4\text{-KAlSi}_2\text{O}_6\text{-SiO}_2$ and $\text{Fe}_3\text{O}_4\text{-Fe}_2\text{O}_3\text{-KAlSi}_2\text{O}_6\text{-SiO}_2$ S or P, $P=200$ MPa. Chemical compositions represent an average of 9 electron microprobe analyses of conjugate Fe-rich (L^m) and Si-rich (L^f) glasses.

Sample	Temperature °C	$f\text{O}_2$		SiO ₂	FeO	Al ₂ O ₃	K ₂ O	P	S	$\delta^{18}\text{O}$	$\Delta^{18}\text{O}$ $\delta^{18}\text{O } L^f - \delta^{18}\text{O } L^m$
A-1	1100	QFM	L^f	84.66	6.43	2.90	2.57			13.8	0.5
			L^m	40.84	51.28	1.30	1.21	0.05		13.3	
AP-1	1100	NNO	L^f	66.05	17.86	7.61	5.57	0.54		12.5	0.8
			L^m	29.8	54.32	3.66	2.04	1.79		11.7	
AS-1	1100	NNO	L^f	88.38	7.94	2.43	1.72		0.1	12.7	0.4
			L^m	25.61	68.26	1.06	0.97		3.42	12.3	
A-1	1200	NNO	L^f	79.42	11.59	2.71	2.03			12.5	0.4
			L^m	40.05	55.69	1.91	0.76			12.1	
AP-1	1200	MH	L^f	82.06	6.79	4.32	4.22	0.36		18.6	0.3
			L^m	26.47	57.39	1.83	0.74	1.45		18.3	
AP-1	1200	QFM	L^f	84.66	6.43	2.90	2.57	0.01		13.4	0
			L^m	40.84	51.28	3.30	1.20	0.05		13.4	
AS-1	1200	MH	L^f	78.74	9.23	4.70	3.81		0.09	12.2	-0.2
			L^m	33.49	55.28	1.62	1.47		3.12	12.4	

In this study, Fe-rich liquids (L^m) contain 42-61 wt% more $\text{FeO}_{\text{total}}$ and 34 to 58 wt% less SiO_2 than conjugate Si-rich liquids (L^f) (Table 4-2). In comparison, conjugate melts in the anhydrous system $\text{Fe}_2\text{SiO}_4\text{-KAlSi}_2\text{O}_6\text{-SiO}_2$ at 1180°C differ by only 16-17 wt% FeO and 17-24 wt% SiO_2 (Kyser et al., 1998). If ^{18}O proportioning between the immiscible liquids is controlled by the relative abundance of tetrahedral Si-O and Al-O bonds in the two melts, as suggested by experimentally and theoretically determined fractionation factors for mineral pairs by O'Neil (1986) and Kyser (1987), then $\Delta^{18}\text{O}$ ($\delta^{18}\text{O } L^f - \delta^{18}\text{O } L^m$) values for the more compositionally diverse melts generated through the addition of H_2O with or without, P or S should be greater

than those reported for the anhydrous system. However, the $\Delta^{18}\text{O}$ values of the volatile-rich conjugate melts pairs synthesized herein do not differ significantly from those of the anhydrous system. The $\Delta^{18}\text{O}$ values for melts with or without H_2O are nearly identical, ranging from 0.4 - 0.6 permil, regardless of experimental $f\text{O}_2$ (Figure 4-1).

No oxygen isotope fractionation data between immiscible melts in the systems Fe_3O_4 - Fe_2O_3 - KAlSi_2O_6 - SiO_2 + P or S have been reported, so a comparison of $\Delta^{18}\text{O}$ values in melts with or without H_2O in combination with P and S cannot be made. To test the relationship between oxygen isotope fractionation and differences in the degree of melt polymerization produced by varying melt composition and $f\text{O}_2$, we use the parameter $(\text{nbo}/\text{t}^{\text{m}})/(\text{nbo}/\text{t}^{\text{f}})$, where nbo = number of non-bridging oxygens in the melt, t: tetrahedrally-coordinated network-forming cations; f: the felsic-silicate melt and m: the mafic silicate melt, (Bogaerts and Schmidt, 2006) to describe the proportioning of oxygen bound in tetrahedral coordination between the conjugate melts.

Oxygen isotope proportioning as a function of the ratio of nbo/t (L^{m}) to nbo/t (L^{f}) in the conjugate melts (Figure 4.2) indicates no correlation between $\Delta^{18}\text{O}$ values and the proportioning of tetrahedral oxygen between conjugate melts in the anhydrous experiments, or in experiments with H_2O , or H_2O + S (Figure 4.2). In contrast, the $\Delta^{18}\text{O}$ values of glasses with H_2O + P record a negative correlation with nbo/t (L^{m}) to nbo/t (L^{f}). Melts in the H_2O -bearing experiments are in equilibrium with a vapour phase and are considered to be oversaturated with respect to H_2O .

The depolymerizing effects of such high concentrations of H_2O in the experimental melts are not considered in the calculation of nbo/t values here. However, even if the Si-Al network structure in the melts were fully depolymerized by the inclusion of H_2O , as has been demonstrated in some hydrous silicate melts (e.g. $\text{NaAlSi}_3\text{O}_8$ - H_2O : Mysen, 1991), the $\Delta^{18}\text{O}$

values of conjugate liquids should correlate with the partitioning of SiO_2 or $\text{FeO}_{\text{total}}$. No such correlation is observed in the melts produced here.

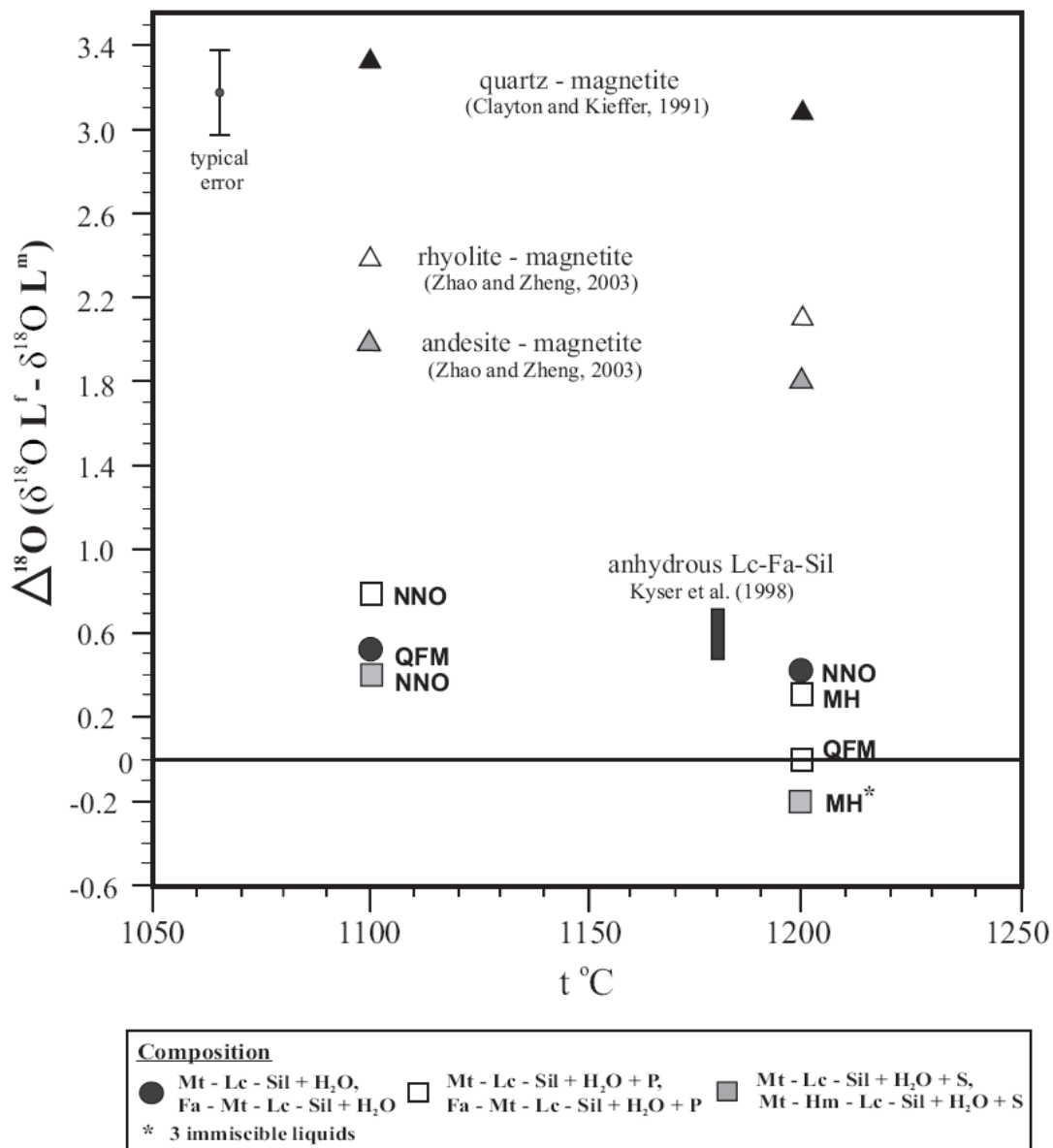


Figure 4-1: $\Delta^{18}\text{O}$ between coexisting Si- and Fe-rich glasses, melt-mineral pairs and mineral-mineral pairs at temperatures of 1100 °C, 1180 °C, and 1200 °C. The pressures are 200 MPa for the experiments in this study and 0.1 MPa for Kyser et al. (1998). $\Delta^{18}\text{O}$ values between melt-mineral pairs and mineral-mineral pairs are theoretical.

The temperature dependence of oxygen isotope fractionation between the conjugate melts is small over the experimental range of 1100 °C - 1200 °C. However, the $\Delta^{18}\text{O}$ values for all compositions with H_2O , and $\text{H}_2\text{O} + \text{P}$ at 1100 °C are slightly greater than those recorded at 1200 °C (Figure 4-1). The trend is consistent with the negative temperature dependence of isotopic fractionation in melt-mineral and mineral-mineral pairs of similar compositions (e.g., Zhao and Zheng, 2003; Clayton and Kieffer, 1991), although the magnitude of the fractionation is much smaller for the melt-melt systems in this study.

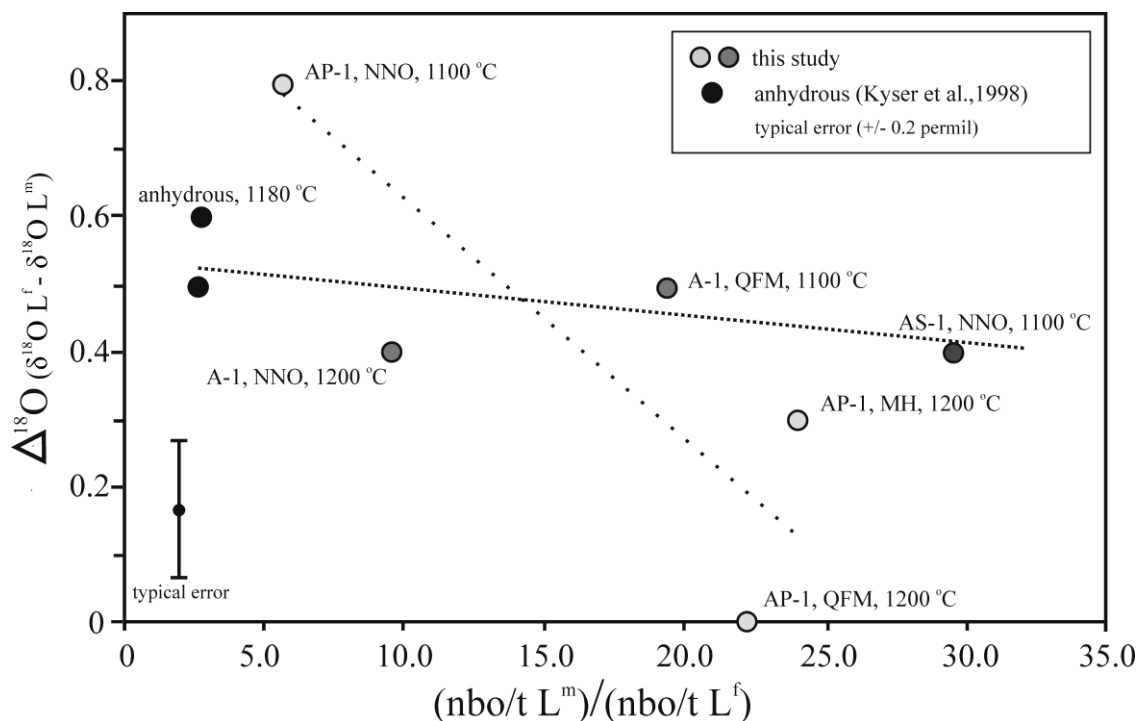


Figure 4-2: Oxygen isotope proportioning as a function of tetrahedral oxygen partitioning in conjugate immiscible Si- and Fe- rich glasses at temperatures of 1100 °C, 1180 °C, and 1200 °C, $P = 200$ MPa and 0.1 MPa (Kyser et al., 1998). Disparity in the degree of melt polymerization between conjugate-liquid pairs increases from left to right.

Variation in the $\Delta^{18}\text{O}$ values of the melts as a function of $f\text{O}_2$ can be isolated in the systems Fa-Mt- Lc-Sil + $\text{H}_2\text{O} + \text{P}$ and Mt-Hm-Lc-Sil + $\text{H}_2\text{O} + \text{P}$ at 1200 °C, $\Delta^{18}\text{O}$ values are

slightly higher at the more oxidizing conditions, showing an increase of 0.3 permil at MH over QFM. In theory, variations in fO_2 could affect oxygen isotope proportioning in silicate melts by influencing the nature and distribution of oxygen-cation bonds between the conjugate melts, e.g. the concentrations of, and partitioning between, melts of Fe_2SiO_4 , Fe_3O_4 and Fe_2O_3 (Kress and Carmichael, 1991) and S^{2-} and SO_4^{2-} (Carroll and Webster, 1994; Moretti and Ottonello, 2003). However, the effect observed in the $H_2O + P$ -bearing systems is not significant over the fO_2 range of the experiments (QFM-MH).

Comparison of theoretically-proposed $\Delta^{18}O$ values at 1100 °C and 1200 °C for andesite-magnetite, rhyolite-magnetite and quartz-magnetite pairs (Figure 4-1) show that ^{18}O proportions preferentially into the Si-rich phase but $\Delta^{18}O$ values for the melt-mineral and mineral-mineral pairs are significantly higher than those observed for the immiscible melts. Although the compositional range of the melt-mineral and mineral-mineral pairs is broadly analogous to the melt compositions in the present study, their theoretical $\Delta^{18}O$ values are not good proxies for immiscible silicate melts.

4.6 Concluding remarks

Liquid-phase separation in silicate melts with H_2O and $H_2O + P$ or S is attended by variations in the distribution of oxygen isotopes in conjugate melts. Thus the $\delta^{18}O$ values of the silicate-rich liquid are 0-0.8 permil higher than those of the Fe-rich liquid. Although the preferential fractionation of ^{18}O into the silicate melts is consistent with crystallochemical effects on oxygen isotope distribution trend determined for mineral-mineral and melt-minerals pairs, the variation in ^{18}O ratios in immiscible melts does not correlate with variations in the distribution of Si-O and Al-O networks between the immiscible melts examined here. No systematic change

occurs in oxygen isotope proportioning in the conjugate melts as the result of varying fO_2 over the range QFM-MH. The $\Delta^{18}O$ values for immiscible liquids as well as the variation in $\delta^{18}O$ values that results from the presence of small, geologically reasonable quantities of network-modifying constituents in the melts suggest that the variations in oxygen isotope ratios cannot be used to identify the involvement of liquid-phase separation in volatile-rich silicate melts.

Chapter 5

DISCUSSION

5.1 Introduction

Subsequent to reviewing fluid and melt inclusion evidence for liquid immiscibility in magmatic differentiation, Edwin Roedder (1991), whose investigation of silicate-liquid immiscibility comprised over 6000 experiments, noted that (p. 5) “complete unequivocal statements of the course of evolution of the fluids in such natural systems may never be possible”. Nonetheless, the data presented herein serve to broaden significantly understanding of the controls on miscibility gaps in volatile-rich silicate melts and thereby to improve the interpretation of data obtained from natural systems by characterizing some of the effects of common magmatic constituents on liquid-phase separation.

In the course of designing experiments to investigate igneous processes, researchers commonly choose between natural samples or compositions and chemically-simplified analogues of natural systems. The latter approach was selected for the present research because it represents a progressive, incremental, first step out from studies of immiscibility in anhydrous silicate melts. Further, because of the sensitivity of two-liquid systems to minor changes in composition and temperature, the application of experimental data obtained from natural compositions is likely to be applicable to a limited range of P - T - X conditions. In contrast, studies of chemically-simplified silicate melts have identified general trends in system behaviour that have in the main part proven applicable to more complex natural melts, e.g., the effects of individual major oxide melt constituents and proportions on the temperature-composition

stability of miscibility gaps (Bogaert and Schmidt, 2006; Watson, 1976; Naslund, 1983; Visser and van Groos, 1970).

The following subsections discuss some of the implications, applications and limitations, of the results of this study, and outline specific approaches to clarify further liquid phase separation in silicate melts and its role in petrogenesis.

5.2 Phase relations of volatile-rich immiscible silicate melts.

The occurrence of stable liquid immiscibility in natural silicate melts is dependent on the position of the low temperature surface of the two-liquid field relative to the system liquidus. The phase assemblage data reported for the systems considered here (Figure 2-2) show that H₂O alone, or in combination with P, S or F, acts to lower the liquidus surface and affect element partitioning such that both the temperature and composition range of the two-liquid fields are increased relative to those of compositionally equivalent anhydrous melts. The expansion of the miscibility gap that results from the addition of network-modifying constituents to the chemically-simplified systems considered here is likely to extend to more complex natural melts, but the extent of expansion and the relative positions of the boundary between the liquidus and two-liquid field in volatile-rich natural systems are expected to vary as a function of composition. Melt parameters that directly or indirectly affect the configuration of the liquidus, such as the coordination of Ca, the availability of cations to charge-balance tetrahedrally-coordinated Fe³⁺ and Al, and the inclusion of Mg and Ti, will plausibly change the extent and the configuration of the liquidus-binodal intersect from the results presented here. The following experiments are suggested to constrain further the phase behaviour of volatile-rich silicate melts such that the data can be applied directly to liquid-phase separation in natural

magmatic systems. Phase assemblage and major element partition data should be obtained for glasses produced from synthetic melts with compositions in the complex systems FeO_x - KAlSi_3O_8 - SiO_2 - CaO - MgO - TiO_2 - H_2O +/- P, S and F that more closely approximate natural melts and used for comparison with the results of this study and those of Bogaerts and Schmidt (2006), thereby identifying systematic changes that occur in the two-liquid field. The results would provide a more complete and accurate means to discriminate between coexisting Fe- and Si- rich lithologies that have undergone liquid-phase separation and those produced by crystal fractionation.

The phase relations of the system FeO_x - KAlSi_2O_6 - SiO_2 - H_2O -S are complex. The $f\text{O}_2$ dependence of the liquid-phase assemblages and the commensurate sensitivity of the system to any parameter that effects $f\text{O}_2$, considered in conjunction with the potential for significant partitioning of transition metals between the three liquids, suggest the need for further study to define the T - X - $f\text{O}_2$ limits of the three-liquid miscibility gap and to evaluate the potential role of three-liquid phase separation in the evolution of some ore deposit types, e.g. iron oxide +/- copper-gold deposits (Naslund et al., 2003) and magmatic sulfide deposits such as those of the Duluth Complex (Ripley et al., 1998). Of particular interest are the constraints imposed by melt composition and $f\text{O}_2$ on sulfide-liquid saturation in two-liquid systems and trace element partitioning between three-liquid immiscible melts as well as the partitioning of elements between liquid and mineral phases.

The most important implication of this study may be the inferred increased pressure range of two-liquid fields in H_2O -rich melts and the potential for the generation of immiscible melts in supra-subduction zones (section 2.4.5). The conjecture, based on the H_2O -induced liquidus suppression observed in the melt-systems studied here, the experimental study of

liquidus suppression in the basaltic system (Medard and Grove, 2008), the molar properties of hydrous silicate melts at high pressure (e.g. Hack and Thompson, 2010), and the H₂O enrichment in volatile-rich, primary melts (Grove et. al., 2006), although theoretically sound, requires rigorous testing to evaluate the *P-T-X* limits of two-liquid fields in hydrated melts at high pressure. To test the inferred stability of two-liquid fields in more complex analogues of natural magmas, experimental melts with compositions in the system FeO_x-KAlSi₃O₈-SiO₂-H₂O- CaO-MgO +/-P and S at temperatures of 1100 °C, 1200 °C and 1300 °C and pressures of 1.5 and 2.5 GPa, could be synthesized, and analytical data from the quenched run products used to constrain the *P-T-X* behavior of two-liquid fields in subduction-zone environments.

5.3 Trace element partitioning between volatile-rich immiscible silicate melts

The results of this (e.g., Figure 3-1) and previous studies of trace element partitioning between both chemically-simplified (Vincenzi et al., 1994; Watson, 1976), and natural immiscible silicate melts (e.g. Shearer, 2001) suggest that patterns of trace element partitioning between Si-rich and Fe-rich liquids in two-liquid systems can potentially provide a means to identify rocks produced by liquid-phase separation. Partitioning trends of REE are nearly independent of melt composition. The magnitude of the partition coefficients of individual elements varies as a function of composition, but in most of the experimental melts the relative change in magnitude is consistent across the suite of REEs and therefore the partitioning trends remain the same. In contrast, the partitioning behaviour of transition metals in the experimental melts varies significantly as a function of the inclusion of H₂O, P, S or F in the melt.

Experimentally determined transition metal partition patterns can potentially be used as a means to discriminate between lithologies formed by liquid phase separation and those produced

by crystal fractionation, but the sensitivity of transition metal partitioning behavior to minor variation in melt composition, particularly network-modifying components, suggests that partitioning data from immiscible melts that include a broad range of more complex natural compositions are required to more accurately predict transition metal partitioning trends between natural, immiscible magmas. Natural magmas generally contain multiple network-modifying volatile components and the partitioning data from melts with both P and S (Table 3-2) demonstrate that the effect of multiple network modifiers on transition metal partitioning is not trivial.

Direct application of melt-melt partitioning data to natural samples is limited to whole-rock composition data from coexisting magmas or partitioning data from melt inclusions, because melt-melt partitioning patterns are likely to be altered during progressive crystallization of the magma. The limitation could be addressed, in part, by determining partitioning data between immiscible melts and primary liquidus mineral phases. For example, Fe-rich lithologies that have been interpreted as originating from silicate liquid-phase separation, such as Kiruna and El Laco- type iron-oxide deposits, contain significant quantities of magnetite. Data from experiments that rigorously define trace element partitioning trends between Fe- and volatile - rich immiscible liquids and magnetite could provide a basis for assessing the role of immiscibility in some natural systems.

5.4 Stable isotopes

Oxygen isotope fractionation values determined for immiscible silicate melts in this study and by Kyser (1998) are probably too small (0-0.8 permil), to serve as a means to recognize the involvement of immiscibility in natural samples. It cannot, however, be assumed that the limited

range of fractionations observed for oxygen isotopes in the experimental melts studied herein extends to other stable-isotope systems. Studies of Fe-rich magmatic systems that have arguably undergone liquid phase separation generally contain significant amounts of sulphur and become saturated with sulphide minerals at some point in their liquid lines of descent (Laroque and Stimac, 2000). Further, it is likely that the liquid line of descent for many of these magmas intersect T - X - fO_2 conditions in which sulphur would occur as both sulfide and sulphate species in the melt. The $\delta^{34}\text{S}_{(\text{sulphate-sulphide})}$ values calculated for natural basalt samples at 1200 °C exceed 2 permil (Yang and Lentz, 2009). The magnitude of ^{34}S fractionation (above), considered in conjunction with the partitioning of sulphide and sulphate between the conjugate liquids, suggests that investigation of the fractionation of sulfur stable isotopes between conjugate immiscible liquids could provide a useful method to evaluate an immiscible petrogenetic hypothesis in natural samples. Other possible isotope systems that may display significant fractionation include redox-sensitive elements such as H, C, Mo, Fe and U.

SUMMARY AND CONCLUSIONS

**6.1 Experiments on liquid immiscibility in silicate melt with H₂O, P, S, F and Cl:
implications for volatile-rich natural magmas**

The addition of H₂O alone or in combination with small amounts of P, S or F (1, 2, and 6 wt% oxide totals respectively) to melts in the systems Fe₂SiO₄-Fe₃O₄-KAlSi₂O₆-SiO₂, Fe₃O₄-KAlSi₂O₆-SiO₂ and Fe₃O₄-Fe₂O₃-KAlSi₂O₆-SiO₂ expands the *T-X* range of the two-liquid miscibility gap. P and S partition strongly into the mafic melt, whereas F is nearly equally partitioned between the conjugate melts. Liquid phase separation in melts with H₂O + Cl is restricted to a narrow composition range as the result of the Cl-induced increase in the stability of silica minerals. The addition of 2 wt% S to the system Fe₃O₄-Fe₂O₃-KAlSi₂O₆-SiO₂ stabilizes three immiscible melts, with Fe-rich mafic silicate, Fe-poor felsic silicate, and FeS compositions.

Power-law curves calculated for D_i - nbo/t^f relationships for the elements Fe, Si, and P in the melts produced in this study are similar to, but distinct from, those calculated for the same elements in immiscible basaltic melts. The results show that the power-law equations calculated for the basaltic system by Bogaerts and Schmidt, (2006) can be applied to assess coexisting volatile rich magmas over a wide range of *P-T-X-fO₂* conditions. Further, the method is applicable even if the H₂O and Fe³⁺ contents of the magmas are not considered in calculating the polymerization parameter, nbo/t^f .

Water-induced suppression of liquidus temperatures in the experimental systems, considered with the effects of pressure on the temperature and composition ranges of two-liquid

fields in silicate melts, suggests that liquid phase separation may occur in some H₂O-rich silicate magmas at pressures up to 2GPa.

6.2 Effect of H₂O, P, S, F, and Cl on trace element partitioning in immiscible silicate melts

Trace element partition coefficients calculated for experimental melts confirm the prediction that H₂O, alone or in combination with geologically reasonable quantities of P, S, F or Cl, influences trace element partitioning behaviour between conjugate immiscible liquid pairs. The addition of H₂O to experimental melts significantly increases the partitioning of HFSE's and REE's into the Fe-rich melt relative to anhydrous melts of similar composition, regardless of fO_2 . Preferential partitioning of Rb and Cs into the silicate-rich melt for anhydrous immiscible systems is strongly reduced or reversed in the H₂O-bearing melts produced here, particularly those with F. REE partitioning trends in the experimental melts generally conform to those observed in rocks formed from volatile-rich, conjugate Fe- and Si- rich magma pairs, although the partitioning of these elements into the Fe-rich melt is predicted to be greater in volatile-rich systems. REE and HFSE partitioning trends are generally sub-parallel, regardless of initial melt composition, but partitioning trends for transition elements vary significantly as a function of the species of the network-modifiers in the melt and, to a lesser degree, on the major element composition.

Magma generally contains multiple network-modifying constituents, such as H₂O, P, S, F and Cl, and trace element partitioning trends in natural two-liquid systems will reflect the combined effects of these components. The data herein clearly demonstrate that liquid phase separation is an effective mechanism for concentrating a broad array of trace elements in FeO-rich melts. Some of the transition element partitioning patterns that result from the inclusion of

H₂O, P, S, F or Cl in the immiscible melts produced in this study (Figure 2-1) are remarkably similar to element enrichment trends observed in some ore deposit types such as iron oxide-copper-gold (Naslund et al., 2003) and Cu- Mo-Au porphyry (Aude'tat and Pettke, 2006) systems. These results demonstrate the need for further study of the potential role played by silicate liquid immiscibility in the evolution of magmatic-hydrothermal ore systems.

REE partitioning trends in Fe- and Si- rich lithologies that result from the liquid-phase separation of volatile-rich magmas should conform to the general pattern observed in the data collected in this study, but conjugate-immiscible magmas with H₂O, P, S, F, or Cl are subject to continued chemical evolution, including the exsolution of a vapour phase, magmatic recharge and the assimilation of country rock, that may alter melt-melt trace element partitioning trends. The further investigation of the effects of multiple network-modifying components on trace element partitioning in immiscible melts with more complex natural compositions is warranted to more accurately predict trace element partitioning in natural systems.

6.3 Oxygen isotopic partitioning in immiscible silicate liquids with H₂O, P and S

$\Delta^{18}\text{O}$ values ($\delta^{18}\text{OL}^m - \delta^{18}\text{OL}^f$) for conjugate Si-rich and Fe-rich immiscible melts in the systems Fe₂SiO₄-Fe₃O₄-KAlSi₂O₆-SiO₂, Fe₃O₄-KAlSi₂O₆-SiO₂ and Fe₃O₄-Fe₂O₃-KAlSi₂O₆-SiO₂ with 10 wt% H₂O, +/- P or S are only 0.4- 0.6 permil and do not differ significantly from the $\Delta^{18}\text{O}$ values of anhydrous melt pairs of similar composition. $\Delta^{18}\text{O}$ values for melts with added H₂O + P or S range more variably, from 0-0.8 permil. Although ¹⁸O preferentially partitions into the Si-rich melt as was previously observed in melt-mineral and mineral-mineral pairs wherein ¹⁸O is enriched in the more polymerized phase, the limited ¹⁸O proportioning in the network modifier-bearing immiscible melts indicates that the relative degree of polymerization and *f*O₂ do not

significantly affect oxygen isotope partitioning. The small range of $\Delta^{18}\text{O}_{L^m/L^f}$ values (<1 permil), and the variation in the $\delta^{18}\text{O}$ values between conjugate melts that occurs with the inclusion of network-modifying constituents, suggest that theoretically-derived melt-mineral pairs are not good analogues for melt-melt partitioning of oxygen isotopes, and that variations in conjugate-melt oxygen isotope ratios cannot be reliably used as a means to identify liquid-phase separation in petrogenesis.

6.4 Concluding remarks

This study constitutes an extension of the experimental investigation of silicate liquid immiscibility that has been ongoing for over 80 years. Beginning with Greig's (1927) investigation of liquid phase separation in binary oxide melts, the compositions of the experimental melts used have systematically progressed to more chemically-complex systems and a wider range of P - T - $f\text{O}_2$ conditions in an attempt to understand the role of liquid-phase separation in natural melts. With the addition of the data presented herein to those presented in previous investigations, the effects of all of the common major and minor elemental components of magmas on silicate immiscibility have now been surveyed. Nonetheless, a robust understanding of the role of silicate liquid immiscibility in magmatic systems and petrogenesis has yet to be achieved. Significant progress can be made toward this objective by the implementation of the research proposed in section 5.2, particularly the investigation of the hypothesis that two-liquid fields may be stable in magmas in supra-subduction zone P - T - X regimes. Understanding the extent and nature of silicate liquid phase separation in magmatic systems is important because the process can segregate, concentrate and spatially redistribute elements on a cumulatively significant scale.

References

- Almeev, R., Holtz, F., Koepke, J., Parat, F., and Botcharnikov, R.E., 2007, The effect of H₂O on olivine crystallization in MORB: experimental calibration at 200 MPa: *American Mineralogist*, v. 92, p. 670-674.
- Aude'tat, A., and Pettke, T., 2006 Evolution of a porphyry-Cu mineralized magma system at Santa Rita, New Mexico (USA): *Journal of Petrology*, v. 47, 10, p. 2021–2046.
- Botcharnikov, R.E., Almeev RR, Koepke, J., and Holtz, F., 2008, Phase relations and liquid lines of descent in hydrous ferrobasalt -implications for the Skaergaard intrusion and Columbia River flood basalts: *Journal of Petrology*, v. 49, 9, p.1687-1727.
- Bogaerts, M., and Schmidt, M.W., 2006, Experiments on silicate immiscibility in the system Fe₂SiO₄-KAlSi₃O₈-SiO₂-CaO-MgO -TiO₂-P₂O₅: *Contributions to Mineralogy and Petrology*, v. 152, p. 257-274.
- Bowen, N.L., 1925, Concerning evidence of immiscibility in a silicate magma, Agate Point, Ontario. *Journal of Geology*, v. 23, p.629-631.
- Carroll, M.R., and Webster, J.D., 1994, Solubilities of sulfur, noble gases, nitrogen, chlorine, and fluorine in magmas: In: Carroll MR, Holloway JR (eds) *Volatiles in magmas*, Mineralogical Society of America, *Reviews in Mineralogy*, v. 30, p.231-279.
- Chen H., Clark A.H., Kyser T.K., Ullrich, T.D., Baxter, R., Chen, Y., and Moody, T.C., 2010, Evolution of the giant Marcona-Mina Justa iron oxide-copper-gold district, south-central Peru: *Economic Geology*, v.105,1, p.155-185.
- Chou, M., and Cygan, G.L., 1990, Quantitative redox control and measurement in hydrothermal experiments, In: *Fluid–Mineral Interactions: A Tribute to H. P. Eugster*: Geochemical Society Special Publication (Spencer, R.J., Chou, I-M., eds.) v.2, p.3-15.

- Clark, A.H., and Kontak, D.J., 2004, Fe-Ti-P oxide melts generated through magma mixing in the Antauta subvolcanic center, Peru: implications for the origin of nelsonite and iron oxide-dominated hydrothermal deposits: *Economic Geology*, v. 99, 2, p.377-395.
- Clayton, R.N., and Kieffer, S.W., 1991, Oxygen isotopic thermometer calibrations: *In Stable Isotope geochemistry: A Tribute to Samuel Epstein*, The Geochemical Society Special Publication., v .3, p.3-10.
- Clayton, R.N., and Mayeda, T.K., 1963, The use of bromine pentafluoride in the extraction of oxygen from oxides and silicates for isotopic analysis: *Geochimica et Cosmochimica Acta*, v .27, p. 43-52.
- Darling, R.S., and Florence, F.P., 1995, Apatite light rare earth element chemistry of the Port Leyden nelsonite, Adirondack Highlands, New York; implications for the origin of nelsonite in anorthosite suite rocks: *Economic Geology*, v. 90, 4, p.964-968.
- Dixon, S., and Rutherford, M.J., 1979, Plagiogranites as late-stage immiscible liquids in ophiolite and mid-ocean ridge suites: an experimental study: *Earth and Planetary Science Letters*, v. 45, p.45–60.
- Dolejs, D., and Baker, D.R., 2007, Liquidus Equilibria in the system $K_2O-Na_2O-Al_2O_3-SiO_2-F_2O_{1-H_2O}$ to 100 MPa: Differentiation paths of fluorosilicic magmas. In hydrous systems: *Journal of Petrology*, v. 48, 4, p.807-828.
- Freestone, I.C., and Powell, R., 1983, The low temperature field of liquid immiscibility in the system $K_2O-Al_2O_3-FeO-SiO_2$ with special reference to the join fayalite-leucite-silica: *Contributions to Mineralogy and Petrology*, v .82, p.291-299.
- Frost, R.B., 1991, Introduction to oxygen fugacity and its petrologic importance: in *Oxide minerals: Petrologic and magnetic significance* (Lindsley D.H., ed.), *Reviews in Mineralogy*, v. 25, p.5-24.

- Gaetani, G.A., Grove, T., and Bryan, W.B., 1994, Experimental phase relations of basaltic andesite from Hole 839b under hydrous and anhydrous conditions, *In Proceedings of the Ocean Drilling Program, Scientific Reports*, Hawkins, J.W. et al., (eds), v. 135, 32 p. 557-563.
- Grieg, J.W., 1927, Immiscibility in silicate melts: *American Journal of Science*, v.13, p. 1-154.
- Grove, T.L., Chatterjee, N., Parman, S.W., and Médard, E., 2006, The influence of H₂O on mantle wedge melting: *Earth and Planetary Science Letters*, v. 249, p.74–89.
- Hamilton, D.L., Frestone, I., Dawson, F., and Donalson, C.H., 1979, Origin of carbonatites by liquid immiscibility: *Nature*, v. 279, p.52-54.
- Hack, A.C., and Thompson, A.B., 2011, Density and viscosity of hydrous magmas and related fluids and their role in subduction zone processes: *Journal of Petrology* v. 52, 7-8, p.1333-1362.
- Haughton, D.H., Roeder, P.L., and Skinner, B.J., 1974, Solubility of sulfur in mafic magmas: *Economic Geology*, v. 69,4, p.451-467.
- Hess, P.C., and Daniel, G.H., 1974, Experimental liquid line of descent and liquid immiscibility for basalt 70017: *Proceedings of the 5th Lunar Science Conference*, v.1, p.569-583.
- Hess, P.C., Rutherford, M.J., Guillmette, R.N., Ryerson, F.J., and Tuchfeld, H.A., 1975, Residual products of fractional crystallization of lunar magmas: an experimental study: *Proceedings of the 6th Lunar and Planet Science Conference*, v. 1, p.895-909.
- Hitzman, M.W., Oreskes, N., and Einaudi, M.T., 1992, Geological characteristics and tectonic settings of Proterozoic iron oxide (Cu-U-Au-REE) deposits: (in Gaal, G., Schulz, K., eds.), *Precambrian Research*, v.58, p.241-287.
- Holloway, J.R., 1971, Internally heated pressure vessels: (in Ulmer, G.C., and Barnes, H.E., Eds.), *Research Techniques for High Temperature and Pressure*, Springer-Verlag, New York, p.217-257.

- Holloway, J.R., Dixon, J.E., and Pawley, A.R., 1992, An internally heated, rapid-quench, high-pressure vessel: *American Mineralogist*, v. 77, p.643-646.
- Hudon, P., and Baker, D.R., 2002, The nature of phase separation in binary oxide melts and glasses in silicate systems: *Journal of Non-Crystalline Solids*, v. 303, p.299-345.
- Johnson, K., Barnes, C.G., Browning, J. M., and Karlsson, H.R., 2002, Petrology of iron-rich magmatic segregations associated with strongly peraluminous trondhjemite in the Cornucopia stock, northeastern Oregon: *Contributions to Mineralogy and Petrology*, v. 142, 5, p. 564-581.
- Kress, V.C., and Carmichael, I.S.E., 1991, The compressibility of silicate liquids containing Fe₂O₃ and the effect of composition, temperature, oxygen fugacity and pressure on their redox states: *Contributions to Mineralogy and Petrology*, v. 108, p.82-92.
- Kyser, T.K., 1987 Equilibrium fractionation factors for stable isotopes: (In: Kyser, T.K., ed) *Short Course in Stable Isotope Geo-chemistry of Low Temperature Fluids*, Mineralogical Association of Canada, v.13, pp1-84.
- Kyser, T.K., 1990, Stable isotopes in the continental lithospheric mantle: (in: Menzies, M., ed.) *The Continental Lithospheric Mantle*. Oxford University Press, N.Y., pp 127-156.
- Kyser, T.K., Leshner, C.E., and Walker, D., 1998, The effects of liquid immiscibility and thermal diffusion on oxygen isotopes in silicate liquids: *Contributions to Mineralogy and Petrology*, v. 3, p. 373-381.
- Laroque, A., Stimac, J., Keith, J., and Huminiki, M., 2000, Evidence for open system behaviour in immiscible Fe-S-O liquids in silicate magmas: implications for contribution of metal and sulphur to ore-forming fluids: *Canadian Mineralogist*, v. 38, p.1233-1249.

- Lester, G.W., 2002, *The Effects of Excess H₂O and H₂O in Combination with F, Cl S, or P on Liquid immiscibility in the system Si- Fe-Al-K-O at 2 Kbar: Implications for the Genesis of Iron-oxide Magmas*: Unpublished M.A. thesis, State University of New York at Binghamton, p.66.
- Longhi, J., 1990, Silicate liquid immiscibility in isothermal crystallization experiments: Proceedings of the 20th Lunar and Planetary Science Conference, 20th, p.13-24.
- McBirney, A.R., 1975, Differentiation of the Skaergaard intrusion: *Nature*, v. 253, p. 691-694.
- Me´dard, A., and Grove, T., 2008, The effect of H₂O on the olivine liquidus of basaltic melts: experiments and thermodynamic models: *Contributions to Mineralogy and Petrology*, v. 155, p.417-452.
- Moore, G., Vennemann, T., and Carmichael, I.S.E., 1998, An empirical model for the solubility of H₂O in magmas to 3 kilobars: *American Mineralogist*, v. 83, p.36-42.
- Naldrett, A.J., 2005, A history of our understanding of magmatic Ni-Cu sulfide deposits: *Canadian Mineralogist*, v. 43, p. 2069-2098.
- Naldrett, A.J., 2010, Secular variation of magmatic sulfide deposits and their source magmas: *Economic Geology*, v. 105, p.669-688.
- Naslund, H.R., 1983, The effect of oxygen fugacity on liquid immiscibility in iron-bearing silicate melts: *American Journal of Science*, v. 283, p.1034-1059.
- Naslund, H.R., Henriquez, F., Nystrom, J.O., Aguirre, R., and Lledo, H., 2003, El Laco, Chile: evidence for the eruption of an immiscible Fe–O–S–P melt: *The Geological Society of America, 2003 Annual Meeting, Abstract with Programs, Geological Society of America*, v. 35, 6, p. 394.
- Nyström, J.O., and Henríquez, F., 1994, Magmatic features of iron ores of the Kiruna type in Chile and Sweden; ore textures and magnetite geochemistry: *Economic Geology*, v. 89, 4, p. 820-839.

- O'Neil, J.R., 1986, Theoretical and experimental aspects of isotope fractionations: (in: Valley, J.W., Taylor, H.P., and O'Neil, J.R., eds.) *Stable Isotopes in High Temperature Geological Processes*, Reviews in Mineralogy, Mineralogical Society of America, Washington, DC, v. 16, p. 1-37.
- Philpotts, A.R., 1976, Silicate liquid immiscibility: its probable extent and petrogenetic significance: *American Journal of Science*, v. 276, p. 1147-1177.
- Philpotts, A.R., 1982, Compositions of immiscible liquids in volcanic rocks: *Contributions to Mineralogy and Petrology*, v. 80, p. 201–218.
- Philpotts, A.R., 2008, Comments on: Liquid Immiscibility and the Evolution of Basaltic Magma; *Journal of Petrology*, v. 49, 12, p. 2171-2175.
- Philpotts, A.R., and Doyle, C.D., 1983, Effect of magmas oxidation state on the extent of silicate liquid immiscibility in a tholeiitic basalt: *American Journal of Science*, v. 283, p. 967-986.
- Pineau, F., Javoy, M., and Bottinga, Y., 1976, $^{13}\text{C}/^{12}\text{C}$ ratios of rocks and inclusions in popping rocks of the Mid-Atlantic ridge and their bearing on the problem of deep-seated carbon: *Earth and Planetary Science Letters*, v.29, p. 413-421.
- Rajesh, H.M., 2003, Outcrop-scale silicate liquid immiscibility from an alkali syenite (A-type granitoid)-pyroxenite association near Puttetti, Trivandrum Block, South India: *Contributions to Mineralogy and Petrology*, v. 145, p. 612-627.
- Ripley, E.M., 1998, Evidence for sulfide and Fe-Ti-P immiscibility in the Duluth Complex; *Minnesota: Economic Geology*, v. 93, p. 1052-1062.
- Roedder, E.W., 1951, Low temperature liquid immiscibility field in the system $\text{K}_2\text{O}-\text{FeO}-\text{Al}_2\text{O}_3-\text{SiO}_2$: *American Mineralogist*, v. 36, p. 282-286.
- Roedder, E.W., 1978, Silicate liquid immiscibility in magmas and in the system $\text{K}_2\text{O}-\text{FeO}-\text{Al}_2\text{O}_3-\text{SiO}_2$: an example of serendipity: *Geochimica et Cosmochimica Acta* , v.42, p. 1597-1617.

- Roedder, E.W., 1991 Fluid inclusion evidence for liquid immiscibility in magmatic differentiation: *Geochimica et Cosmochimica Acta*, v. 56,1, p. 5-20.
- Roedder, E.W., and Weiblen, P.W., 1971, Petrology of silicate melt inclusions, Apollo 11 and 12, and terrestrial equivalents: *Proceedings of the Lunar Science Conference*, 2nd, p. 507-528.
- Ryerson, F.J., and Hess, P.C. 1978, Implications of liquid-liquid distribution coefficients to mineral-liquid partitioning: *Geochimica et Cosmochimica Acta*, v. 42, p.921-932.
- Ryerson, .F.J., and Hess, P.C., 1980, The role of P₂O₅ in silicate melt: *Geochimica et Cosmochimica Acta* v.44, p. 611-624.
- Scrope, G.P., 1825, *Consideration on Volcanoes, the Probable Cause of their Phenomena, the Laws which Determine their March, the Disposition of their Product and the Connexion with the Present State and Past History of the Globe; Leading to the Establishment of a New Theory of the Earth*, W. Phillips, London, 270 pp.
- Schuessler, J. A., Roman, R.E., Botcharnikov, E., Behrens, H., Misiti, V., and Freda, C., 2008, Oxidation state of iron in hydrous phono-tephritic melts: *American Mineralogist* v. 93, p, 1493-1504.
- Shearer, C.K., Papike, J.J., and Spilde, M.N., 2001, Trace-element partitioning between immiscible lunar melts: An example from naturally occurring lunar melt inclusions: *American Mineralogist*, v. 3, 86, p. 238-246.
- Sillitoe, R.H., 2003, IOCG deposits: an Andean view: *Mineralium Depositum*, v. 38, p. 787-812.
- Taylor, H.P., Epstein, S., 1962, Relationship between ¹⁸O/¹⁶O ratios in coexisting minerals of igneous and metamorphic rocks part I: *Geological Society of America Bulletin*, v.73, p 461-480.

- Taylor, H.P., and Sheppard, S.M.F. 1986, Igneous rocks. I. Processes of isotopic fractionation and isotope systematic : (in: Valley J.W., Taylor H.P., O'Neil J.R., eds.) *Stable Isotopes in High Temperature Geological Processes*. Reviews in Mineralogy, 16, Mineralogical Society of America, p. 227-272.
- Ulmer, P., 2001, Partial melting in the mantle wedge and the role of H₂O in the genesis of mantle-derived arc-related magmas: *Physics of the Earth and Planetary Interiors*, v. 127, 1-4, p 215-232.
- Veksler, .IV., Dorfman, A.M., Danyushevsky, L.V., Jakobsen, J.K., and Dingwell, D.B., 2006, Immiscible silicate liquid partition coefficients: implications for crystal-melt element partitioning and basalt petrogenesis: *Contributions to Mineralogy and Petrology*, v. 152, p. 685-702.
- Vicenzi, E., Green, T., and Sie, S., 1994, Effect of oxygen fugacity on trace-element partitioning between immiscible silicate melts at atmospheric pressure: a proton and electron microprobe study: *Chemical Geology*, v. 117, p. 355-360.
- Visser, W., and Koster van Groos, A.F., 1979a, Phase relations in the system K₂O-FeO-Al₂O₃-SiO₂ at 1 atmosphere with special emphasis on low temperature liquid immiscibility: *American Journal of Science*, v. 279, p. 70-91.
- Visser, W., and Koster van Groos, A.F., 1979b, Effect of pressure on liquid immiscibility in the system K₂O-FeO-Al₂O₃-SiO₂- P₂O₅: *American Journal of Science*, v. 279, p.1160-1175.
- Visser, W., and Koster van Groos, A.F., 1979c, Effect of P₂O₅ and TiO₂ on liquid-liquid equilibria in the system K₂O-FeO-Al₂O₃-SiO₂: *American Journal of Science*, v. 279, p. 970-988.
- Wallace P.J., and Carmichael I.S.E. (1994) S speciation in submarine basaltic glasses as determined by XK α X-ray wavelength shifts. *American Mineralogist*, 79: p.161-167.
- Watson, E.B., 1976a, Two-liquid partition coefficients: experimental data and geochemical implications: *Contributions to Mineralogy and Petrology*, v. 56, p. 119–134.

- Watson, E.B., 1976b, *Experimental Studies Bearing on the Nature of Silicate Melts and their Role in Trace Element Geochemistry*. Ph.D. Thesis, Massachusetts Institute of Technology, Cambridge, USA.
- Watson, E.B., and Naslund, H.R., 1976 The effects of pressure on liquid immiscibility in the system $K_2O-FeO-Al_2O_3-SiO_2-CO_2$. *Carnegie Institute Yearbook*, 1976-77, p. 410-414.
- Webster, J.D., and De Vivo, B., 2002, Experimental and modeled solubilities of chlorine in aluminosilicate melts, consequences of magma evolution, and implications for exsolution of hydrous chloride melt at Mt. Somma-Vesuvius: *American Mineralogist*, v. 87, p. 1046-1061.
- Yang, X., and Lentz, D., 2009, Estimate of mole sulfate ratios in magmatic rocks: *Geochemical Journal*, v. 43, p. 371-377.
- Zhao, Z.F., and Zheng, Y.F., 2003, Calculation of oxygen isotope fractionation in magmatic rocks: *Chemical Geology*, v. 193, p. 59-80.

Appendix A

Experimental procedure

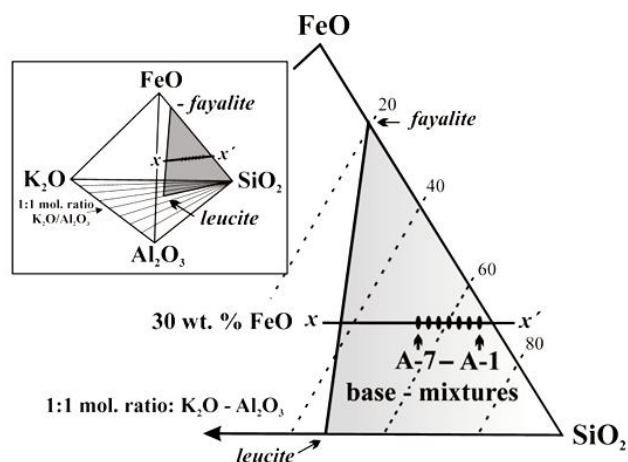
Facilities

All experiments were conducted at the Depths of the Earth Laboratories at the Department of Geological Sciences, Arizona State University, Tempe, Arizona. Dr. Gordon Moore was in charge of laboratory operations during the period the experiments these were conducted.

Materials

Starting materials for the experiments included seven anhydrous base compositions prepared from SiO₂ (cristobalite), Al₂O₃, K₂Si₂O₅, FeO and Fe₂O₃. Each base-mixture plots as a composition point on the 30 wt% FeO isopleth on the ternary join fayalite-leucite-silica. Base-compositions have an Al/K molar ratio of 1 (Table 2-1). To minimize the f_{O_2} gradient between melts and external solid buffers, $\text{Fe}^{3+} / \Sigma \text{Fe}$ values for the melts synthesized in this study were estimated with the method of Schuessler et al. (2008) at the quartz-fayalite-magnetite (QFM), nickel-nickel oxide (NNO) or magnetite-hematite (MH) oxygen buffers at, $T=1200$ °C and $P=200$ MPa. The 30 wt% FeO_{total} component of each base-mixture comprises FeO and Fe₂O₃, with Fe₂P, FeS, FeCl₂, or FeF₂ in proportions that approximate the $\text{Fe}^{3+} / \Sigma \text{Fe}$ values calculated for the selected experimental conditions. Oxygen fugacity in the experimental capsules was controlled using the conventional double capsule, metal-metal oxide or metal oxide-silicate + water configuration (Chou and Cygan, 1990).

Experimental starting compositions containing either 1 wt% P, 2 wt% S, 6 wt% Cl or 6 wt% F (total wt. oxides) were prepared by the addition of Fe₂P, FeS, FeCl₂, or FeF₂ to the anhydrous base- mixtures.



Base - mixture compositions A-7 - A-1 plot on the 30 wt.% FeO isopleth ($x - x'$) of the ternary join fayalite - leucite - silica. The join defines a plane bounded by the 1:1 molar ratio $K_2O - Al_2O_3$ segment in the composition system $SiO_2 - FeO - Al_2O_3 - K_2O$ (inset). Experimental starting compositions comprising base - mixtures and; H_2O , or H_2O and P, S, F, or Cl.

Base compositions (wt%).

base composition	SiO_2	FeO_{total}	Al_2O_3	K_2O	An_{50}^a
A - 1	66.05	30	2.06	1.89	-
A - 2	64.46	30	2.88	2.66	-
A - 3	62.86	30	3.71	3.43	-
A - 4	60.13	30	5.13	4.74	-
A - 5	57.48	30	6.51	6.01	-
A - 6	55.88	30	7.34	6.78	-
A - 7	54.32	30	8.15	7.53	-
An_{50}	65.2	29.62	2.03	1.87	1.3

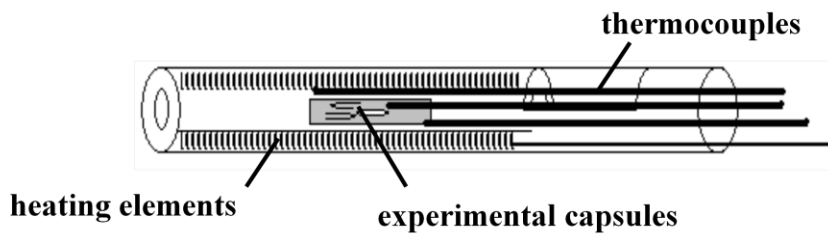
^a $(Ca_{.5} Na_{.5}) Al_{1.5} Si_{2.5} O_8$

Fe-salts were selected as the source of P, S F and Cl in order to minimize the loss of volatile components during the welding of experimental capsules.

Hydrous experiments incorporated 10 wt% H_2O (total wt. solids). Plagioclase-bearing experiments contain 1.3 wt% (total wt. solids) An_{50} , constituting 43 wt% of the normative feldspar component. The dry experiment components were weighed, mixed and ground 3 times under ethanol then dried and stored in an oven at $125^\circ C$.

Experiments were carried out by loading the desired quantity of starting material, or starting material + H₂O, into a 2mm (outside diameter) platinum capsule. Three- to five- experimental capsules were loaded into a 5 mm (outside diameter) platinum capsule containing H₂O and one of the selected metal-metal oxide or metal oxide-silicate buffers, QFM, NNO or MH. Both inner experimental capsules and outer buffer-bearing capsules were sealed by welding.

Experiments were carried out in Kanthal™ or platinum-wound furnaces placed in an internally-heated pressure vessel under isobaric conditions (200, +/- 10 MPa), isothermally at 1075, 1150 or 1200 °C for two hours using argon as the pressure medium.



Kanthal or Pt furnace (above) Experimental capsule contains H₂O and oxygen buffers and three to five individual experimental charges.

The pressure vessel, similar in design to that described by Holloway (1971), was modified to allow the vessel to rotate from the horizontal run position to a vertical quench position.



Internally heated pressure vessel. Dimensions, diameter-eight inches, length 23 inches, cylindrical bore (furnace volume) 1.3 x 22 inches. External cooling by copper water coil.

Rapid isobaric cooling of the experimental capsules was achieved as the vessel was rotated towards the vertical, causing the capsule to drop from the hot spot to the unheated, water-cooled end of the pressure chamber ($T < 250^\circ\text{C}$). The quench rate is inferred to be 500°C/s , similar to that reported by Holloway (1992) for a rapid-quench furnace with an equivalent thermal profile. The rotating furnace design used in this study provides a significant degree of control on the thermal characteristics of the critical heating zone. The temperature along the length of the experimental capsules was measured using three iconel-sheathed, chrome-alumel thermocouples. Temperature differences between the distal thermocouples ranged from 1 to 16°C , $\pm 2^\circ\text{C}$. The argon medium pressure was measured using a Bourdon tube-gauge, accurate to $\pm 5\text{ MPa}$.

Reversal experiments were performed to determine the time required to achieve chemical equilibrium in the experimental charges. Capsules containing experimental base-compositions + 10 wt% H₂O, were heated for two hours at a temperature of 1210 °C and then cooled to 1075, 1150 or 1200 °C for one, two or four hours, and subsequently quenched. The chemical compositions and textural characteristics observed in the experimental products produced in the reverse experiments are identical to those produced in forward experiments run at the same temperature and it is therefore concluded that equilibrium was obtained at heating durations of less than one hour. Chemical composition data for glasses produced during the reverse experiments is given in appendix B. Solid-oxide buffer reactants were evaluated after cooling using X-ray powder diffraction analysis or microscopic phase identification.

Trace elements experiment compositions

Experimental starting compositions containing 2.06 wt% P, 2.14 wt% S, 1.26 wt% F or 2.36 wt% Cl total solids (i.e. 6.66×10^{-4} mols /gr) were prepared by the addition of Fe₂P, FeS, FeCl₂, or FeF₂ to the anhydrous base-mixtures (above). Hydrous experiments incorporated 10 wt% H₂O (total wt. solids). Plagioclase-bearing experiments contain 1.3 wt% (total wt. solids) An₅₀, constituting 43 wt% of the normative feldspar component. Trace elements were added as mixtures of 7, 8 or 10 oxides in the amount of 1.25 wt% total weight solids. Peraluminous compositions contain 1.3 wt % Al₂O₃ total weight % solids in addition to the Al₂O₃ content listed for the given base composition.

Starting mixtures: base compositions A-1, A-1_p (peraluminous), A-3, and An₅₀ plus 10 wt% H₂O (total wt. solids) and 6.66×10^{-4} mols/gr of P, S, F or Cl.

base compositions (wt% oxide)	SiO ₂	FeO _{total}	Al ₂ O ₃	K ₂ O	An ₅₀
A-1	66.05	30.0	2.06	1.89	-
A-1 _p	66.05	30.0	2.06	1.89	-
A-3	62.86	30.0	3.71	3.43	-
An ₅₀ ^a	65.20	29.62	2.03	1.87	1.3

^a (Ca₅ Na₅) Al_{1.5} Si_{2.5}O₈

Preparation of oxygen isotope experimental material for analysis

Immiscible glasses and cryptocrystalline aggregates produced in experimental runs were finely ground and placed and magnetically separated while under suspension in ethanol. Separation of the Fe-rich and Si rich material was accomplished by varying the strength of the magnetic field and producing aliquots of distinct magnetic susceptibility. The process was repeated until the desired sample material was obtained (> 96 volume percent of the conjugate glass or Fe-rich aggregate).

Appendix B

Preparation of trace element doping mixtures and major element composition data for trace element partitioning experiments

Trace elements were doping mixtures were prepared by grinding equal atomic proportions of the selected elements in the form of element-oxide compounds. The mixtures were added to experimental charges in the quantity of 1.3 wt% of the total dry weight of the base compositions. Trace element mixtures designated R1, R2 and Xm contained the following oxide compounds: R1- Rb₂O, ZrO₂, NbO₂, HfO, UO₂, ThO, R2- La₂O₃, NdO₃, SmO₃, ErO₃, DyO₃ and Xm- MnO₂, CoO, MoO₃, NiO, Cu₂O, ZnO, CrO₃, V₂O₅, TiO₂ and Ag₂O. Major element compositions for the immiscible glasses and crystal aggregate produced in the trace element experiments are listed below.

Experiments were carried out by loading the desired quantity of starting material, or starting material + H₂O, into a 2mm (outside diameter) platinum capsule. Three- to five- experimental capsules were loaded into a 5 mm (outside diameter) platinum capsule containing H₂O and one of the selected metal-metal oxide or metal oxide-silicate buffers, QFM, NNO or MH. Both inner experimental capsules and outer buffer-bearing capsules were sealed by welding.

Experiments were carried out in Kanthal™ or platinum-wound furnaces placed in an internally-heated pressure vessel under isobaric conditions (200, +/- 10 MPa), isothermally at 1200 °C for two hours using argon as the pressure medium. Major element compositions for the immiscible glasses and crystal aggregate were obtained using a SX-100 electron microprobe at the University of Manitoba. Analytical conditions were set to an accelerating voltage of 15 kV, a 15 nA beam current. Major-element concentrations are listed below.

starting composition: AP-1 Xm	mt 3-4	SiO ₂	FeO	Al ₂ O ₃	K ₂ O	P	total
temp. = 1200 °C	liq 1	16.8	71.5	1.0	0.4	0.0	89.9
f_{O_2} = nickel - nickel oxide	std. dev.,	3.5	3.6	0.1	0.1	0.0	0.9
P= 2 kbar							
duration = 2 hours	liq 2	83.8	4.8	3.0	2.3	0.0	93.9
	std. dev.,	0.5	0.1	0.1	0.4	0.0	0.3
	D Fe/Si	0.2	15.0	0.3	0.2	0.4	
starting composition: AP-1 R-1	mt 4-1	SiO ₂	FeO	Al ₂ O ₃	K ₂ O	P	total
temp. = 1200 °C	liq 1	28.3	57.9	1.3	0.8	8.0	96.3
f_{O_2} = nickel - nickel oxide	std. dev.,	0.1	0.4	0.1	0.0	0.1	0.2
P= 2 kbar							
duration = 2 hours	liq 2	74.8	11.0	5.7	5.7	0.7	97.9
	std. dev.,	0.4	0.0	0.2	0.1	0.0	0.2
	D Fe/Si	0.4	5.3	0.2	0.1	11.6	
starting composition: APS-1 R1	mt 6-1	SiO ₂	FeO	Al ₂ O ₃	K ₂ O	P	total
temp. = 1200 °C	liq 1	16.5	60.9	0.5	0.1	18.0	95.9
f_{O_2} = nickel - nickel oxide	std. dev.,	0.9	1.7	0.4	0.0	2.0	2.9
P= 2 kbar							
duration = 2 hours	liq 2	81.7	7.9	2.8	2.8	0.6	95.7
	std. dev.,	0.5	0.2	0.1	0.3	0.0	0.6
	D Fe/Si	0.2	7.7	0.2	0.1	30.1	
starting composition: QAP Xm	mt 6-5	SiO ₂	FeO	Al ₂ O ₃	K ₂ O	P	total
temp. = 1200 °C	liq 1	28.3	56.3	1.4	1.4	9.7	97.1
f_{O_2} = quartz - fayalite - magnetite	std. dev.,	0.2	0.4	0.2	0.1	0.1	0.2
P= 2 kbar							
duration = 2 hours	liq 2	80.0	7.2	6.0	5.9	0.6	99.7
	std. dev.,	4.2	1.8	1.0	1.1	0.3	0.2
	D Fe/Si	0.4	7.9	0.2	0.2	15.6	
starting composition: MHAP-1 R-1	mt 7-3	SiO ₂	FeO	Al ₂ O ₃	K ₂ O	P	total
temp. = 1200 °C	liq 1	20.4	67.9	1.3	0.7	2.6	93.0
f_{O_2} = magnetite - hematite	std. dev.,	0.2	2.1	0.1	0.0	2.1	0.1
P= 2 kbar							
duration = 2 hours	liq 2	82.9	7.1	2.5	2.2	0.6	95.4
	std. dev.,	0.4	0.1	0.0	0.4	0.0	0.6
	D Fe/Si	0.2	9.5	0.5	0.3	4.1	
starting composition: MHAP-1 R-1, per:	mt 7-4	SiO ₂	FeO	Al ₂ O ₃	K ₂ O	P	total
temp. = 1200 °C	liq 1	13.1	59.7	0.4	0.1	21.8	95.0
f_{O_2} = nickel - nickel oxide	std. dev.,	0.1	0.1	0.0	0.0	0.2	0.2
P= 2 kbar							
duration = 2 hours	liq 2	81.6	7.9	2.9	2.0	0.6	95.0
	std. dev.,	0.3	0.1	0.0	0.2	0.0	0.5
	D Fe/Si	0.2	7.5	0.1	0.0	33.6	

starting composition: QAP-1 R-2	mt 8-1	SiO ₂	FeO	Al ₂ O ₃	K ₂ O	P	total
temp. = 1200 °C	liq 1	25.3	55.3	1.3	1.1	11.0	93.9
f_{O_2} = quartz - fayalite - magnetite	std. dev.,	0.3	0.5	0.1	0.0	0.2	0.6
P= 2 kbar							
duration = 2 hours	liq 2	82.7	6.3	4.9	4.6	0.7	99.3
	std. dev.,	5.3	1.5	1.1	1.0	0.5	1.1
	D Fe/Si	0.3	8.7	0.3	0.2	15.1	
starting composition: QA-1 R-2	mt 8-2	SiO ₂	FeO	Al ₂ O ₃	K ₂ O	P	total
temp. = 1200 °C	liq 1	35.0	53.7	0.8	1.0	0.1	90.6
f_{O_2} = quartz - fayalite - magnetite	std. dev.,	0.8	1.1	0.1	0.1	0.0	0.3
P= 2 kbar							
duration = 2 hours	liq 2	71.5	15.0	3.6	4.4	0.0	94.6
	std. dev.,	0.2	0.1	0.2	0.2	0.0	0.4
	D Fe/Si	0.5	3.6	0.2	0.2	7.3	
starting composition: AP-1 R-2	mt 8-4	SiO ₂	FeO	Al ₂ O ₃	K ₂ O	P	total
temp. = 1200 °C	liq 1	26.7	57.3	1.8	0.5	6.5	92.9
f_{O_2} = nickel - nickel oxide	std. dev.,	7.4	0.1	0.5	0.4	7.9	0.5
P= 2 kbar							
duration = 2 hours	liq 2	82.8	6.2	2.4	1.9	0.3	93.7
	std. dev.,	0.2	0.1	0.0	0.3	0.0	0.5
	D Fe/Si	0.3	9.3	0.7	0.3	20.8	
starting composition: AP-1 An50 R-1	mt 9-3	SiO ₂	FeO	Al ₂ O ₃	K ₂ O	P	total
temp. = 1200 °C	liq 1	5.6	50.4	0.8	0.2	29.0	86.0
f_{O_2} = nickel - nickel oxide	std. dev.,	0.2	0.3	0.0	0.0	0.2	0.3
P= 2 kbar							
duration = 2 hours	liq 2	81.6	7.5	2.9	2.1	0.5	94.5
	std. dev.,	0.2	0.1	0.0	0.2	0.0	0.3
	D Fe/Si	0.1	6.7	0.3	0.1	52.8	
starting composition: AP-1 Xm	mt 10-1	SiO ₂	FeO	Al ₂ O ₃	K ₂ O	P	total
temp. = 1200 °C	liq 1	13.8	59.1	0.6	0.2	20.2	93.9
f_{O_2} = nickel - nickel oxide	std. dev.,	0.2	0.7	0.0	0.0	0.1	0.9
P= 2 kbar							
duration = 2 hours	liq 2	87.1	4.5	2.3	1.9	0.3	96.0
	std. dev.,	0.2	0.1	0.0	0.2	0.0	0.3
	D Fe/Si	0.2	13.2	0.3	0.1	72.2	
starting composition: MHAP-1 Xm	mt 10- 4	SiO ₂	FeO	Al ₂ O ₃	K ₂ O	P	total
temp. = 1200 °C	liq 1	18.7	55.2	4.7	0.2	15.1	93.8
f_{O_2} = magnetite - hematite	std. dev.,	0.3	0.4	2.6	0.0	0.4	2.4
P= 2 kbar							
duration = 2 hours	liq 2	84.0	7.4	2.3	2.0	0.3	96.0
	std. dev.,	0.3	0.2	0.0	0.2	0.0	0.3
	D Fe/Si	0.2	7.4	2.0	0.1	48.8	

starting composition: AP-1 R-2,	mt 11-2	SiO ₂	FeO	Al ₂ O ₃	K ₂ O	P	total
temp. = 1200 °C peraluminous,	liq 1	26.5	57.4	1.8	0.7	8.4	94.9
f_{O_2} = nickel - nickel oxide	std. dev.,	0.6	1.0	0.4	0.3	0.6	1.3
P= 2 kbar							
duration = 2 hours	liq 2	82.1	6.8	4.3	4.2	0.4	97.8
	std. dev.,	0.9	0.5	0.1	0.2	0.0	0.7
	D Fe/Si	0.3	8.4	0.4	0.2	23.7	
starting composition: MHAP-1 R-2	mt 11-4	SiO ₂	FeO	Al ₂ O ₃	K ₂ O	P	total
temp. = 1200 °C	liq 1	16.8	52.6	7.5	0.2	14.1	91.3
f_{O_2} = magnetite - hematite	std. dev.,	1.5	4.8	4.4	0.0	1.3	3.1
P= 2 kbar							
duration = 2 hours	liq 2	83.7	7.4	2.4	2.0	0.3	95.8
	std. dev.,	0.2	0.2	0.2	0.2	0.0	0.2
	D Fe/Si	0.2	7.1	3.1	0.1	52.8	
starting composition: AP-1 An50 Xm	mt 13 -4	SiO ₂	FeO	Al ₂ O ₃	K ₂ O	P	total
temp. = 1200 °C	liq 1	21.2	57.3	1.9	0.2	14.3	94.9
f_{O_2} = nickel - nickel oxide	std. dev.,	0.9	2.0	0.8	0.1	0.7	1.0
P= 2 kbar							
duration = 2 hours	liq 2	84.7	5.3	2.6	2.3	0.5	95.4
	std. dev.,	0.3	0.1	0.0	0.2	0.0	0.2
	D Fe/Si	0.2	10.8	0.7	0.1	29.3	
starting composition: A-1 R-2	mt 14-1	SiO ₂	FeO	Al ₂ O ₃	K ₂ O	P	total
temp. = 1200 °C	liq 1	38.2	49.7	2.5	1.3	0.0	91.7
f_{O_2} = nickel - nickel oxide	std. dev.,	0.3	0.6	0.4	0.1	0.0	0.4
P= 2 kbar							
duration = 2 hours	liq 2	83.7	1.0	5.3	5.6	0.0	95.6
	std. dev.,	0.3	0.1	0.1	0.2	0.0	0.1
	D Fe/Si	0.5	51.9	0.5	0.2	1.3	
starting composition: ACl-1 R-2	mt 14-2	SiO ₂	FeO	Al ₂ O ₃	K ₂ O	P	total
temp. = 1200 °C	liq 1	39.2	50.1	2.8	1.0	0.0	93.1
f_{O_2} = nickel - nickel oxide	std. dev.,	0.3	1.4	0.4	0.1	0.0	1.0
P= 2 kbar							
duration = 2 hours	liq 2	71.6	16.7	3.6	3.5	0.0	93.1
	std. dev.,	0.3	0.2	0.0	0.1	0.0	1.0
	D Fe/Si	0.5	3.0	0.8	0.3	1.2	
starting composition: QAP-1 R-1	mt 15-2	SiO ₂	FeO	Al ₂ O ₃	K ₂ O	P	total
temp. = 1200 °C	liq 1	25.6	55.8	1.7	1.0	11.5	95.6
f_{O_2} = quartz - fayalite - magnetite	std. dev.,	0.2	0.3	0.1	0.0	0.1	0.5
P= 2 kbar							
duration = 2 hours	liq 2	91.7	3.3	2.4	2.1	0.2	99.8
	std. dev.,						
	D Fe/Si	0.3	16.7	0.7	0.5	52.2	

starting composition: QA-1 R-1	mt 15-3	SiO ₂	FeO	Al ₂ O ₃	K ₂ O	P	total
temp. = 1200 °C	liq 1	40.8	51.3	3.3	1.2	0.0	96.7
f_{O_2} = quartz - fayalite - magnetite	std. dev.,	0.2	0.5	0.1	0.0	0.0	0.2
P= 2 kbar							
duration = 2 hours	liq 2	84.7	6.4	2.9	2.6	0.0	96.6
	std. dev.,	0.2	0.1	0.0	0.2	0.0	0.3
	D Fe/Si	0.5	8.0	1.1	0.5	-6.5	
starting composition: AS-1 Xm	mt 3-5	SiO ₂	FeO	Al ₂ O ₃	K ₂ O	S	total
temp. = 1200 °C	liq 1	28.7	58.7	1.2	0.8		89.4
f_{O_2} = nickel - nickel oxide	std. dev.,	0.7	0.7	0.5			1.2
P= 2 kbar							
duration = 2 hours	liq 2	81.3	8.2	4.2	4.5		98.1
	std. dev.,	3.1	1.1	0.5	1.2		0.2
	D Fe/Si	0.4	7.2	0.3	0.2		
starting composition: AS-3 Xm	mt 6-2	SiO ₂	FeO	Al ₂ O ₃	K ₂ O	S	total
temp. = 1200 °C	liq 1	39.2	53.9	1.9	1.0		95.9
f_{O_2} = nickel - nickel oxide	std. dev.,	0.3	0.5	0.0	0.3		0.7
P= 2 kbar							
duration = 2 hours	liq 2	66.2	22.9	3.4	3.4		95.8
	std. dev.,	0.4	0.5	0.1	0.7		0.8
	D Fe/Si	0.6	2.4	0.6	0.3		
starting composition: AS-1 Xm	mt 10 -2	SiO ₂	FeO	Al ₂ O ₃	K ₂ O	S	total
temp. = 1200 °C peraluminous	liq 1	36.6	55.5	2.7	1.0	0.4	96.1
f_{O_2} = nickel - nickel oxide	std. dev.,	0.4	1.2	0.6	0.2	0.0	0.3
P= 2 kbar							
duration = 2 hours	liq 2	77.6	9.2	5.9	4.5	0.0	97.3
	std. dev.,	0.5	0.3	0.3	0.5	0.0	0.5
	D Fe/Si	0.5	6.0	0.5	0.2	24.9	
starting composition: AS-1 An50 Xm	mt 13 -3	SiO ₂	FeO	Al ₂ O ₃	K ₂ O	S	total
temp. = 1200 °C	liq 1	33.5	55.3	1.6	0.5	3.1	94.0
f_{O_2} = nickel - nickel oxide	std. dev.,	1.1	1.4	0.1	0.0	0.1	0.4
P= 2 kbar							
duration = 2 hours	liq 2	78.7	9.2	4.7	3.8	0.1	96.6
	std. dev.,	0.5	0.2	0.1	0.4	0.0	0.4
	D Fe/Si	0.4	6.0	0.3	0.1	36.6	
starting composition: AS-3 R-2	mt 16 -3	SiO ₂	FeO	Al ₂ O ₃	K ₂ O	S	total
temp. = 1200 °C	liq 1	29.0	54.3	2.0	0.2	0.9	86.4
f_{O_2} = nickel - nickel oxide	std. dev.,	0.1	0.4	0.0	0.0	0.0	0.3
P= 2 kbar							
duration = 2 hours	liq 2	74.4	12.4	4.2	2.0	0.1	93.2
	std. dev.,	0.6	0.6	0.2	0.6	0.0	1.0
	D Fe/Si	0.4	4.4	0.5	0.1	8.4	

starting composition: AF-1 R-2	mt 12-3	SiO ₂	FeO	Al ₂ O ₃	K ₂ O	F	total
temp. = 1200 °C, peraluminous	liq 1	21.1	63.2	0.9	0.5	0.1	85.8
fO_2 = nickel - nickel oxide	std. dev.,	0.2	0.2	0.2	0.0	0.0	0.5
P= 2 kbar							
duration = 2 hours	liq 2	74.4	7.0	9.3	8.0	0.1	98.8
	std. dev.,	0.4	0.2	0.0	0.1	0.0	0.4
	D Fe/Si	0.3	9.1	0.1	0.1	1.4	
starting composition: AF-1 R-2	mt 14-3	SiO ₂	FeO	Al ₂ O ₃	K ₂ O	F	total
temp. = 1200 °C	liq 1	32.2	57.8	1.9	1.0	0.7	93.5
fO_2 = nickel - nickel oxide	std. dev.,	0.6	0.8	0.1	0.1	0.3	0.0
P= 2 kbar							
duration = 2 hours	liq 2	83.2	7.6	2.6	2.8	1.1	97.3
	std. dev.,	0.2	0.1	0.1	0.0	0.1	0.2
	D Fe/Si	0.4	7.6	0.7	0.3	0.7	

An50

starting composition: A-1 An50 R-1	mt 4-3	SiO ₂	FeO	Al ₂ O ₃	K ₂ O	Na ₂ O	CaO
temp. = 1200 °C	liq 1	46.0	44.3	1.9	0.7	0.0	0.2
fO_2 = nickel - nickel oxide	std. dev.,	0.1	1.5	0.0	0.0	0.0	0.0
P= 2 kbar							
duration = 2 hours	liq 2	83.2	7.3	3.2	1.4	0.0	0.1
	std. dev.,	0.7	0.2	1.1	0.0	0.0	0.0
	D Fe/Si	0.6	6.1	0.6	0.5	-1.5	1.2
starting composition: AS-1 R-2 An50	mt 16-1	SiO ₂	FeO	Al ₂ O ₃	K ₂ O	Na ₂ O	CaO
temp. = 1200 °C	liq 1	37.8	42.4	2.8	0.4	0.1	1.7
fO_2 = nickel - nickel oxide	std. dev.,	0.5	0.7	0.4	0.0	0.0	0.1
P= 2 kbar							
duration = 2 hours	liq 2	82.0	7.4	3.1	1.8	0.2	0.4
	std. dev.,	0.8	0.3	0.6	0.0	0.0	0.0
	D Fe/Si	0.5	5.7	0.9	0.2	0.5	4.6
starting composition: AP-1 R-2 An50	mt 16-2	SiO ₂	FeO	Al ₂ O ₃	K ₂ O	Na ₂ O	CaO
temp. = 1200 °C	liq 1	5.2	49.6	0.9	0.8	0.2	2.6
fO_2 = nickel - nickel oxide	std. dev.,	0.4	0.0	0.0	0.0	0.0	0.0
P= 2 kbar							
duration = 2 hours	liq 2	86.8	4.1	2.6	2.0	0.2	0.1
	std. dev.,	0.8	0.2	0.3	0.1	0.0	0.0
	D Fe/Si	0.1	12.2	0.4	0.4	1.4	50.4
starting composition: APS-1 R-2	mt 16-4	SiO ₂	FeO	Al ₂ O ₃	K ₂ O		
temp. = 1200 °C	liq 1	18.5	64.6	1.1	0.1		
fO_2 = nickel - nickel oxide	std. dev.,	0.2	2.5	0.1	0.0		
P= 2 kbar							
duration = 2 hours	liq 2	86.5	4.7	2.8	2.4		
	std. dev.,	0.9	0.5	0.1	0.1		
	D Fe/Si	0.2	13.8	0.4	0.0		

starting composition: AP-3 R-2	mt 16-5	SiO ₂	FeO	Al ₂ O ₃	K ₂ O		
temp. = 1200 °C	liq 1	27.4	59.5	2.1	0.4		
fO_2 = nickel - nickel oxide	std. dev.,	0.6	0.8	0.5	0.0		
P= 2 kbar							
duration = 2 hours	liq 2	85.1	6.7	2.3	1.7		
	std. dev.,	0.2	0.0	0.0	0.0		
	D Fe/Si	0.3	8.9	0.9	0.3		
starting composition: QAP-1 R-1	mt 18-1	SiO ₂	FeO	Al ₂ O ₃	K ₂ O	P	total
temp. = 1200 °C	liq 1	17.6	59.2	0.6	0.3	17.2	95.3
fO_2 =	std. dev.,	0.2	0.6	0.0	0.0	0.1	0.6
P= 2 kbar							
duration = 2 hours	liq 2	72.0	13.3	4.3	3.3	1.2	94.2
	std. dev.,	0.4	0.1	0.0	0.2	0.0	0.5
	D Fe/Si	0.2	4.4	0.2	0.1	14.1	1.0
starting composition: QAP-1 R-2	mt 18-3	SiO ₂	FeO	Al ₂ O ₃	K ₂ O	P	total
temp. = 1200 °C	liq 1	10.8	53.5	1.7	0.3	23.7	91.8
fO_2 =	std. dev.,	0.5	0.1	0.1	0.0	0.7	1.1
P= 2 kbar							
duration = 2 hours	liq 2	76.0	10.2	4.4	3.4	1.1	95.1
	std. dev.,	0.2	0.1	0.0	0.4	0.0	0.2
	D Fe/Si	0.1	5.3	0.4	0.1	22.0	1.0
starting composition: QAP-1 XM	mt 18-4	SiO ₂	FeO	Al ₂ O ₃	K ₂ O	P	total
temp. = 1200 °C	liq 1	14.6	54.0	1.2	0.2	18.0	88.5
fO_2 =	std. dev.,	0.2	0.3	0.5	0.0	0.1	0.5
P= 2 kbar							
duration = 2 hours	liq 2	74.8	11.1	4.4	3.3	1.1	94.8
	std. dev.,	0.2	0.1	0.1	0.2	0.0	0.2
	D Fe/Si	0.2	4.9	0.3	0.1	16.6	0.9